Global Genetic Cartography of Urban Metagenomes and Anti-Microbial Resistance

David Danko[1, 2, †], Daniela Bezdan[1, 2, †], Ebrahim Afshinnekoo[1, 2, ⋆], Sofia Ahsanuddin[3, ⋆], Chandrima Bhattacharya[1, 2, ⋆], Daniel J Butler[1, 2, ⋆], Kern Rei Chng[4, ⋆], Daisy Donnellan[1, 2, ⋆], Jochen Hecht[5, ⋆], Katerina Kuchin[1, 2, ⋆], Mikhail Karasikov[6, ⋆], Abigail Lyons[1, 2, ⋆], Lauren Mak[1, 2, ⋆], Dmitry Meleshko[1, 2, ⋆], Harun Mustafa[6, ⋆], Beth Mutai[8, 9, ⋆], Russell Y Neches[7, ⋆], Amanda Ng[4, ⋆], Olga Nikolayeva[10, ⋆], Tatyana Nikolayeva[10, ⋆], Eileen Png[4, ⋆], Krista Ryon[1, 2, ⋆], Jorge L Sanchez[1, 2, ⋆], Heba Shaaban[1, 2, ⋆], Maria A Sierra[1, 2, ⋆], Dominique Thomas[1, 2, ⋆], Ben Young[1, 2, ⋆], Omar O. Abudayyeh[11, ⋆], Josue Alicea[1, 2, ⋆], Malay Bhattacharyya[12, 13, ⋆], Ran Blekhman[14, ⋆], Eduardo Castro-Nallar[15, ⋆], Ana M Cañas[1, 2, ⋆], Aspassia D Chatziefthimiou[1, 2, ⋆], Robert W Crawford[16, ⋆], Francesca De Filippis[17, 18, ⋆], Youping Deng[19, ⋆], Christelle Desnues[20, ⋆], Emmanuel Dias-Neto[21, ⋆], Marius Dybwad[22, ⋆], Eran Elhaik[23, ⋆], Danilo Ercolini[17, 18, ⋆], Alina Frolova[24, ⋆], Dennis Gankin[11, ⋆], Jonathan S. Gootenberg[11, ⋆], Alexandra B Graf[25, ⋆], David C Green[26, ⋆], Iman Hajirasouliha[1, 2, ⋆], Mark Hernandez[27, ⋆], Gregorio Iraola[28, 29, 30, ⋆], Soojin Jang[31, ⋆], Andre Kahles[6, ⋆], Frank J Kelly[26, ⋆], Kaymisha Knights[1, 2, ⋆], Nikos C Kyrpides[7, ⋆], Paweł P Łabaj[59, ⋆], Patrick K H Lee[32, ⋆], Marcus H Y Leung[32, ⋆], Per Ljungdahl[33, ⋆], Gabriella Mason-Buck[26, ⋆], Ken McGrath[34, ⋆], Cem Meydan[1, 2, ⋆], Emmanuel F Mongodin[35, ⋆], Milton Ozorio Moraes[36, ⋆], Niranjan Nagarajan[4, ⋆], Marina Nieto-Caballero[27, ⋆], Houtan Noushmehr[37, ⋆], Manuela Oliveira[38, ⋆], Stephan Ossowski[39, 40, ⋆], Olayinka O Osuolale[41, ⋆], Orhan Özcan[45, ⋆], David Paez-Espino[7, ⋆], Nicolas Rascovan[42, ⋆], Hugues Richard[43, ⋆], Gunnar Rätsch[6, ⋆], Lynn M Schriml[35, ⋆], Torsten Semmler[44, ⋆], Osman U Sezerman[45, ⋆], Leming Shi[46, 47, ⋆], Tieliu Shi[48, ⋆], Le Huu Song[49, ⋆], Haruo Suzuki[50, ⋆], Denise Syndercombe Court[26, ⋆], Scott W Tighe[51, ⋆], Xinzhao Tong[32, ⋆], Klas I Udekwu[33, ⋆], Juan A Ugalde[52, ⋆], Brandon Valentine[1, 2, ⋆], Dimitar I Vassilev[53, ⋆], Elena Vayndorf[54, ⋆], Thirumalaisamy P Velavan[55, ⋆], Jun Wu[48, ⋆], María M Zambrano[56, ⋆], Jifeng Zhu[1, 2, ⋆], Sibo Zhu[57, 58, ⋆], Christopher E Mason[1, 2, ‡], and The International MetaSUB Consortium[⋆]

[†]Equal contribution
[⋆]Listed alphabetically
[‡]Corresponding author
[⋆]Full list attached
[1]Weill Cornell Medicine
[2]The Bin Talal Bin Abdulaziz Alsaud Institute for Computational Biomedicine
[3]Icahn School of Medicine at Mount Sinai
[4]Genome Institute of Singapore
[5]Centre for Genomic Regulation (CRG), The Barcelona Institute of Science and Technology, Barcelona, Spain
[6]ETH Zurich, Department of Compter Science, Biomedical Informatics Group
[7]Department of Energy, Joint Genome Institute, Walnut Creek, California 94598, USA.
[8]Kenya Medical Research Institute / US Army medical Research Directrorate - Kenya
[9]Centre for Genomic Regulation (CRG), The Barcelona Institute of Science and Technology, Barcelona, Spain.
[10]ETH Zurich, Functional Genomics Center Zurich
[11]Massachusetts Institute of Technology, McGovern Institute for Brain Research
[12]Machine Intelligence Unit, Indian Statistical Institute, Kolkata
[13]Centre for Artificial Intelligence and Machine Learning, Indian Statistical Institute, Kolkata
[14]University of Minnesota
[15]Universidad Andrés Bello, Center for Bioinformatics and Integrative Biology, Facultad de Ciencias de la Vida
[16]California State University Sacramento

[17]Department of Agricultural Sciences, Division of Microbiology, University of Naples Federico II

[18]Task Force on Microbiome Studies, University of Naples Federico II

[19]University of Hawaii John A. Burns School of Mecidine

[20]Aix-Marseille Université, Mediterranean Institute of Oceanology, Université de Toulon, CNRS, IRD, UM 110

[21]A.C. Camargo Cancer Center

[22]Norwegian Defence Research Establishment FFI, Kjeller, Norway

[23]Department of Animal Plant Sciences, University of Sheffield

[24]Institute of Molecular Biology and Genetics of National Academy of Science of Ukraine

[25]University of Applied Sciences Vienna

[26]Department of Analytical, Environmental and Forensic Sciences

[27]University of Colorado at Boulder

[28]Microbial Genomics Laboratory, Institut Pasteur de Montevideo, Uruguay

[29]Center for Integrative Biology, Universidad Mayor, Santiago de Chile, Chile

[30]Wellcome Sanger Institute, Hinxton, United Kingdom

[31]Institut Pasteur Korea

[32]School of Energy and Environment, City University of Hong Kong, Hong Kong SAR, China

[33]Stockholm University

[34]Microba

[35]University of Maryland School of Medicine, Institute for Genome Sciences

[36]Fundação Oswaldo Cruz

[37]University of São Paulo, Ribeirão Preto Medical School

[38]Instituto de Patologia e Imunologia Molecular da Universidade do Porto

[39]Institute of Medical Genetics and Applied Genomics, University of Tübingen, Tübingen, Germany

[40]Centre for Genomic Regulation (CRG), The Barcelona Institute of Science and Technology, Barcelona, Spain. 3) Universitat Pompeu Fabra, Barcelona, Spain.

[41]Applied Environmental Metagenomics and Infectious Diseases Research (AEMIDR), Department of Biological Sciences, Elizade University

[42]Aix-Marseille Université, IRD, AP-HM, IHU Méditerranée Infection

[43]Sorbonne University, Faculty of science, Institute of Biology Paris-Seine, Laboratory of Computational and Quantitative Biology

[44]Robert Koch Institute Berlin

[45]Acibadem Mehmet Ali Aydınlar University

[46]Center for Pharmacogenomics, School of Life Sciences and Shanghai Cancer Center, Fudan University

[47]State Key Laboratory of Genetic Engineering (SKLGE) and MOE Key Laboratory of Contemporary Anthropology, School of Life Sciences

[48]The Center for Bioinformatics and Computational Biology, Shanghai Key Laboratory of Regulatory Biology, the Institute of Biomedical Sciences and School of Life Sciences, East China Normal University

[49]Institute of Tropical Medicine, Vietnamese-German Center of Excellence

[50]Keio University

[51]University of Vermont

[52]Millennium Initiative for Collaborative Research on Bacterial Resistance

[53]Faculty of Mathematics and Informatics, Sofia University "St. Kliment Ohridski"

[54]Institute of Arctic Biology, University of Alaska Fairbanks

[55]Institute of Tropical Medicine, Univeristätsklinikum Tübingen, Tübingen

[56]Corporación Corpogen

[57]State Key Laboratory of Genetic Engineering (SKLGE) and MOE Key Laboratory of Contemporary Anthropology, School of Life Sciences, Fudan University

[58]. Department of Epidemiology, School of Public Health, Fudan University

[59]Małopolska Centre of Biotechnology, Jagiellonian University

Abstract

Although studies have shown that urban environments and mass-transit systems have distinct genetic profiles, there are no systematic worldwide studies of these dense, human microbial ecosystems. To address this gap in knowledge, we created a global metagenomic and antimicrobial resistance (AMR) atlas of urban mass transit systems from 60 cities, spanning 4,728 samples and 4,424 taxonomically-defined microorganisms collected for three years. This atlas provides an annotated, geospatial profile of microbial strains, functional characteristics, antimicrobial resistance markers, and novel genetic elements, including 10,928 novel predicted viral species, 1302 novel bacteria, and 2 novel archaea. Urban microbiomes often resemble human commensal microbiomes from the skin and airways, but also contain a consistent "core" of 31 species which are predominantly not human commensal species. Samples show distinct microbial signatures which may be used to accurately

2

12 predict properties of their city of origin including population, proximity to the coast, and taxonomic
13 profile. These data also show that AMR density across cities varies by several orders of magnitude,
14 including many AMRs present on plasmids with cosmopolitan distributions. Together, these results
15 constitute a high-resolution, global metagenomic atlas, which enables the discovery of new genetic
16 components of the built human environment, highlights potential forensic applications, and provides
17 an essential first draft of the global AMR burden of the world's cities.

18 **Keywords:** Built Environment, metagenome, global health, antimicrobial resistance

1   Introduction

The high-density urban environment has historically been home to only a fraction of all people, with the majority living in rural areas or small villages. In the last two decades, the situation has reversed; 55% of the world's population now lives in urban areas (Ritchie and Roser, 2020; United Nations, 2018). Since the introduction of germ theory and John Snow's work on cholera, it has been clear that people in cities interact with microbes in ways that can be markedly different than in rural areas (Neiderud, 2015). Microbes in the built environment have been implicated as a possible source of contagion (Cooley et al., 1998) and certain syndromes, like allergies, are associated with increasing urbanization (Nicolaou et al., 2005). It is now apparent that cities in general have an impact on human health though the mechanisms of this impact are broadly variable and often little understood. Indeed, our understanding of microbial dynamics in the urban environment outside of pandemics has only begun (Gilbert and Stephens, 2018).

Technological advances in next-generation sequencing (NGS) and metagenomics have created an unprecedented opportunity for rapid, global studies of microorganisms and their hosts, providing researchers, clinicians, and policymakers with a more comprehensive view of the functional dynamics of microorganisms in a city. NGS facilitates culture-independent sampling of the microorganisms in an area with the potential for both taxonomic and functional annotation; this is particularly important for surveillance of microorganisms as they acquire antimicrobial resistance (AMR) (Fresia et al., 2019). Metagenomic methods enable nearly real-time monitoring of organisms, AMR genes, and pathogens as they emerge within a given geographical location, and have the potential to reveal hidden microbial reservoirs and detect microbial transmission routes as they spread around the world (Zhu et al., 2017). There are several different drivers and sources for AMR; including agriculture, farming, and livestock in rural and suburban areas, household and industrial sewage, usage of antimicrobials, hard metals, and biocides, as well as human and animal waste, all these factors contribute to the complexity of AMR transmission (Allen et al., 2009; Martínez, 2008; Singer et al., 2016; Thanner et al., 2016; Venter et al., 2017). A molecular map of urban environments will enable significant new research on the impact of urban microbiomes on human health.

The United Nations projects that by 2050, over two-thirds of the world's population will live in urban areas (Ritchie and Roser, 2020). Consequently, urban transit systems - including subways and buses - are a daily contact interface for billions of people who live in cities. Notably, urban travelers bring their commensal microorganisms with them as they travel and come into contact with organisms and mobile elements present in the environment, including AMR markers. The study of the urban microbiome and the microbiome of the built environment spans several different projects and initiatives including work focused on transit systems (Afshinnekoo et al., 2015; Hsu et al., 2016; Kang et al., 2018; Leung et al., 2014; MetaSUB International Consortium. Mason et al., 2016), hospitals (Brooks et al., 2017; Lax et al., 2017), soil (Hoch et al., 2019; Joyner et al., 2019), and sewage (Fresia et al., 2019; Maritz et al., 2019), among others. However, these efforts for the most part have only been profiled with comprehensive metagenomic methods in a few selected cities on a limited number of occasions. This leaves a gap in scientific knowledge about a microbial ecosystem, with which the global human population readily interacts. Human commensal microbiomes have been found to vary widely based on culture, and thus the geography and geographically constrained studies may to miss key differences (Brito et al., 2016). Moreover, data on urban microbes and AMR genes are urgently needed in developing nations, where antimicrobial drug consumption is expected to rise by 67% by 2030 (United Nations, 2016; Van Boeckel et al., 2015), both from changes in consumer demand for livestock products and an expanding use of antimicrobials - both of which can alter AMR profiles of these cities.

The International Metagenomics and Metadesign of Subways and Urban Biomes (MetaSUB) Consortium was launched in 2015 to address this gap in knowledge on the density, types, and dynamics of urban metagenomes and AMR profiles. Since then, we have developed standardized collection and sequencing protocols to process 4,728 samples across 60 cities worldwide (Table S1). Sampling took place at three major time points: a pilot study in 2015-16 and two global city sampling days (gCSD, June 21st) in 2016 and 2017. Each sample was sequenced with 5-7M 125bp paired-end reads using Illumina NGS sequencers (see Methods). To deal with the challenging analysis of our large dataset, we generated an open-source analysis pipeline (MetaSUB Core Analysis Pipeline, CAP), which includes a comprehensive set of state-of-the-art, peer-reviewed, metagenomic tools for taxonomic identification, k-mer analysis, AMR gene prediction, functional profiling, de novo assembly, annotation of particular microbial species, and geospatial mapping.

To our knowledge this study represents the first and largest global metagenomic study of urban microbiomes - with a focus on transit systems - that reveals a consistent "core" urban microbiome across

all cities, as well as distinct geographic variation that may reflect epidemiological variation and that enables a new forensic, source-tracking capabilities. More importantly, our data demonstrate that a significant fraction of the urban microbiome remains to be characterized. Though 1,000 samples are sufficient to discover roughly 80% of the observed taxa and AMR markers, we continued to observe taxa and genes at an ongoing discovery rate of approximately one new species (previously non-observed) and one new AMR marker for every 10 samples. Notably, this genetic variation is affected by various environmental factors (e.g., climate, surface type, latitude, etc.) and samples show greater diversity near the equator. Moreover, sequences associated with AMR markers are widespread, though not necessarily abundant, and show geographic specificity. Here, we present the results of our global analyses and a set of tools developed to access and analyze this extensive atlas, including: two interactive map-based visualizations for samples (`metasub.org/map`) and AMRs (`resistanceopen.org`), an indexed search tool over raw sequence data (`dnaloc.ethz.ch/`), a Git repository for all analytical pipelines and figures, and application programming interfaces (APIs) for computationally accessing results (`github.com/metasub/metasub_utils`).

2 Results

We have collected 4,728 samples from from the mass transit systems of 60 cities around the world (Table 1, Supplementary table S1). These samples were collected from various common surfaces in the mass transit systems such as railings, benches, and ticket kiosks and were subjected to metagenomic sequencing. We use the microbiome of mass transit systems as a proxy for the urban microbiome as a whole and present our key findings here.

A Core Urban Microbiome Centers Global Diversity

We first investigated the distribution of microbial species across the global urban environment. Specifically, we asked whether the urban environment represents a singular type of microbial ecosystem or a set of related, but distinct, communities, especially in terms of biodiversity. We observed a bi-modal distribution of taxa prevalence across our dataset, which we used to define two separate sets of taxa based on the inflection points of the distribution: the putative "sub-core" set of urban microbial species that are consistently observed ($>70\%$ of samples) and the less common "peripheral" ($<25\%$ of samples) species. We also defined a set of true "core" taxa which occur in essentially all samples ($>97\%$ of samples). Applying these thresholds, we identified 1,145 microbial species (Figure 2C) that make up the sub-core urban microbiome with 31 species in the true core microbiome (Figure 2A). Core and sub-core taxa classifications were further evaluated for sequence complexity and genome coverage on a subset of samples. Of the 1,206 taxa with prevalence greater than 70%, 69 were flagged as being low quality classifications (see methods). The sub-core microbiome was principally bacterial, with just one eukaryotic taxon identified and not flagged: *Saccharomyces cerevisiae*. Notably, no archaea or viruses were identified in the group of sub-core microorganisms (note that this analysis did not include viruses newly discovered in this study). For viruses in particular, this may be affected by the sampling or DNA extraction methods used, by limitations in sequencing depth, or by missing annotations in the reference databases used for taxonomic

Table 1: Sample Counts, The number of samples collected from each region.

Region	Pilot	CSD16	CSD17	Other	Total
North America	28	284	371	276	959
East Asia	34	26	1297	0	1357
Europe	177	310	939	1	1427
Sub Saharan Africa	0	116	192	0	308
South America	20	44	199	68	331
Middle East	0	100	15	0	115
Oceania	0	94	32	0	126
Background Control	0	0	40	0	40
Lab Control	0	0	20	6	26
Positive Control	0	0	33	6	39
Total	259	974	3138	357	4728

classification, which is principally problematic with phages. It is worth noting that potentially prevalent RNA viruses are omitted with our DNA-based sampling. The three most common bacterial phyla across the world's cities ordered by the number of species observed were *Proteobacteria*, *Actinobacteria*, and *Firmicutes*. To test for possible geographic bias in our data, we normalized the prevalence for each taxa by the median prevalence within each city. The two normalization methods broadly agreed (Figure 2).

Despite their global prevalence, the core taxa are not uniformly abundant across all cities. Many species exhibited a high standard deviation and kurtosis (calculated using Fisher's definition and normal kurtosis of 0) than other species (Figure 2B). Furthermore, some species show distinctly high mean abundance, often higher than the core species, but more heterogeneous global prevalence. For example, *Salmonella enterica* is identified in less than half of all samples but is the 12th most abundant species based on the fraction of DNA that can be ascribed to it. The most relatively abundant microbial species was *Cutibacterium acnes* (Figure 2D) which had a comparatively stable distribution of abundance across all samples; *Cutibacterium acnes* is known as a prominent member of the human skin microbiome. To test for any biases arising from uneven geographic sampling, we measured the relative abundance of each taxon by calculating the fraction of reads classified to each particular taxon, and compared the raw distribution of abundance to the distribution of median abundance within each city (This process is analogous to the one used for Figure 2C, Figure 2B); the two measures closely aligned. Also, an examination of the positive and negative controls indicates that these results are not likely due to contamination or batch effect (Supp. Figure S13). In total, we observed 31 core taxa ($>97\%$), 1,145 sub-core taxa (70-97%) 2,466 peripheral taxa ($<25\%$), and 4,424 taxa across all samples. We term the set of all taxa observed *the urban panmicrobiome*.

To estimate the number of taxa present in our samples but which were not detected by our experimental techniques, we performed a rarefaction analysis on the taxa that were identified. By estimating the number of taxa identified for different numbers of samples, we see a diminishing trend (Figure 2D), which indicates that at some point, the species in every new sample were likely already identified in a previous one. Our rarefaction curve did not reach a plateau and, even after including all samples, it still shows an expected marginal discovery rate of roughly 1 additional species for every 10 samples added to the study. For clarity we note that this analysis only considers taxa already present in reference databases, not newly discovered taxa (below). Despite the remaining unidentified taxa, we estimate that most (80%) of the classifiable taxa in the urban microbiome could be identified with roughly 1,000 samples. However, as noted below, this new diversity is likely not evenly distributed across regions.

As humans are a major part of the urban environment, the DNA in our samples could be expected to resemble commensal human microbiomes. To investigate this, we compared non-human DNA fragments from our samples to a randomized set of 50 samples from 5 commensal microbiome sites in the Human Microbiome Project (HMP) (Consortium et al., 2012) (stool, skin, airway, gastrointestinal tract, urogenital tract). We used MASH to perform a k-mer based comparison of our samples vs. the selected HMP samples, which showed a roughly uniform dissimilarity between MetaSUB samples and those from different human body sites (Figure 2E, Supp. Figure S2A B). Samples taken from surfaces that were likely to have been touched more often by human skin, such as doorknobs, buttons, railings, and touchscreens, were indeed more similar to human skin microbiomes than surfaces like bollards, windows, and the floor. Given that a large fraction of DNA in our samples could not be classified and that a k-mer based comparison did not find significant body-site specificity, it is possible that the unclassified DNA in our samples is from novel taxa which are not human commensals. Of note, the taxonomic composition of our samples do not closely resemble soil samples. We processed 28 metagenomic soil samples (Bahram et al., 2018) using the same pipeline as the rest of the data and compared soil samples to our samples using MASH. Our samples were very dissimilar from the soil samples (Figure 2F) even in comparison to human skin microbiomes. This suggests that the unclassified DNA may represent heretofore uncharacterized taxa that are not known commensals being shed into the environment.

We next estimated the fraction of sequences in our data that did not resemble sequences in known reference databases. We took a subset of 10,000 reads from each sample and aligned these reads to a number of reference databases using BLASTn (Altschul et al., 1990). We then identified reads that mapped to sequences in the reference databases at 80%, 90%, and 95% Average Nucleotide Identity (ANI) (Figure 2G). We used a broad set of databases for reference: RefSeq, NCBI's NT Environmental, a large database of Metagenome Assembled Genomes (MAGs) from Pasolli et al. (2019), and MAGs from MetaSUB itself (Section 2.4). At 80% ANI, the most permissive threshold, 34.6% of reads did not map to any database while 47.3% of reads did not map or only mapped to MAGs from MetaSUB itself. This mirrors results seen by previous urban microbiome works (Afshinnekoo et al., 2015; Hsu et al., 2016).

Next, we analyzed the fraction of sequences that aligned to these same databases by region. Sur-

prisingly, samples from Europe had the highest fraction of unaligned reads, followed by the middle east, while samples from Sub Saharan Africa had the smallest fraction of unaligned reads (Supp. Figure S1C). The proportion of reads aligned to each database did not vary significantly by region. We further investigated the relationship between geography and sample composition. In ecology, an increasing distance from the equator is associated with a decrease in taxonomic diversity (O'Hara et al., 2017). The MetaSUB data recapitulates this result and identifies a significant decrease in taxonomic diversity (though with significant noise, $p < 2e16$, $R^2 = 0.06915$) as a function of absolute latitude; samples are estimated to lose 6.9672 species for each degree of latitude away from the equator (Supp. Figure S1A). The effect of latitude on species diversity is not purely monotonic, since several cities have higher species diversity then their latitude would predict. This is expected as latitude is only a rough predictor of a city's climate. While this is an observation consistent with ecological theory, we note that our samples are heavily skewed by the location of the target cities, as well as the prevalence of those cities in specific latitude zones of the northern hemisphere.

2.1 Global Diversity Varies According to Covariates

Despite the core urban microbiome present in almost all samples, there was also geographic variation in taxonomy and localization. We calculated the Jaccard distance between samples measured by the presence and absence of species (which is robust to noise from relative abundance) and performed a dimensionality reduction of the data using UMAP (Uniform Manifold Approximation and Projection, McInnes et al. (2018)) for visualization (Figure 2A). Jaccard distance was correlated with distance based on Jensen-Shannon Divergence (which accounts for relative abundance) and k-mer distance calculated by MASH (which is based on the k-mer distribution in a sample, so cannot be biased by a database) (Supp. Figure S10A, B, C). In principle, Jaccard distance could be influenced by read depth as low abundance species drop below detection thresholds. However we expect this issue to be minor as the total number of species identified stabilized at 100,000 reads (Supp. Figure S9B) compared to an average of 6.01M reads per sample. Samples collected from North America and Europe were distinct from those collected in East Asia, but the separation between other regions was less clear. A similar trend was found in an analogous analysis based on functional pathways rather than taxonomy (Supp. Fig S5D), which indicates geographic stratification of the metagenomes at both the functional and taxonomic levels. Subclusters identified by UMAP roughly corresponded to city and climate but not surface type (Supp. Figure S5A, B, C). These findings confirm and extend earlier analyses performed on a fraction of the MetaSUB data which were run as a part of CAMDA Challenges in years 2017, 2018, and 2019 (`camda.info`).

We quantified the degree to which metadata covariates influence the taxonomic composition of our samples using MAVRIC, a statistical tool to estimate the sources of variation in a count-based dataset (Moskowitz and Greenleaf, 2018). We identified covariates which influenced the taxonomic composition of our samples: city, population density, average temperature in June, region, elevation above sea-level, surface type, surface material, elevation above or below ground and proximity to the coast. The most important factor, which could explain 19% of the variation in isolation, was the city from which a sample was taken followed by region which explained 11%. The other four factors ranged from explaining 2% to 7% of the possible variation in taxonomy in isolation (Supp. Table S2). We note that many of the factors were confounded with one another, so they can explain less diversity than their sum. One metadata factor tested, the population density of the sampled city, had no significant effect on taxonomic variation overall.

To quantify how the principle covariates, climate, continent, and surface material impacted the taxonomic composition of samples, we performed a Principal Component Analysis (PCA) on our taxonomic data normalized by proportion and identified principal components (PCs) which were strongly associated with a metadata covariate in a positive or negative direction (PCs were centered so an average direction indicates an association). We found that the first two PCs (representing 28.0% and 15.7% of the variance of the original data, respectively) associated strongly with the city climate while continent and surface material associate less strongly (Figure 2B).

Next, we tested whether geographic proximity (in km) of samples to one another had any effect on the variation, since samples taken from nearby locations could be expected to more closely resemble one another. Indeed, for samples taken in the same city, the average JSD (Jensen-Shannon distance) was weakly predictive of the taxonomic distance between samples, with every increase of 1km in distance between two samples representing an increase of 0.056% in divergence ($p < 2e16$, $R^2 = 0.01073$, Supp. Figure S1B). This suggests a "neighborhood effect" for sample similarity analogous to the effect described by Meyer et al. (2018), albeit a very minor one. To reduce bias that could be introduced by samples
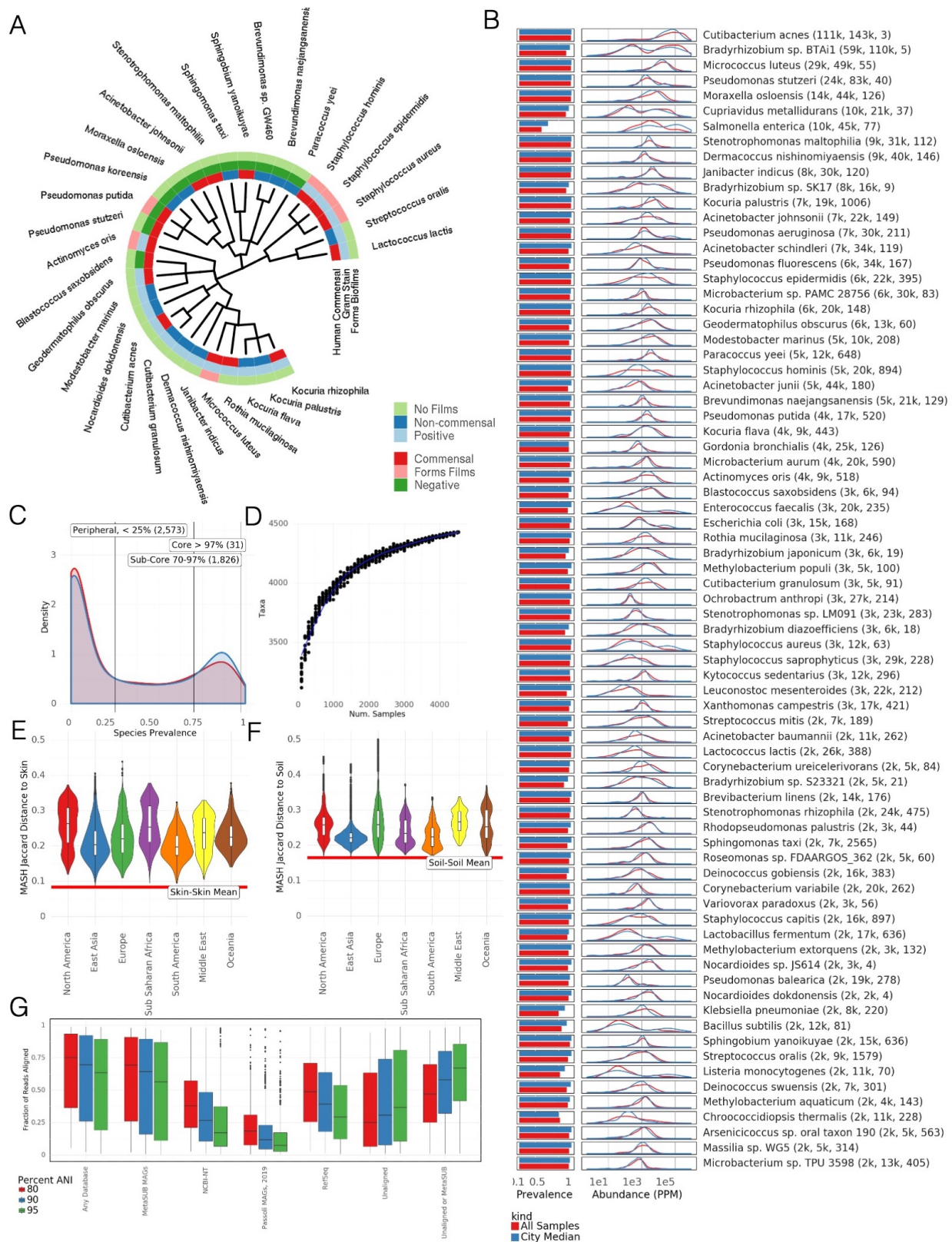
Figure 1: The core microbiome A) Taxonomic tree showing 31 core taxa, colored by phylum and annotated according to gram stain, ability to form biofilms, predicted association with a virus, and whether the bacteria is a human commensal species. B) prevalence and distribution of relative abundances of the 75 most abundant taxa. Mean relative abundance, standard deviation, and kurtosis of the abundance distribution are shown. C) Distribution of species prevalence from all samples and normalized by cities. Vertical lines show defined group cutoffs. D) Rarefaction analysis showing the number of species detected in randomly chosen sets of samples. E) MASH (k-mer based) similarity between MetaSUB samples and HMP skin microbiome samples, by continent. F) MASH (k-mer based) similarity between MetaSUB samples and soil microbiome samples, by continent. G) Fraction of reads aligned (via BLAST) to different databases at different Average Nucleotide Identities.
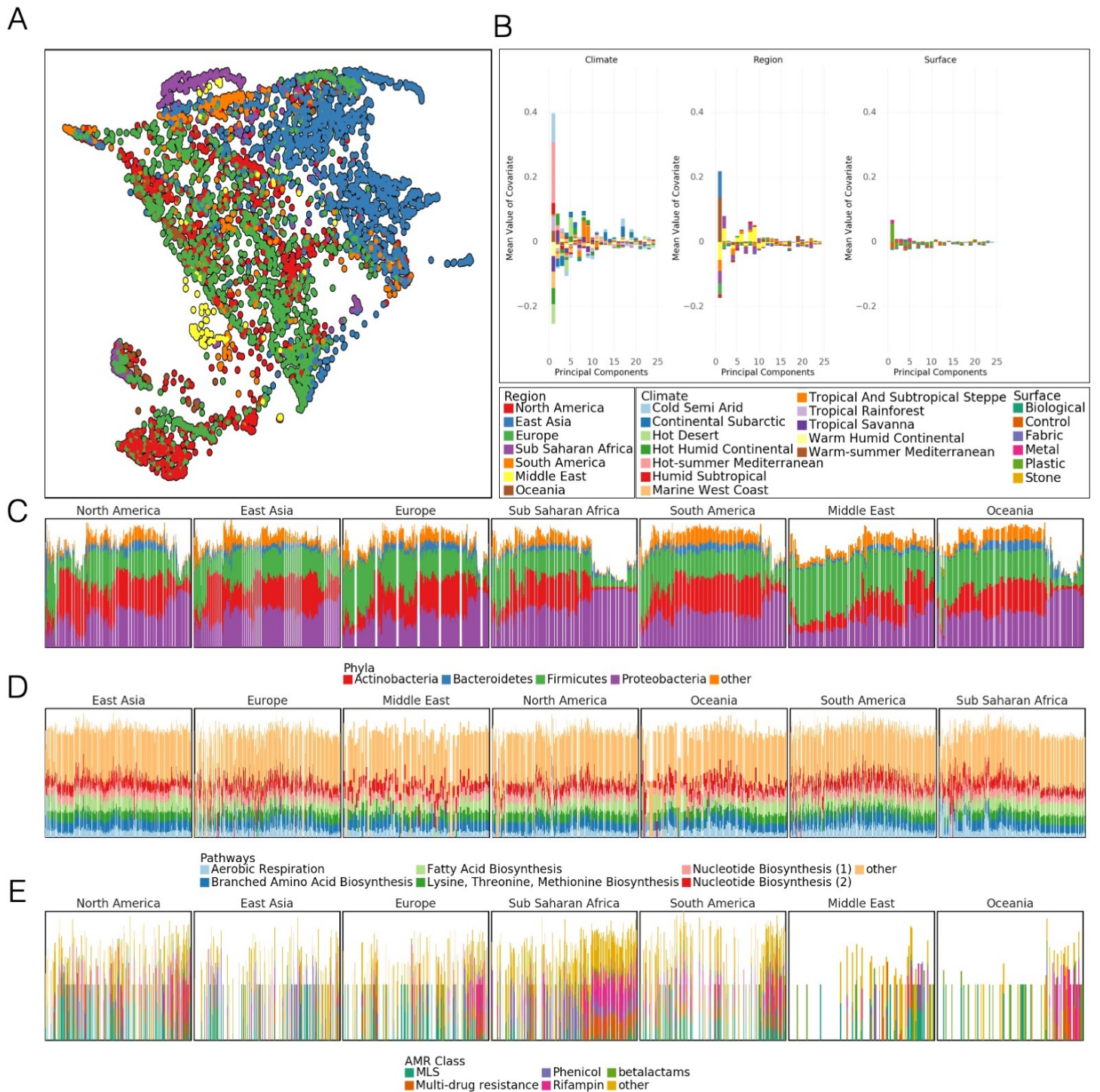
Figure 2: Differences at global scale A) UMAP of taxonomic profiles based on Jaccard distance between samples. Colored by the region of origin for each sample. Axes are arbitrary and without meaningful scale. The color key is shared with panel B. B) Association of the first 25 principal components of sample taxonomy with climate, continent, and surface material. C) Distribution of major phyla, sorted by hierarchical clustering of all samples and grouped by continent. D) Distribution of high-level groups of functional pathways, using the same order as taxa (C). E) Distribution of AMR genes by drug class, using the same order as taxa (C). Note that MLS is macrolide-lincosamide-streptogramin.

taken from precisely the same object we excluded all pairs of samples within 1km of one another.

At a global level, we examined the prevalence and abundance of taxa and their functional profiles between cities and continents. These data showed a fairly stable phyla distribution across samples, but the relative abundance of these taxa is unstable (Figure 2C) with some continental trends. In contrast to taxonomic variation, functional pathways were much more stable across continents, showing relatively little variation in the abundance of high level categories (Figure 2D). This pattern may also be due to the more limited range of pathway classes and their essential role in cellular function, in contrast to the much more wide-ranging taxonomic distributions examined across metagenomes. Classes of antimicrobial resistance were observed to vary by continent as well. Clusters of AMR classes were observed to occur in groups of taxonomically similar samples (Figure 2E).

We quantified the relative variation of taxonomic and functional profiles by comparing the distribution of pairwise distances in taxonomic and functional profiles. Both profiles were equivalently normalized to give the probability of encountering a particular taxon or pathway. Taxonomic profiles have a mean pairwise Jensen-Shannon Divergence (JSD) of 0.61 while pathways have a mean JSD of 0.099. The distributions of distances are significantly different (Welch's t-test, unequal variances, $p < 2e - 16$). This is consistent with observations from the Human Microbiome Project, where metabolic function varied less than taxonomic composition (Consortium et al., 2012; Lloyd-Price et al., 2017) within samples from a given body site.

2.2 Microbial Signatures Reveal Urban Characteristics

To facilitate characterization of novel sequences we created GeoDNA, a high-level web interface (Figure 3A) to search raw sequences against our dataset. Users can submit sequences to be processed against a k-mer graph-based representation of our data. Query sequences are mapped to samples and a set of likely sample hits is returned to the user. This interface will allow researchers to probe the diversity in this dataset and rapidly identify the range of various genetic sequences.

We sought to determine whether a samples taxonomy reflected the environment in which it was collected. To this end we trained a Random Forest Classifier (RFC) to predict a sample's city of origin from its taxonomic profile. We trained an RFC with 100 components on 90% of the samples in our dataset and evaluated its classification accuracy on the remaining 10%. We repeated this procedure with multiple subsamples of our data at various sizes and with 5 replicates per size to achieve a distribution (Fig. 3B). The RFC achieved 88% on held out data which compares favorably to the 7.01% that would be achieved by a randomized classifier. These results from our RFC demonstrate that city specific taxonomic signatures exist and can be predictive.

We expanded our analysis of environmental signatures in taxonomy to the prediction of features in cities not present in our training set. To do this we collated a set of 7 features for each city: population, surface material, elevation, proximity to the coast, population density, region, ave June temperature, and Koppen climate classification. We trained a RFCs to predict each feature based on all samples that were not taken from a given city then used the relevant RFC to predict the feature for samples from the held out city and recorded the classification accuracy (Figure 3D). While not all features and cities were equally predictable (in particular features for a number of British cities were roughly similar and could be predicted effectively) in general the predictions exceeded random chance by a significant margin (Supp. Figure S3A). This suggests that certain features of cities generate microbial signatures that are present globally and distinct from city specific signatures. The successful geographic classification of samples demonstrates distinct city-specific trends in the detected taxa, that may enable future forensic biogeographical capacities.

However, unique, city-specific taxa are not uniformly distributed (Figure 3B). To quantify this, we developed a score to reflect how endemic a given taxon is within a city, which reflects upon the forensic usefulness of a taxon. We define the Endemicity Score (ES) of a taxa as term-frequency inverse document frequency where the document consists of samples from some metadata defined group such as a city or region. This score is designed to simultaneously reflect the chance that a taxon could identify a given city and that that taxon could be found within the given city. A high ES for a taxon in a given city could be evidence of the evolutionary advantage that the taxon has in a particular cities environment. However, neutral evolution of microbes within a particular niche is also possible and the ES alone does not distinguish between these two hypotheses.

Note that while the ES only considers taxa which are found in a city, a forensic classifier could also take advantage of the absence of taxa for a similar metric. ES show a roughly bimodal distribution for regions (Fig. 3C). Each region possesses a number of taxa with ES scores close to 1 and a slightly larger
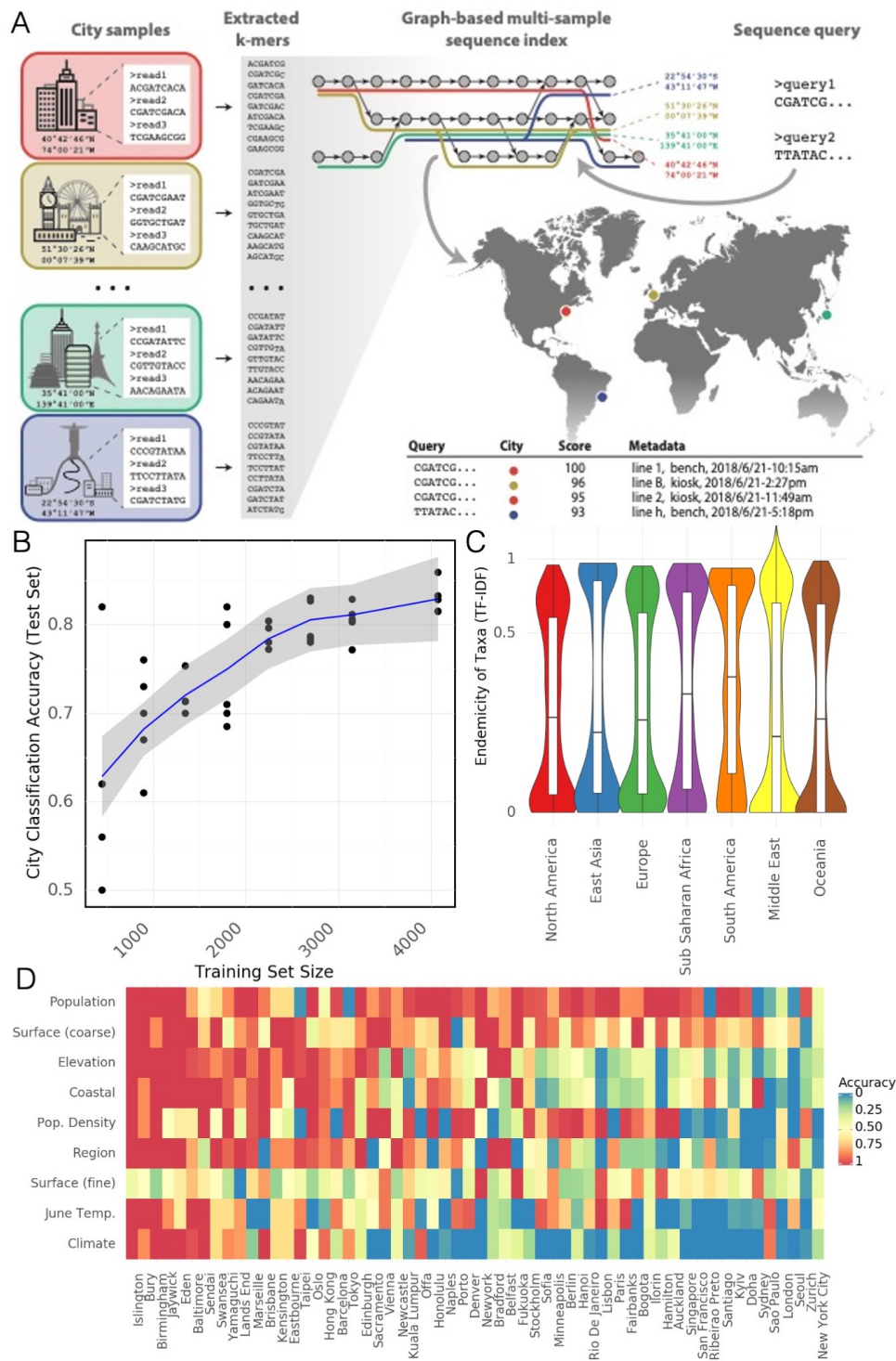
Figure 3: Microbial Signatures A) Schematic of GeoDNA representation generation – Raw sequences of individual samples for all cities are transformed into lists of unique k-mers (left). After filtration, the k-mers are assembled into a graph index database. Each k-mer is then associated with its respective city label and other informative metadata, such as geo-location and sampling information (top middle). Arbitrary input sequences (top right) can then be efficiently queried against the index, returning a ranked list of matching paths in the graph together with metadata and a score indicating the percentage of k-mer identity (bottom right). The geo-information of each sample is used to highlight the locations of samples that contain sequences identical or close to the queried sequence (middle right). B) Classification accuracy of a random forest model for assigning city labels to samples as a function of the size of training set. C) Distribution of Endemicity scores (term frequency inverse document frequency) for taxa in each region. D) Prediction accuracy of a random forest model for a given feature (rows) in samples from a city (columns) that was not present in the training set. Rows and columns sorted by average accuracy. Continuous features (e.g. Population) were discretized.

11

283 number close to 0 (note that ES is not bounded in $[0, 1]$). Some cities, like Offa (Nigeria), host many
284 unique taxa while others, like Zurich (Switzerland), host fewer endemic species (Supp. Figure S3B).
285 Large numbers of endemic species in a city may reflect geographic bias in sampling. However, some
286 cities from well sampled continents (e.g., Lisbon, Hong Kong) also host many endemic species which
287 would suggest that ES may indicate interchangeability and local pockets of microbiome variation for
288 some locations.

2.3   Antimicrobial Resistance Genes Form Distinct Clusters

290 Quantification of antimicrobial diversity and AMRs are key components of global antibiotic stewardship.
291 Yet, predicting antibiotic resistance from genetic sequences alone is challenging, and detection accuracy
292 depends on the class of antibiotics (i.e., some AMR genes are associated to main metabolic pathways
293 while others are uniquely used to metabolize antibiotics). As a first step towards a global survey of
294 antibiotic resistance in urban environments, we mapped reads to known antibiotic resistance genes,
295 using the MegaRES ontology and alignment software. We quantified their relative abundance using
296 reads/kilobase/million mapped reads (RPKM) for 20 classes of antibiotic resistance genes detected in
297 our samples (Figure 4A B). 2,210 samples had some sequence which were identified as belonging to an
298 AMR gene, but no consistent core set of genes was identified. The most common classes of antibiotic
299 resistance genes were for macrolides, lincosamides, streptogamines (MLS), and betalactams, yet the most
300 common class of antibiotic resistance genes, MLS was found in only 56% of the samples where AMR
301 sequence was identified.

302   Despite being relatively common, antibiotic resistance genes were universally in low abundance com-
303 pared to functional genes, with RPKM values for resistance classes typically ranging from $0.1 - 1$ com-
304 pared to values of 10 - 100 for typical housekeeping genes (AMR classes contain many genes so RPKM
305 values may be lower than they would be for individual genes). In spite of the low abundance of the genes
306 themselves, some samples contained sequences from hundreds of distinct AMR genes. Clusters of high
307 AMR diversity were not evenly distributed across cities (Figure 4C). Some cities had more resistance
308 genes identified on average (15-20X) than others (e.g. Bogota) while other cities had bimodal distribu-
309 tions (e.g. San Francisco) where some samples had hundreds of genes while others very few. We note
310 that 99% of the cases where we detected an AMR genes had an average depth of 2.7x, indicating that
311 our global distribution would not dramatically change with altered read depth (Supp. Figure S6E).

312   As with taxa, AMR genes can be used to classify samples to cities - albeit with much less accuracy.
313 A random forest model analogous to the one trained to predict city classification from taxonomic profiles
314 was trained to predict from profiles of antimicrobial resistance genes. This model achieved 37.6% accuracy
315 on held out test data (Supp. Figure S6A). While poor for actual classification this accuracy far exceeds
316 the 7.01% that would be achieved by randomly assigning labels and indicates that there are possibly
317 weak, city specific signatures for antimicrobial resistance genes.

318   Multiple AMR genes can be carried on a single plasmid and ecological competition may cause mul-
319 tiple taxa in the same sample to develop antimicrobial resistance. As a preliminary analysis into these
320 phenomenons we identified clusters of AMR genes that co-occurred in the same samples (Figure 4D).
321 We measured the Jaccard distance between all pairs of AMR genes found in at least 1% of samples and
322 performed agglomerative clustering on the resulting distance matrix. We identified three large clusters of
323 genes and numerous smaller clusters. Of note, these clusters often consist of genes from multiple classes
324 of resistance. At this point we do not posit a specific ecological mechanism for this co-occurrence, but
325 we note that the large clusters contain far more genes than are typically found on plasmids.

326   We performed a rarefaction analysis on the set of all resistance genes in the dataset, which we call
327 the "panresistome" (Figure (Supp. Figure S6B). Similar to the rate of detected species, the panresistome
328 also shows an open slope with an expected rate of discovery of 1 previously unobserved AMR gene per
329 10 samples. Given that AMR gene databases are rapidly expanding and that no AMR genes were found
330 in some samples, it is likely that future analyses will identify many more resistance genes in this data.

331   Additionally, AMR genes show a "neighbourhood" effect within samples that are geographically prox-
332 imal analogous to the effect seen for taxonomic composition (Supp. Figure S6C). Excluding samples
333 where no AMR genes were detected, the Jaccard distance between sets of AMR genes increases with
334 distance for pairs of samples in the same city. As with taxonomic composition. the overall effect is weak
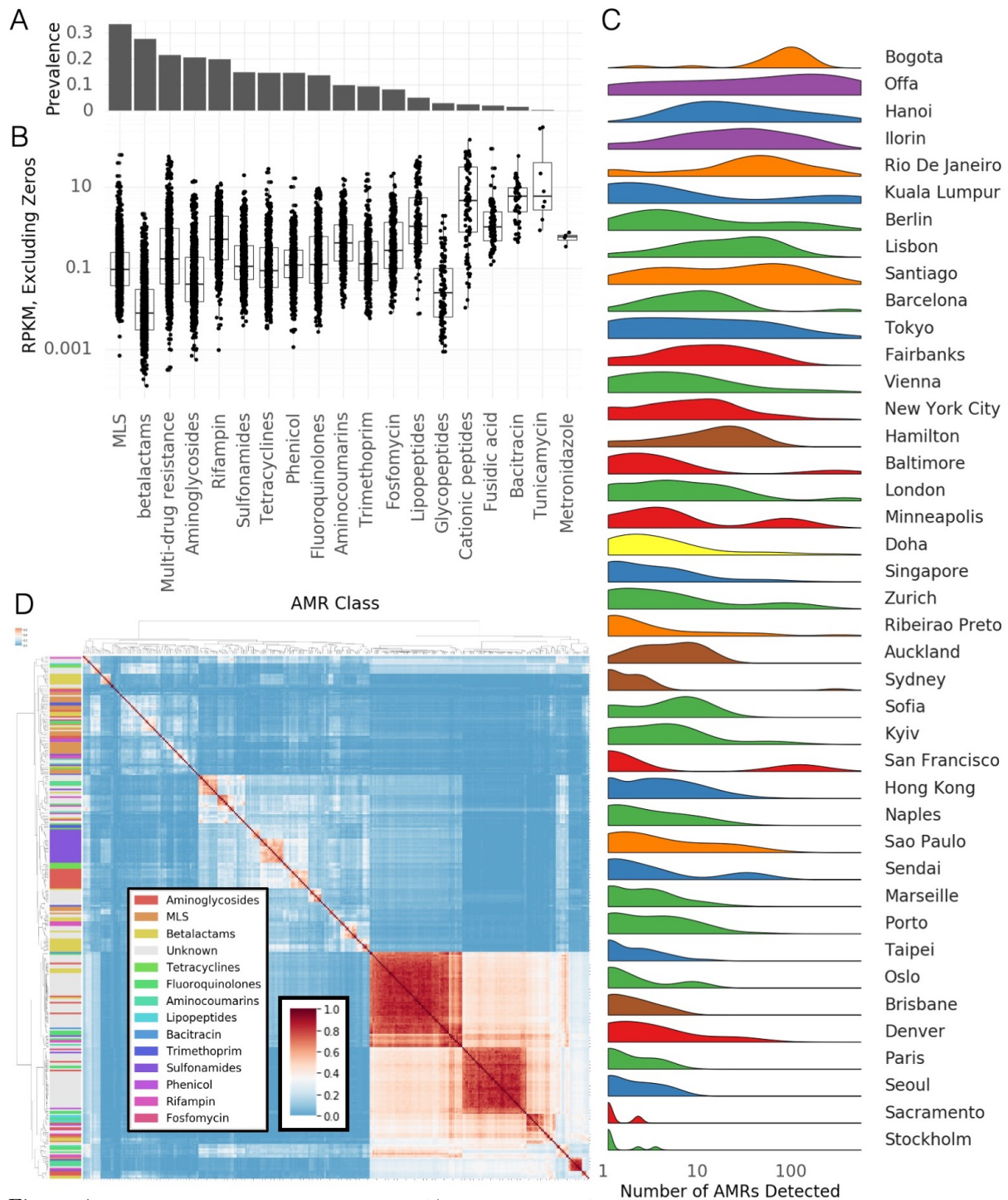335 and noisy, but significant.

Figure 4: Antimicrobial Resistance Genes. A) Prevalence of AMR genes with resistance to particular drug classes. B) Abundance of AMR gene classes when detected, by drug class. C) Number of detected AMR genes by city. D) Co-occurrence of AMR genes in samples (Jaccard index) annotated by drug class.
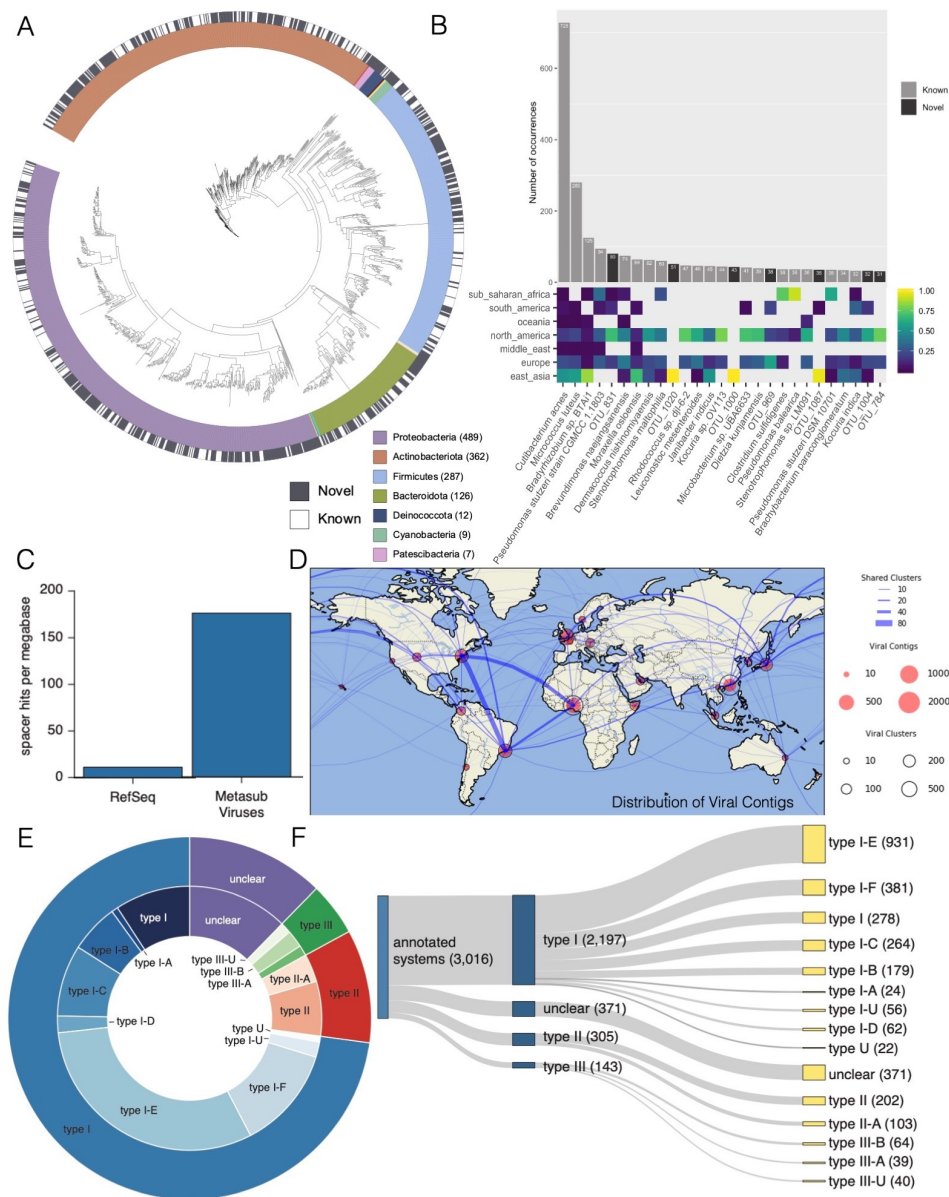
Figure 5: Novel Biology A) Taxonomic tree for Metagenome Assembled Genomes (MAGs) found in the MetaSUB data. Outer black and white ring indicates if the MAG matches a known species, inner ring indicates phyla of the MAG. B) Top: the number of samples where the most prevalent MAGs were found. Bottom: The regional breakdown of samples where the MAG was found. C) Mapping rate of CRISPR Spacers from MetaSUB data to viral genomes in RefSeq and viral genomes found in MetaSUB data. D) Geographic distribution of viral genomes found in MetaSUB data. E & F) Fractional breakdowns of identifiable CRISPR systems found in the MetaSUB data

2.4 Widespread Discovery of Novel Biology

To examine these samples for novel genetic elements, we assembled and identified Metagenome Assembled Genomes (MAGs) for viruses, bacteria, and archaea and analyzed them with several algorithms. This includes thousands of novel CRISPR arrays that reflect the microbial biology of the cities and 1,304 genomes from our data, of which 748 did not match any known reference genome within 95% average nucleotide identity (ANI). 1302 of the genomes were classified as bacteria, and 2 as archaea. Bacterial genomes came predominantly from four phyla: the Proteobacteria, Actinobacteria, Firmicutes, and Bacteroidota. Novel bacteria were evenly spread across phyla (Figure 5A).

Assembled bacterial genomes were often identified in multiple samples. Several of the most prevalent bacterial genomes were novel species (Figure 5B). Some assembled genomes, both novel and not, showed regional specificity while others were globally distributed. The taxonomic composition of identifiable genomes roughly matched the composition of the core urban microbiome (Section 2). The number of identified bacterial MAGs was somewhat based on read depth and the sample count per city (Supp. Figure S7A). The number of bacterial MAGs discovered in a city which did not match a known species was closely correlated to the total number of bacterial MAGs discovered in that city (Supp. Figure S7B). Bacterial MAGs were roughly evenly distributed geographically with the notable exception of Offa, which had dramatically more novel bacterial species than other cities.

We investigated assembled contigs from our samples to identify 16,584 predicted uncultivated viral genomes (UViGs). Taxonomic analysis of predicted UViGS to identify viral species yielded 2,009 clusters containing a total of 6,979 UViGs and 9,605 singleton UViGs for a total of 11,614 predicted viral species. Predicted viral species (Section ??) from samples collected within 10, 100 and 1000 kilometers of one another were agglomerated to examine their planetary distribution at different scales (Figure ??C). At any scale, most viral clusters appear to be weakly cosmopolitan; the majority of their members are found at or near one location, with a few exceptions.

We compared the predicted species to known viral sequences in the JGI IMG/VR system, which contains viral genomes from isolates, a curated set of prophages and 730k viral MAGs from other studies. Of the 11,614 species discovered in our data 94.1% did not match any viral sequence in IMG/VR (Paez-Espino et al., 2019) at the species level for a total of 10,928 novel viruses. We note that this number is surprisingly high but was obtained using a conservative pipeline (99.6% precision) and corresponded well with our identified CRISPR arrays (below). This suggests that urban microbiomes contain significant diversity not observed in other environments.

Next, we attempted to identify possible bacterial and eukaryotic hosts for our predicted viral MAGs. For the 686 species with similar sequences in IMG/VR, we projected known host information onto 2,064 MetaSUB viral MAGs. Additionally, we used CRISPR-Cas spacer matches in the IMG/M system to assign possible hosts to a further 1,915 predicted viral species. Finally, we used a database of 20 million metagenome-derived CRISPR spacers to provide further rough taxonomic assignments. Our predicted viral hosts aligned with our taxonomic profiles, 41% of species in the core microbiome (Section 2) had predicted viral-host interactions. Many of our viral MAGs were found in multiple locations (Figure 5D). Many viruses were found in South America, North America and Africa. Viral MAGs in Japan often corresponded to those in Europe and North America.

We identified 838,532 CRISPR arrays in our data of which 3,245 could be annotated for specific systems. The annotated CRISPR arrays were principally type 1-E and 1-F btu a number of type two and three systems were identified as well (Figure 5E, F). A number of arrays had unclear or ambiguous type assignment. Critically the spacers in our identified CRISPR arrays closely matched our predicted viral MAGs. We aligned spacers to both our viral MAGs and all viral sequences in RefSeq. The total fraction of spacers which could be mapped to our viral MAGS and RefSeq was similar (Supp. Figure S7C) but the mapping rate to our viral MAGs dramatically exceeded the mapping rate to RefSeq (Figure 5C). We present this as additional evidence supporting these novel viral MAGs.

3 Discussion

MetaSUB is a global network of scientists and clinicians developing knowledge of urban microbiomes by studying mass transit systems and hospitals within and between cities. We collected and sequenced 4,728 samples from 60 cities worldwide (Tables 1 and S1), constituting the first large scale metagenomic study of the urban microbiome. We also identified species that are geographically constrained and showed that these can be used to determine a samples city of origin (Section 2.1). Many of these species are associated with commensal microbiomes from human skin and airways, but we observed that urban microbiomes are

15

nevertheless distinct from both human and soil microbiomes. Notably, no species from the *Bacteroidetes*, a prominent group of human commensal organisms (Eckburg et al., 2005; Qin et al., 2010), was identified in the core urban microbiome. We conclude that there is a consistent urban microbiome core (Figure 1, 2), which is supplemented by geographic variation (Figure 2) and microbial signatures based on the specific attributes of a city (Figure 3). Our data also indicates that significant diversity remains to be characterized and that novel taxa may be discovered in the data (Figure 5), that environmental factors affect variation, and that sequences associated with AMR are globally widespread but not necessarily abundant (Figure 4). In addition to these results, we present several ways to access and analyze our data including interactive web based visualizations, search tools over raw sequence data, and high level interfaces to computationally access results.

Unique taxonomic composition and association with covariates specific to the urban environment suggest that urban microbiomes should be treated as ecologically distinct from both surrounding soil microbiomes and human commensal microbiomes. Though these microbiomes undoubtedly interact with the urban environment, they nonetheless represent distinct ecological niches with different genetic profiles. While our metadata covariates were associated with the principal variation in our samples, they do not explain a large proportion of the observed variance. It remains to be determined whether variation is essentially a stochastic process or if a deeper analysis of our covariates proves more fruitful. We have observed that less important principal components (roughly PCs 10-100) are generally less associated with metadata covariates but that PCs 1-3 do not adequately describe the data alone. This is a pattern that was observed in the human microbiome project as well, where minor PCs (such as our Figure 2B) were required to separate samples from closely related body sites.

Much of the urban microbiome likely represents novel diversity as our samples contain a significant proportion of unclassified DNA. This finding is comparable to many other metagenomic and microbiome studies including other work done in subway environments (Afshinnekoo et al., 2015; Hsu et al., 2016), airborne microbiomes (Yooseph et al., 2013), work done by the Earth Microbiome Project (Thompson et al., 2017), and others. As noted in in Section ?? more sensitive methodology only marginally increases the proportion of DNA that can be classified. We consider the DNA which would not be classified by a sensitive technique to be true unclassified DNA and postulate that it may derive from novel genes or species. Given that our samples did not closely resemble human commensal microbiomes or soil samples, it is possible this represents novel urban DNA sequences.

Additionally, our discovery of a large number of novel viral sequences in our data suggests that there are likely to be additional novel taxa from other domains. The fraction of predicted viral sequences which belonged to previously unobserved taxa was particularly high in our study (94.1%) however taxonomic associations of these viruses to observed microbial hosts suggests these results are not spurious. This rate of discovery may prove prescient for novel taxa in other domains, and novel discovery of taxa may help to reduce the large fraction of DNA which cannot currently be classified.

Many of the identified taxa are frequently implicated as infectious agents in a clinical setting including specific *Staphylococcus, Streptococcus, Corynebacterium, Klebsiella* and *Enterobacter* species. There is no clear indication that these species identified in the urban environment are pathogenic, and further in-depth study is necessary to determine the clinical impact of urban microbiomes. This includes microbial culture studies, specifically searching for virulence factors and performing strain-level characterization. Seasonal variation also remains open to study as the majority of the samples collected here were from two global City Sampling Days (June 21, 2016 and 2017). Further studies, some generating novel data, will need to explore whether the core microbiome shifts over the course of the year, with particular interest in the role of the microbiome in flu transmission (Cáliz et al., 2018; Korownyk et al., 2018).

As metagenomics and next-generation sequencing becomes more and more available for clinical (Wilson et al., 2019) and municipal use (Hendriksen et al., 2019), it is essential to contextualize the AMR markers or presence of new species and strains within a global and longitudinal context. The most common AMR genes were found for two classes of antibiotic: MLS and beta-lactams. MLS represents macrolides, lincosamides and streptogramins, which are three groups of antibiotics with a mechanism of action of inhibiting bacterial protein synthesis. Macrolides, with strong Gram-positive and limited Gram-negative coverage, are prevalently used to treat upper respiratory, skin, soft tissue and sexually transmitted infections amongst others. Beta-lactam antibiotics are a major class of antibiotics including penicillins, cephalosporins, monobactams, carbapenems and carbacephems that are all used to treat a wide array of infections. Antimicrobial resistance has surged due to the selection pressure of widespread use of antibiotics and is now a global health issue plaguing communities and hospitals worldwide. Antimicrobial resistance genes are thought to spread from a variety of sources including hospitals, agriculture and water (Bougnom and Piddock, 2017; Klein et al., 2018). The antimicrobial classes particularly

impacted by resistance include beta-lactamases, gylcopeptides and fluoroquinolones (Rice, 2012), all of which we found antimicrobial resistance genes for across our samples. We found that there was uneven distribution of AMR genes across cities. This could be the result of some of combination of different levels of antibiotic use, differences in the urban geography between cities (population density, presence of untreated wastewater etc), or reflect the background microbiome in different places in the world. Techniques to estimate antibiotic resistance from sequencing data remain an area of intense research as certain classes of AMR gene (ie. fluoroquinolones) are sensitive to small mutations and it is possible that our methods may not fully reflect true resistance. Further research is needed to fully explore AMR genes in the urban environment, including culture studies which directly measure the phenotype of resistance.

One of the challenges in the field of metagenomics of the built environment is dealing with low biomass samples. Not only does it introduce the challenge of contamination (Kim et al., 2017) which requires standardized sample preparation and the use of positive and negative controls, but there is also the challenge in biases and data interpretation (McLaren et al., 2019). Metagenomic studies rely on bioinformatics analyses that predict relative abundances of taxa, functional genes, antimicrobial resistance genes, etc. When you have low biomass samples, these relative abundances may appear high when their absolute abundance is in fact low when considering where the samples came from. However, this is an inherent component of metagenomics that studies and examines microbiomes and communities based on the metrics and measurements of relative abundances. There are important considerations to be made from sample collection to bioinformatics analysis to ensure limited biases are introduced to a study (McLaren et al., 2019). Moreover, the overall findings must be interpreted with the proper context and scope of the experiment and samples collected.

In summary, this study presents a first molecular atlas of urban and mass-transit metagenomics from across the world. By facilitating large scale epidemiological comparisons, it is a first critical step towards quantifying the clinical role of environmental microbiomes and provides requisite data for tracking changes in ecology or virulence. Moreover, in order to study the transmission of AMRs on a global scales this dataset represents only focuses on some of the sources and vectors of the built environment. Indeed, datasets from rural and suburban areas with livestock and farms, sewage from cities (Fresia et al., 2019; Joseph et al., 2019), and other notable sources of AMRs need to be integrated together to truly capture AMR mechanisms at the global scale (Singer et al., 2016; Thanner et al., 2016). Previous studies have already demonstrated a role for precision clinical metagenomics in managing infectious disease and global health (Afshinnekoo et al., 2017; Gardy and Loman, 2018; Ladner et al., 2019). As demonstrated by the coronavirus disease 2019 (COVID-19) pandemic, as an atlas this data has the potential to aid physicians, public health officers, government officials, and others in tracing, diagnosis, clinical decision making, and policy within their communities.

3.1 Open Science

The MetaSUB dataset is built and organized for full accessibility to other researchers. This is consistent with the concept of Open Science. Specifically, we built our study with the FAIR principles in mind: Findable, Accessible, Interoperable and Reusable.

To make our study reproducible, we released an open source version-controlled pipeline called the MetaSUB Core Analysis Pipeline (CAP). The CAP is intended to improve the reproducibility of our findings by making it easy to apply a number of analyses consistently to a large dataset. This pipeline includes all steps from extracting data from raw sequence data to producing refined results like taxonomic and functional profiles. The CAP itself is principally composed of other open peer-reviewed scientific tools, with only a few custom scripts for mundane tasks. Every tool in the CAP is open source with a permissive license. The CAP is available as a docker container for easier installation in some instances and all databases used in the CAP are available for public download. The CAP is versioned and includes all necessary databases allowing researchers to replicate results. The CAP is not designed to produce highly novel results but is meant to be a good practice agglomeration of open source tools.

However, the output of the CAP still consists of a number of different output formats with multiple files for each sample. To make our results more reproducible and accessible, we have developed a program to condense the outputs of the Core Analysis Pipeline into a condensed data-packet. This data packet contains results as a series of Tidy-style data tables with descriptions. The advantage of this set-up is that result tables for an entire dataset can be parsed with a single command in most high level analysis languages like Python and R. This package also contains Python utilities for parsing and analyzing data packets which streamlines most of the boilerplate tasks of data analysis. All development of the CAP and data packet builder (Capalyzer) package is open source and permissively licensed.

17

In addition to general purpose data analysis tools essentially all analysis in this paper is available as a series of Jupyter notebooks. Our hope is that these notebooks allow researchers to reproduce our results, build upon our results in different contexts, and better understand precisely how we arrived at our conclusions. By providing the exact source used to generate our analyses and figures, we also hope to be able to quickly incorporate new data or correct any mistakes that might be identified.

For less technical purposes, we also provide web-based interactive visualizations of our dataset (typically broken into city-specific groups). These visualizations are intended to provide a quick reference for major results as well as an exploratory platform for generating novel hypotheses and serendipitous discovery. The web platform used, MetaGenScope, is open source, permissively licensed, and can be run on a moderately powerful machine (though its output relies on results from the MetaSUB CAP).

Our hope is that by making our dataset open and easily accessible to other researchers the scientific community can more rapidly generate and test hypotheses. One of the core goals of the MetaSUB consortium is to build a dataset that benefits public health. As the project develops we want to make our data easy to use and access for clinicians and public health officials who may not have computational or microbiological expertise. We intend to continue to build tooling that supports these goals.

3.2 CAMDA

Since 2017 MetaSUB has partnered with the Critical Assessment of Massive Data Analysis (CAMDA) `camda.info`, a full conference track at the Intelligent Systems for Molecular Biology (ISMB) Conference. At this venue a subset of the MetaSUB data were released to the CAMDA community in the form of annual challenge addressing the issue of geographically locating samples: 'The MetaSUB Inter-City Challenge' in 2017 and 'The MetaSUB Forensics Challenge' in 2018 and 2019. In the latter challenge the MetaSUB data has been complemented by data from EMP (Thompson et al., 2017) and other studies (Delgado-Baquerizo et al., 2018; Hsu et al., 2016). This Open Science approach of CAMDA has generated multiple interesting results and concepts relating to urban microbiomics, resulting in several publications `biologydirect.biomedcentral.com/articles/collections/camdaproc` as well as perspective manuscript about moving towards metagenomics in the intelligence (Mason-Buck et al., 2020). The partnership is continued in 2020 with 'The Metagenomic Geolocation Challenge' where the MetaSUB data has been complemented by the climate/weather data in order to construct multi-source microbiome fingerprints and predict the originating ecological niche of the sample.

4 Data Access

Raw sequencing reads from this study contain significant amounts of human DNA and cannot yet be made public. However, reads with the majority of human DNA filtered and low quality bases removed are available for download from Wasabi (an Amazon S3 clone) with individual URLs located here: `https://github.com/MetaSUB/metasub_utils`. In addition to raw reads higher level results (e.g. taxonomic profiles, functional pathways, etc.) are available in the MetaSUB data packet also available for download from Wasabi. For instructional purposes we also provide a simplified data packet for teaching which includes balanced numbers of samples from each city and completely filled metadata tables.

Interactive data visualizations are available on `https://pangea.gimmebio.com/contrib/metasub`, `https://www.metagenscope.com` and GeoDNA, an interface to search query DNA sequences against MetaSUB samples, is available at (`dnaloc.ethz.ch/`). MetaSUB data may be downloaded from `https://pangea.gimmebio.com`. MetaSUB metadata is available in the data-packet, on Pangea, or may be downloaded from `https://github.com/MetaSUB/MetaSUB-metadata`. Programs used for analysis of data may be found at `https://github.com/MetaSUB/MetaSUB_CAP` and `https://github.com/dcdanko/capalyzer`. Jupyter notebooks used to generate the figures and statistics in this study can be found at `https://www.github.com/MetaSUB/main_paper_figures`. Additional tools and resources are described here `https://github.com/MetaSUB/bioinformatics_management`.

5 Acknowledgement

19

don, Natalia Marciniak, Vincent Matthys, Arif Asyraf Md Supie, Irène Mauricette Mendy, Roy Meoded, Mathilde Mignotte, Ryusei Miura, Kunihiko Miyake, Maria D Moccia, Mauricio Moldes, Jennifer Molinet, Orgil-Erdene Molomjamts, Mario Moreno, Maureen Muscat, Cristina Muñoz, Francesca Nadalin, Dorottya Nagy-Szakal, Ashanti Narce, Hiba Naveed, Thomas Neff, Wan Chiew Ng, Elsy Ngwa, Agier Nicolas, Pierre Nicolas, Abdollahi Nika, Javier Quilez Oliete, Nils Ordioni, Mitsuki Ota, Francesco Oteri, Yuya Oto, Coral Pardo-Este, Young-Ja Park, Jananan Pathmanathan, Manuel Perez, Melissa P Pizzi, María Gabriela Portilla, Leonardo Posada, Catherine E. Pugh, Kyrylo Pyrshev, Sreya Ray Chaudhuri, Hubert Rehrauer, Renee Richer, Paula Rodríguez, Paul Roldán, Sandra Roth, Maria Ruiz, Mariia Rybak, Ikuto Saito, Yoshitaka Saito, Khaliun Sanchir, Kai Sasaki, Kaisei Sato, Masaki Sato, Ryo Sato, Seisuke Sato, Yuma Sato, Oli Schacher, Christian Schori, Felipe Sepulveda, Juan C Severyn, Sarah Shalaby, Hikaru Shirahata, Jordana M Silva, Gwenola Simon, Kasia Sluzek, Rebecca Smith, Yuya Sonohara, Nicolas Sprinsky, Stefan G Stark, Chisato Suzuki, Sora Takagi, Kou Takahashi, Naoya Takahashi, Tomoki Takeda, Soma Tanaka, Andrea Tassinari, Eunice Thambiraja, Antonin Thiébaut, Takumi Togashi, Yuto Togashi, Anna Tomaselli, Itsuki Tomita, Nora C Toussaint, Takafumi Tsurumaki, Yelyzaveta Tymoshenko, Mariko Usui, Sophie Vacant, Laura E Vann, Jhovana L Velasco Flores, Fabienne Velter, Riccardo Vicedomini, Tomoro Warashina, Ayuki Watanabe, Tina Wunderlin, Olena Yemets, Tetiana Yeskova, Shusei Yoshikawa, Stas Zubenko.

6 Methods

6.1 Metadata Collection and Cleaning

Metadata from individual cities was collected from a standardized form and set of fields. The principle fields collected were the location of sampling, the material being sampled, the type of object being sampled, the elevation above or below ground, and the station or line where the sample was collected. However, several cities were unable to use the provided apps for various reasons and submitted their metadata as separate spreadsheets. Additionally, certain metadata features, such as those related to sequencing and quality control, were added after initial sample collection.

To collate various metadata sources, we built a publicly available program which assembled a large master spreadsheet with consistent sample UUIDs. After assembling the originally collected data attributes we added normalized attributes based on the original metadata to account for surface material, control status, and features of individual cities. A full description of ontologies used is provided as part of the collating program.

6.2 Sample Collection and Preparation

To obtain a comprehensive picture of microbial communities within a sample it is essential to choose a sampling method which absorbs and preserves biological materials during sampling, transport and storage until DNA extraction. The effectiveness of a swab may be influenced by a number of factors, including most importantly the material of the swab tip affecting the rate at which bacteria are absorbed during the sampling process. Furthermore, the design of the transport tube and DNA preserving liquids affect the integrity of the material during transport. Finally, the amount of background contamination identified for different products should be taken into account.

6.3 Swab Comparisons

In this study we have benchmarked various types of swabs and DNA preservative tubes, including Copan Liquid Amies Elution Swab (ESwab, Copan Diagnostics, Cat.:480C) referred to as 'copan swab' and Isohelix Swabs (Mini-Swab, Isohelix Cat.:MS-02) referred to as 'isohelix swabs', which were combined with 2D Thermo Scientific™ Matrix™ storage tubes (3741-WP1D-BR/Matrix 1.0 ml/EA) referred to as 'matrix tube', which have been prefilled with the preservative liquid Zymo Shield Zymo DNA/RNA Shield™ (R1100-250) referred to as 'Zymo shield'. Copan swabs contain a transport medium for sample preservation. After samples were collected with Copan swabs they were transported at room temperature and stored at -80C until DNA extraction. Isohelix swabs have been stored in matrix tubes containing $400\mu l$ Zymo shield preservative. Matrix tubes were also transported at room temperature and stored at -80C until DNA extraction. We tested the absorption strength of Copan and Isohelix swabs for various biological and surface materials encountered when sampling subway stations. For a designated sampling area of an office desk, a Isohelix swabs were moistened by submerging the swab for a few seconds in

20

preservative media. The desk area was then swabbed for 3 min. Results were compared to sampling with copan swabs, which were similarly used to swab the area for 3 min.

6.4 Sampling Protocol

A standard operating procedure (SOP) was developed for the sample collection to be followed by all members of the MetaSUB consortium participating in CSD. This protocol was adapted from work by Afshinnekoo et al. (2015). The goal was to standardize as much of the sampling procedure and ensure high quality control across the various cities and sampling teams. Thus it was recommended that teams collect samples from surfaces that are present throughout most subway and transit stations and systems around the world. These included ticket kiosks, turnstiles, railings, seats or benches, etc. Some cities had to adapt the SOP according to their city especially if they did not have a subway system and were collecting samples from other transit systems. However, the vast majority of sampling teams collected samples from these surfaces. Moreover, a significant amount of metadata was recorded throughout sample collections to ensure as much information regarding the samples was captured. All cities also developed sampling plans for their collections and submitted them for review to have swabs sent to them, this was to ensure consistency across the various sites.

All principal investigators and MetaSUB city leaders were trained in the sampling instructions and this training was further disseminated to the respective sampling teams to ensure consistent and quality control sampling. Swabbers were instructed to put on gloves before each sample collection. The swab was dipped in the preservative medium to be pre-moistened before collection and sampling was timed to 3 minutes to ensure highest yield. Other key points in training included ensure highest surface area was used for collection (i.e. swab entire bench, not just one area) and avoiding any areas that appeared wet, contaminated, and not consistent with a subway surface. Any other observations or important notes during sample collection that could add more context to data analysis and interpretation were recorded on the notes section of the metadata collection apps.

There were some changes between CSD2016 and CSD2017 sampling protocols that are important to note. First, the swab was changed from Copan (CSD16) to Isohelix (CSD17) this was after the results of benchmarking work comparing the swabs and ensuring we are optimizing the amount of DNA collected from swabbing these surfaces. Moreover a barcoding system was set in place in CSD17 to improve metadata collection and sample tracking compared to the CSD ID system utilized in CSD16 colection (CSD-City Code-00XYZ).

6.4.1 In-Lab controls CSD2016

As positive lab control we used $30\mu l$ ZymoBiOMICS Microbial Community standard (Catalog #D6300), which we added to an empty sterile urine cap, followed by swabbing with Copan Liquid Amies Elution Swab (ESwab,Copan Diagnostics, Cat.:480C) for 1.5min / 3 minutes. As negative (background) lab control we used $50\mu l$ of the final resuspension buffer (MoBio PowerSoil®DNA Isolation Kit, Cat.:12888-100), which we have added to an empty sterile urine cup followed by swabbing for 3 min (Fig.S1). Furthermore, the working space has been swabbed for 1.5 min / 3 min before and after treatment with 10% bleach (Fig. S2) to test for background contamination rates. To identify the background levels of biological material in the air at sample areas, a Copan swab has been held for 1.5 min - 3 min in the air. To estimate the source and amount of contamination in commercial swab and tube products used for MetaSUB, we tested all consumables in triplicates in the sterilized hood (UV light and 10% bleach wiped with ethanol).

6.4.2 DNA Extraction from Isohelix swabs using ZymoBiomics 96 MagBead

The Isohelix swab head and the entire $400\ \mu l$ of DNA/RNA Shield-solubilized sample were transferred into ZR BashingBead Lysis Tubes (0.1 & 0.5 mm) (Cat# S6012-50) to which an additional $600\ \mu l$ of DNA/RNA Shield was added. Mechanical lysis using bead beating was performed on a maximum of 18 samples simultaneously using the Scientific Industries Vortex-Genie 2 with Horizontal-(24) Microtube Adapter (Cat # SI-0236 and SI-H524) at maximum power for 40 minutes. The resulting lysate ($400\ \mu l$) was transferred to Nunc^{TM} 96-Well Polypropylene DeepWell Storage Plates (Cat # 278743), followed by DNA extraction using the ZymoBIOMICS 96 MagBead Kit (Lysis Tubes) (Catalog # D4308) on the Hamilton Star according to manufacturer instructions.

6.4.3 DNA extraction from Copan swabs using MoBio PowerSoil®DNA

Droplets in the Copan Liquid Amies Elution Swab tube (ESwab, Copan Diagnostics, Cat.:480C (http://goo.gl/8a9uCP)) were spun down at 300rpm/1min. Next, the swab pad was transferred to a MoBio PowerSoil®DNA vial containing beads using sterile scissors, which we sterilized by flaming with 100% ethanol. The remaining 400-500μl Copan Amines liquid has been transferred into an Eppendorf tube and centrifuged at full speed to collect bacteria and debris in a pellet. The pellet was finally transferred to the same MoBio PowerSoil®DNA vial also containing the corresponding swab pad. MoBio PowerSoil®DNA Isolation Kit, Cat.:12888-100 (https://goo.gl/65rcn2) was used according to manufacturer's instructions except for the following modifications:

Both swab and pellet have been re-suspended with 135μl C1 buffer (MoBio PowerSoil®DNA). Sample homogenization was performed using either TissueLyser II (Qiagen) with 2 cycles of 3 minutes at 30Hz (https://goo.gl/hBg8Lb), or using the Vortex-Genie 2 (Vortex Catalog #13000-V1-24) adaptor and vortex at maximum speed for 10 minutes. The sequencing centers in Stockholm and Shanghai used different procedures for homogenization. Stockholm used a method based on MPI FASTPREP, while Shanghai added 0.6 grams of 100-micron zirconium-silica beads to 2ml tubes containing the swab pad and the media, followed by bead beating for 1 min. The eluted samples have been additionally purified and concentrated by Beckmann Coulter Agencourt AMPure XP (Cat.:A63881) purification (1.8X) and eluted into 12μl - 50μl elution buffer. Subsequently, DNA was quantified using Qubit® dsDNA HS Assay (Catalog #Q32854).

6.4.4 DNA extraction using Promega Maxwell

We added 300μl Promega Maxwell Lysis buffer and 30μl Promega Maxwell Proteinase K to Copan swab heads or Isohelix swab heads and transferred the swabs back to their respective collection tube. For lysis the sample tubes containing the swabs and the lysis mixture were incubated in a water bath at 54C for 30min. Following lysis, Copan swab heads were cut off their stem using sterile scissors and transferred into a filter tube (Promega V4745). The filter containing the swab was placed into a 2ml Eppendorf tube and spun down at full speed for 2min. This step is necessary since the Copan swab material consists of a foam, which harbors the main liquid containing the extracted DNA. Next, the eluate has been combined with the corresponding sample tube media and added to the first well of the cartridge (Maxwell® RSC Buccal Swab kit AS1640). Cartridges were processed using the Maxwell® RSC Instrument (AS4500) following the manufacturer's default instructions. Extracted DNA was eluted in 50μl Promega Elution Buffer and stored at -80C.

The matrix tubes containing the Isohelix swabs and the lysis buffer have been vortexed at full speed for one minute. The Isohelix swab head material is a non-porous material, which allows for easy collection of the lysate. We transferred the lysate to the first cartridge of the Maxwell® RSC Blood DNA KitAS1400 using syringes (BD 3 mL Syringes with 18G x 1.5" Luer Lok Tip Blunt Fill Needles) and ran the Promega Maxwell using the Blood program according to manufacturer's instructions. Samples were subsequently eluted in 50μl elution buffer and stored at -80C.

Pilot samples collected in Barcelona and Stockholm were prepared for NGS analysis using QIAGEN QIAseq FX DNA Library Kit. Samples from CSD2017 and CSD2018 have been prepped at HudsonAlpha Genome Center described by Afshinnekoo et al. (2015).

6.5 Quality Control

6.5.1 Sequencing quality

We measured sequencing quality based on 5 metrics: number of reads obtained from a sample, GC content, Shannon's entropy of k-mers, post PCR Qubit score, and recorded DNA concentration before PCR. The number of reads in each sample was counted both before and after quality control, we used the number of reads after quality control for our results though the difference was slight. GC content was estimated from 100,000 reads in each sample after low quality DNA and human reads had been removed. Shannon's entropy of k-mers was estimated from 10,000 reads taken from each samples. PCR Qubit score and DNA concentration are described in the wet lab methods.

6.5.2 Sequencing quality scores show expected trends

We measured sequencing quality based on 5 metrics: number of reads obtained from a sample, GC content (taken after removing human reads), Shannon's entropy of k-mers (from 10,000 reads sampled

22

768 from each sample), post PCR Qubit score, and recorded DNA concentration before PCR. We observed
769 good separation of negative and positive controls based on both PCR Qubit and k-mer entropy (Supp.
770 Figure S14). Distributions of DNA concentration and the number of reads were as expected. GC content
771 was broadly distributed for negative controls while positive controls were tightly clustered, expected since
772 positive controls have a consistent taxonomic profile. Comparing the number of reads before and after
773 quality control did not reveal any major outliers.

6.5.3 Batch effect appears minimal

775 A major concern for this low-biomass studies and large-scale studies are batch effects. The median flowcell
776 used in our study contained samples from 3 cities and 2 continents. However, two flowcells covered 18
777 cities from 5 or 6 continents respectively. When samples from these flowcells were plotted using UMAP
778 (see Section 2.1 for details) the major global trends we described were recapitulated (Supp. Figure
779 S15A). Further, when plotting samples by PCR qubit and k-mer entropy (the two metrics that most
780 reliably separated our positive and negative controls) and overlaying the flowcell used to sequence each
781 sample only one outlier flowcell was identified and this flowcell was used to sequence a large number of
782 background control samples (Supp. Figure S15B). Plots of the number of reads against city of origin and
783 surface material (Supp. Figure S15C & D) showed a stable distribution of reads across cities. Analogous
784 plots of PCR Qubit scores were less stable than the number of reads but showed a clear drop for control
785 samples (Supp. Figure S15E & F). These results led us to conclude that batch effects are likely to be
786 minimal.

6.5.4 Strain Contamination

788 We used BLASTn to align nucelotide assemblies from case samples to control samples. We used a
789 threshold of 8,000 base pairs and 99.99% identity as a minimum to consider two sequences homologous.
790 This threshold was chosen to be sensitive without solely capturing conserved regions. We identified all
791 connected groups of homologous sequences and found approximate taxonomic identifications by aligning
792 contigs to NCBI-NT using BLASTn searching for 90% nucleotide identity over half the length of the
793 longest contig in each group.

6.5.5 Strain contamination is rare or absent

795 Despite good separation of positive and negative controls (see Section 6.5.1) we identified several species
796 in our negative controls which were also identified as prominent taxa in the data-set as a whole (See
797 Section 2). Our dilemma was that a microbial species that is common in the urban environment might
798 also reasonably be expected to be common in the lab environment. In general, negative controls had
799 lower k-mer complexity, fewer reads, and lower post PCR Qubit scores than case samples and no major
800 flowcell specific species were observed. Similarly, positive control samples were not heavily contami-
801 nated. These results suggest samples are high quality but do not systematically exclude the possibility
802 of contamination.
803 Previous studies have reported that microbial species whose relative abundance is negatively cor-
804 related with DNA concentration may be contaminants. We observed a number of species that were
805 negatively correlated with DNA concentration (Supp. Figure S13A) but this distribution followed the
806 same shape (but had a greater magnitude) as a null distribution of uniformly randomly generated rela-
807 tive abundances (Supp. Figure S13B) leading us to conclude that negative correlation may simply be a
808 statistical artifact. We also plotted correlation with DNA concentration against each species mean rela-
809 tive abundance across the entire data-set (Supp. Figure S13C). Species that were negatively correlated
810 with DNA concentration were clearly more abundant than uncorrelated species, this suggests that there
811 may be a jackpot effect for prominent species in samples with lower concentrations of DNA but is not
812 generally consistent with contamination.
813 We analyzed the total complexity of case samples in comparison to control samples. Case samples
814 had a significantly higher taxonomic diversity (Supp. Figure S12A) than any type of negative control
815 sample. We also compared the confidence of taxonomic assignments to control assignments for prominent
816 taxa (Supp. Figure S12B) using the number of unique marker k-mers to compare assignments. We found
817 that case samples had more and higher quality assignments than could be found in controls. One species,
818 *Bradyrhizobium sp. BTAi1*, was not clearly better in case samples than controls but in this case we were
819 able to assemble genomes for this species in several unique samples so we feel it is ambiguous.

23

Finally, we compared assemblies from negative controls to assemblies from our case samples searching for regions of high similarity that could be from the same microbial strain. We reasoned that uncontaminated samples may contain the same species as negative controls but were less likely to contain identical strains. Only 137 case samples were observed to have any sequence with high similarity to an assembled sequence from a negative control (8,000 base pairs minimum of 99.99% identity). The identified sequences were principally from *Bradyrhizobium* and *Cutibacterium*. Since these genera are core taxa (See Section 2) observed in nearly every sample but high similarity was only identified in a few samples, we elected not to remove species from these genera from case samples.

6.5.6 K-Mer Based Analyses

We generated 31-mer profiles for raw reads using Jellyfish. All k-mers that occurred at least twice in a given sample were retained. We also generated MASH sketches from the non-human reads of each sample with 10 million unique minimizers per sketch.

We calculated the Shannon's entropy of k-mers by sampling 31-mers from a uniform 10,000 reads per sample. Shannon's entropy of taxonomic profiles was calculated using the CAPalyzer package (Section 4).

6.5.7 K-Mer based metrics correlate with taxonomic metrics

We found clear correlations between three pairwise distance metrics (Supp. Figure S10A, B, C): k-mer based Jaccard distance (MASH), taxonomic Jaccard distance, and taxonomic Jensen-Shannon divergence. This suggests that taxonomic variation reflects meaningful variation in the underlying sequence in a sample.

We also compared alpha diversity metrics (Supp. Figure S10D): Shannon entropy of k-mers, and Shannon entropy of taxonomic profiles. As with pairwise distances these metrics were correlated though noise was present. This noise may reflect sub-species taxonomic variation in our samples.

6.5.8 Sequence Preprocessing

Sequence data were processed with AdapterRemoval (v2.17, Schubert et al. (2016)) to remove low quality reads and reads with ambiguous bases. Subsequently reads were aligned to the human genome (hg38, including alternate contigs) using Bowtie2 (v2.3.0, fast preset, Langmead and Steven L Salzberg (2013)). Read pairs where both ends mapped to the human genome were separated from read pairs where neither mate mapped. Read pairs where only one mate mapped were discarded. Hereafter, we refer to the read sets as human reads and non-human reads.

6.5.9 Unmapped DNA is not similar to any known sequence

A large proportion of the reads in our samples were not mapped to any references sequences. There are three major reasons why a fragment of DNA would not be classified in our analysis 1) The DNA originated from a non-human and non-microbial species which would not be present in the databases we used for classification 2) Our classifier (KrakenUniq) failed to classify a DNA fragment that was in the database due to slight mismatch 3) The DNA fragment is novel and not represented in any existing database. Explanations (1) and (2) are essentially drawbacks of the database and computational model used, and we can quantify them by mapping reads using a more sensitive aligner to a larger database, such as BLASTn (Altschul et al., 1990), or ensemble methods for analysis (McIntyre et al., 2017). To estimate the proportion of reads which could be assigned, we took 10k read subsets from each sample and mapped these to a set of large database using BLASTn (see 2 for details). This resulted in 34.6% reads which could not be mapped to any external database compared to 41.3% of reads mapped using our approach with KrakenUniq. We note that our approach to estimate the fraction of reads that could be classified using BLASTn does not account for hits to low quality taxa which would ultimately be discarded in our pipeline, and so represents a worst-case comparison. Explanation (3) is altogether more interesting and we refer to this DNA as true unclassified DNA. In this analysis we do not seek to quantify the origins of true unclassified DNA except to postulate that it may derive from novel species as have been identified in other similar studies.

6.6 Computational Analysis

6.6.1 Taxonomic Analysis

We generated taxonomic profiles by processing non-human reads with KrakenUniq (v0.3.2 Breitwieser et al. (2018)) using a database based on all draft and reference genomes in NCBI/RefSeq Microbial (bacteria/archaea, fungi and virus) ca. March 2017. KrakenUniq was selected because its high performance, as it has been demonstrated to be comparable or having higher sensitivity than the best tools identified in a recent benchmarking study (McIntyre et al. (2017)) on the same comparative dataset. In addition, KrakenUniq allows for tunable specificity and identifies k-mers that are unique to particular taxa in a database. Reads are broken into k-mers and searched against this database. Finally, the taxonomic makeup of a sample is given by identifying the taxa with the greatest leaf to ancestor weight.

KrakenUniq reports the number of unique marker k-mers assigned to each taxon, as well as the total number of reads, the fraction of available marker k-mers found, and the mean copy number of those k-mers. We found that requiring more k-mers to identify a species resulted in a roughly linear decrease in the total number of species identified without a plateau or any other clear point to set a threshold (Supp. Figure S9A). In an ongoing but unpublished clinical study we have used a threshold of 512 marker k-mers to accurately recapitulate the results of culturing while identifying few species which were not cultured. Since false positives are less problematic in the current study than in a clinical study and because we could use our large number of samples as a partially orthogonal confirmation we chose less strict thresholds for KrakenUniq in this study.

At a minimum we required three reads assigned to a taxa with 64 unique marker k-mers. This setting captures a group of taxa with low abundance but reasonable ($\sim$ 10-20%) coverage of the k-mers in their marker set (Supp. Figure S9C). However, this also allows for a number of taxa with very high (105) duplication of the identified marker k-mers and very few k-mers per read which we believe is biologically implausible (Supp. Figure S9D). We filtered these taxa by applying a further filter which required that the number of reads not exceed $\frac{10}{25}$ times the number of unique k-mers, unless the set of unique k-mers was saturated ($> 90\%$ completeness). We include a full list of all taxonomic calls from all samples including diagnostic values for each call. We do not attempt to classify reads below the species level in this study.

We further evaluated prominent taxonomic classifications for sequence complexity and genome coverage. For each microbe evaluated we calculated two indices generated using a random subset of 152 samples: the average topological entropy of reads assigned to the microbe and the Gini-coefficient of read positions on the microbial genome. For brevity we refer to these as *mean sequence entropy* (MSE) and *coverage equality* (CE). The formula for topological entropy of a DNA sequence is described by Koslicki (2011). Values close to 0 correspond to low-complexity sequences and values near 1 are high complexity. In this work we use a word size of 3 with an overall sequence length of 64 since this readily fits into our reads. To find the MSE of a microbial classification we take the arithmetic mean of the topological entropy of all reads that map to a given microbial genome in a sample. The Gini-coefficient is a classic economic measure of income inequality. We repurpose it here to evaluate the evenness of read coverage over a microbial classification. Reads mapping to a microbial genome are assigned to a contiguous 10kbp bin and the Gini-coefficient of all bins is calculated. Like MSE, the Gini-coefficient is bounded in [0, 1]. Lower values indicate greater inequality, very low values indicate that a taxon may be misidentified from conserved and near conserved regions. We downloaded one representative genome per species evaluated and mapped all reads from samples to using Bowtie2 (sensitive-local preset). Indices were processed from alignments using a custom script. Species classifications with an average MSE less than 0.75 or CE less than 0.1 were flagged.

To determine relative abundance of taxa where applicable we rarefied samples to 100,000 classified reads, computed the proportion of reads assigned to each taxon, and took the distribution of values from all samples. This was the minimum number of reads sufficient to maintain taxonomic richness (Supp. Figure S9B). We chose sub-sampling (sometimes referred to as rarefaction in the literature) based on the study by Weiss et al. (2017), showing that sub-sampling effectively estimates relative abundance. Note that we use the term prevalence to describe the fraction of samples where a given taxon is found at any abundance and we use the term relative abundance to describe the fraction of DNA in a sample from a given taxon.

We compared our samples to metagenomic samples from the Human Microbiome Project and a metagenomic study of European soil samples using MASH (Ondov et al., 2016), a fast k-mer based comparison tool. We built MASH sketches from all samples with 10 million unique k-mers to ensure a sensitive and accurate comparison. We used MASH's built-in Jaccard distance function to generate

distances between our samples and HMP samples. We then took the distribution of distances to each particular human commensal community as a proxy for the similarity of our samples to a given human body site.

We also compared our samples to HMP and soil samples using taxonomic profiles generated by MetaPhlAn v2.0 (Segata et al., 2012). We generated taxonomic profiles from non-human reads using MetaPhlAn v2.0 and found the cosine similarity between all pairs of samples.

We used the Microbe Directory (Shaaban et al., 2018) to annotate taxonomic calls. The Microbe Directory is a hand curated, machine readable, database of functional annotations for 5,000 microbial species.

6.6.2 Functional Analysis

We analyzed the metabolic functions in each of our samples by processing non-human reads with HUMAnN2 (Franzosa et al., 2018). We aligned all reads to UniRef90 using DIAMOND (v0.8.36, (Buchfink et al., 2014)) and used HUMAnN2 to produce estimate of pathway abundance and completeness. We filtered all pathways that were less than 50% covered in a given sample but otherwise took the reported pathway abundance as is after relative abundance normalization (using HUMAnN2's attached script).

High level categories of functional pathways were found by grouping postively correlated pathways and manually annotating resulting clusters.

6.7 Assembly and Plasmid Annotations

All samples were assembled using metaSPAdes (v3.8.1 Nurk et al. (2017)) with default settings. Assembled scaffolds of at least 1,500bp of length were annotated using PlasFlow (v1.1 Krawczyk et al. (2018)) using default settings. PlasFlow predicts whether a contig is likely from a chromosome or a plasmid and gives a rough taxonomic annotation. Predicting which sequences are from plasmids is a difficult problem and some annotations may be incorrect.

6.7.1 Analysis of Antimicrobial Resistance Genes

We generated profiles of antimicrobial resistance genes using MegaRes (v1.0.1, Lakin et al. (2017)). To generate profiles from MegaRes, we mapped non-human reads to the MegaRes database using Bowtie2 (v2.3.0, very-sensitive presets, Langmead and Steven L Salzberg (2013)). Subsequently, alignments were analyzed using ResistomeAnalyzer (commit 15a52dd `github.com/cdeanj/resistomeanalyzer`) and normalized by total reads per sample and gene length to give RPKMs. MegaRes includes an ontology grouping resistance genes into gene classes, AMR mechanisms, and gene groups. AMR detection remains a difficult problem and we note that detection of a homologous sequence to a known AMR gene does not necessarily imply an equivalent resistance in our samples. Currently, the gold standard for detecting AMR is via culturing.

Known AMR genes can come from gene families with homologous regions of sequence. To reduce spurious mapping from gene homology we used BLASTn to align all MegaRes AMR genes against themselves. We considered any connected group of genes with an average nucleotide identity of 80% across 50% of the gene length as a set of potentially confounded genes. We collapsed all such groups into a single pseudo-gene with the mean abundance of all constituent genes. Before clustering genes we removed all genes which were annotated as requiring SNP verification to predict resistance.

In addition to MegaRes we mapped non-human reads from all samples to the amino acid gene sequences in the Comprehensive Antibiotic Resistance Database (McArthur et al., 2013) using DIAMOND. While we do not use this analysis explicitly in this study we provide the results as a data table.

Assembled contigs were annotated for AMR genes using metaProdigal (Hyatt et al., 2010), HMMER3 (Eddy, 2011), and ResFam (Gibson et al., 2015) as described by Rahman et al. (2018). All predicted gene annotations with an e-value higher than 10^{-10} were discarded.

6.7.2 Beta Diversity

Inter-sample (beta) diversity was measured by using Jaccard distances. We note that Jaccard distances do not use relative abundance information. Matrices of Jaccard distances were produced using built in SciPy functions treating all elements greater than 0 as present. Hierarchical clustering (average linkage) was performed on the matrix of Jaccard distances using SciPy (https://www.scipy.org/).

⁹⁷⁵ Dimensionality reduction of taxonomic and functional profiles was performed using UMAP (McInnes
⁹⁷⁶ et al., 2018) on the matrix of Jaccard distances with 100 neighbours (UMAP-learn package, random
⁹⁷⁷ seed of 42). We did not use Principal Component Analysis as a preprocessing step before UMAP as is
⁹⁷⁸ sometimes done for high dimensional data.

6.7.3   Alpha Diversity

⁹⁸⁰ Intra-sample (alpha) diversity was measured by using Species Richness and Shannon's Entropy. We
⁹⁸¹ took species richness as the total number of detected species in a sample after rarefaction to 1 million
⁹⁸² reads. Shannon's entropy is robust to sample read depth and accounts for the relative size of each
⁹⁸³ group in diversity estimation. Shannon's entropy is typically defined as $H = \sum a_i log_2 a_i$ where a_i is the
⁹⁸⁴ relative abundance of taxon i in the sample. For alpha diversity based on k-mers or pathways, we simply
⁹⁸⁵ substitute the relative abundance of a species for the relative abundance of the relevant type of object.

6.7.4   GeoDNA Sequence Search

⁹⁸⁷ For building the sequence graph index, each sample was processed with KMC (version 3, [1]) to convert
⁹⁸⁸ the reads in FASTA format into lists of k-mer counts, using different values of k ranging from 13 to 19 in
⁹⁸⁹ increments of 2. All k-mers that contained the character "N" or occurred in a sample less than twice were
⁹⁹⁰ removed. For each value of k, we built a separate index, consisting of a labeled de Bruijn graph, using an
⁹⁹¹ implicit representation of the complete graph and a compressed label representation based on Multiary
⁹⁹² Binary Relation Wavelet Trees (Multi-BRWT). For further details, we refer to the manuscript [2]. To
⁹⁹³ build the index, for each sample the KMC k-mer count lists were transformed into de Bruijn graphs, from
⁹⁹⁴ which path covers in the form of contig sets were extracted and stored as intermediate FASTA files. The
⁹⁹⁵ contig sets of each sample were then transformed into annotation columns (one column per sample) by
⁹⁹⁶ mapping them onto an implicit complete de Bruijn graph of order k. All annotation columns were then
⁹⁹⁷ merged into a joint annotation matrix and transformed into Multi-BRWT format. Finally, the topology
⁹⁹⁸ of the Multi-BRWT representation was optimized by relaxing its internal tree arity constraints to allow
⁹⁹⁹ for a maximum arity of 40.

6.8   Novel Biology

6.9   Identifying Bacteria and Archaea

Metagenomic Assembly and Binning   All samples were re-assembled with metaSPAdes (v3.10.1
Nurk et al., 2017); generated contigs with length <1000nt were excluded from further analysis. Remaining
contigs were binned with MetaBAT2 (v2.12.1 Kang et al. (2019)) with default parameters, resulting in
14,080 bins. As MetaBAT2 uses contig abundance (mean base coverage) in its analysis, we mapped reads
back to their respective contigs via Bowtie2 (v2.3.4.1 Langmead and Steven L Salzberg (2013))with the
flags –local –very-sensitive-local to provide accurate coverage metrics. Draft genome quality was assessed
via CheckM (v1.0.13 Parks et al. (2015)) lineage_wf workflow with default parameters. Using the
strategy proposed by Parks et al. (2018) we filtered bins by quality score, defined as QS = completeness -
5 * contamination; bins with QS < 50 were removed from consideration. The remaining 6,107 bins were
labeled by quality based on the MIMAG standard (Bowers et al. (2018)), with some modification: 1,448
high quality (completeness >90%, contamination <5%, strain heterogeneity <0.5%) bins, 4,532 medium
quality (completeness >50%, contamination <5%) bins, all others low quality. Bins of at least medium
quality were selected as acceptable MAGs (5,980 total).

MAG Dereplication   OTUs (MAG representatives) were chosen with a two-step clustering strategy.
Single-linkage clustering formed primary clusters of MAGs based on Mash ANI (v2.1.1), with intra-cluster
identity at 90%. Though Mash ANI can be inaccurate for potentially incomplete genomes (Olm et al.
(2017)), we can leverage the technique's speed for the many pairwise comparisons needed in this granular
step. Within primary clusters, MAGs were compared pairwise by a more accurate whole-genome ANI
(gANI) via dnadiff (v1.3) from MUMmer (v3.23 Kurtz et al. (2004)). Secondary, more refined clusters
were grouped based n gANI using average-linkage hierarchical clustering from the R package dendextend
(v1.12.0 Galili (2015)). A gANI cut-off of 95% resulted in 1,304 representative OTUs.

OTU to Reference Genome Matching OTUs were compared against reference genomes from Ref-Seq (release 96 from November 2019, complete bacterial and archaeal genomes only, with "Exclude anomalous" and "Exclude derived from surveillance project" applied) as well as the full Integrated Gut Genomes (IGG) dataset (v1.0 Nayfach et al. (2019); 23,790 representative genomes). A MinHash sketch was created for each reference genome via Mash (v2.1.1) with default parameters to find Mash distances and select candidate "best matches" from each reference database. Then, dnadiff (v1.3) was used to further quantify differences between each OTU and its best match from either database. ANI between OTUs and their matches was found as "M-to-M AvgIdentity" in the query report column (ANI 95% over 60% OTU sequence qualified as a match).

OTU Taxonomic Assignment OTUs were placed into a bacterial or archaeal reference tree (based on the Genome Database Taxonomy, GTDB) and then assigned taxonomic classifications using GTDB-Tk (v1.0.2 Chaumeil et al. (2019)). GTDB-Tk relies on 120 bacterial and 122 archaeal marker genes; domain assignment is chosen based on domain-specific marker content of the OTU sequence. Using the GTDB-Tk placements, we built an OTU-only bacterial phylogeny with FastTree (v2.1.10 Price et al. (2010)). The tree was visualized using iTOL (v5.5 Letunic and Bork (2019)).

6.9.1 Viral Discovery

We followed the protocol described by Paez-Espino et al. (2017). Briefly, we used an expanded and curated set of viral protein families (VPFs) as bait in combination with recommended filtering steps to identify 16,584 UViGs directly from all MetaSUB metagenomic assemblies greater than 5kb. Then, the UViGs were clustered with the content of the IMG/VR system (a total of over 730k viral sequences including isolate viruses, prophages, and UViGs from all kind of habitats). The clustering step relied on a sequence-based classification framework (based on 95% sequence identity across 85% of the shortest sequence length) followed by the markov clustering (mcl). This approach yielded 2,009 viral clusters (ranging from 2-611 members) and 9,605 singletons (or viral clusters of 1 member), sequences that failed to cluster with any sequence from the dataset or the references from IMG/VR, resulting in a total of 11,614 vOTUs. We define viral species from vOTUs as sequences sharing at least 95% identity over 85% of their length. Out of this total MetaSUB viral diversity, only 686 vOTUs clustered with any known viral sequence in IMG/VR.

6.9.2 Identifying Host Virus Interactions

We used two computational methods to reveal putative host-virus connections (Paez-Espino et al., 2016a). (1) For the 686 vOTUs that clustered with viral sequences from the IMG/VR system, we projected the known host information to all the members of the group (total of 2,064 MetaSUB UViGs). (2) We used bacterial/archaeal CRISPR-Cas spacer matches (from the IMG/M 1.1 million isolate spacer database) to the UViGs (allowing only for 1 SNP over the whole spacer length) to assigned a host to 1,915 MetaSUB vOTUs. Additionally, we also used a database of over 20 million CRISPR-Cas spacers identified from metagenomic contigs from the IMG/M system with taxonomy assigned. Since some of these spacers may derive from short contigs these results should be interpreted with caution.

6.9.3 CRISPR Array Detection and Annotation

Using CRISPRCasFinder the MetaSUB database was investigated to predict CRISPR arrays and annotate them with their corresponding predicted type based on CRISPR-Cas genes in their vicinity. CRISPRCasFinder was run with default parameters, "-so" and "-cas" options to identify cas genes. The precision and recall of the virus detection was 99.6% and 37.5% respectively, as previously reported by (Paez-Espino et al., 2016b).

CRISPR-Cas types were assigned to arrays based on detected cas genes within a 10 kilobases vicinity. Cases where CRISPRCasFinder associated several cas genes of contradicting CRISPR-Cas types with the same CRISPR array were regarded as unclear annotation. This procedure yielded 838,532 predicted CRISPR arrays (with additional CRISPR arrays predicted with default parameters for PILER-CR), of which, 3,245 CRISPR arrays had unambiguous annotation, resulting in 43,656 unique spacers queried against genomic databases using BLASTN.

6.10   Organisms/BLAST Databases

In order to associate detected spacers within defined groups (plasmids, prophages, viruses) four different genomic databases were aggregated to be searched with BLASTN. The aggregated database consisted of IMG/VR, PHASTER, and PLSDB alongside bacterial and archaeal genomic sequences from the National Center for Biotechnology Information (NCBI). All database downloads were made on the 28th January 2020. Detected and annotated spacers were searched against the databases mentioned above using BLASTN with the following additional arguments, which correspond to the default parameters of CRISPRTarget: word_size=7, evalue=1, gapopen=10, gapextend=2, penalty=-1, reward=1.

6.11   MetaSUB Genomic Database and Statistical Analysis

Genomic data was acquired from the MetaSUB database and matched by sample names to the corresponding metadata downloaded from the MetaSUB-metadata github repository (https://github.com/MetaSUB/MetaSUB-metadata). All data derived from MetaSUB and the subsequent steps described above was then analysed using Python 3.6. Python packages plotly, matplotlib and seaborn where used for plotting as well as pandas to create and manage dataframes. The heatmap is clustered by Euclidean distance on the columns.

References

Afshinnekoo, E., Chou, C., Alexander, N., Ahsanuddin, S., Schuetz, A. N., and Mason, C. E. (2017). Precision metagenomics: Rapid metagenomic analyses for infectious disease diagnostics and public health surveillance. *Journal of Biomolecular Techniques*, 28(1):40–45.

Afshinnekoo, E., Meydan, C., Chowdhury, S., Jaroudi, D., Boyer, C., Bernstein, N., Maritz, J. M., Reeves, D., Gandara, J., Chhangawala, S., Ahsanuddin, S., Simmons, A., Nessel, T., Sundaresh, B., Pereira, E., Jorgensen, E., Kolokotronis, S. O., Kirchberger, N., Garcia, I., Gandara, D., Dhanraj, S., Nawrin, T., Saletore, Y., Alexander, N., Vijay, P., Hénaff, E. M., Zumbo, P., Walsh, M., O'Mullan, G. D., Tighe, S., Dudley, J. T., Dunaif, A., Ennis, S., O'Halloran, E., Magalhaes, T. R., Boone, B., Jones, A. L., Muth, T. R., Paolantonio, K. S., Alter, E., Schadt, E. E., Garbarino, J., Prill, R. J., Carlton, J. M., Levy, S., and Mason, C. E. (2015). Geospatial Resolution of Human and Bacterial Diversity with City-Scale Metagenomics. *Cell Systems*, 1(1):72–87.

Allen, H. K., Moe, L. A., Rodbumrer, J., Gaarder, A., and Handelsman, J. (2009). Functional metagenomics reveals diverse β-lactamases in a remote alaskan soil. *The ISME journal*, 3(2):243–251.

Altschul, S. F., Gish, W., Miller, W., Myers, E. W., and Lipman, D. J. (1990). Altschul et al.. 1990. Basic Local Alignment Search Tool.pdf.

Bahram, M., Hildebrand, F., Forslund, S. K., Anderson, J. L., Soudzilovskaia, N. A., Bodegom, P. M., Bengtsson-Palme, J., Anslan, S., Coelho, L. P., Harend, H., Huerta-Cepas, J., Medema, M. H., Maltz, M. R., Mundra, S., Olsson, P. A., Pent, M., Põlme, S., Sunagawa, S., Ryberg, M., Tedersoo, L., and Bork, P. (2018). Structure and function of the global topsoil microbiome.

Bougnom, B. P. and Piddock, L. J. (2017). Wastewater for Urban Agriculture: A Significant Factor in Dissemination of Antibiotic Resistance.

Bowers, R. M., Kyrpides, N. C., Stepanauskas, R., Harmon-Smith, M., Doud, D., Reddy, T. B. K., Schulz, F., Jarett, J., Rivers, A. R., Eloe-Fadrosh, E. A., Tringe, S. G., Ivanova, N. N., Copeland, A., Clum, A., Becraft, E. D., Malmstrom, R. R., Birren, B., Podar, M., Bork, P., Weinstock, G. M., Garrity, G. M., Dodsworth, J. A., Yooseph, S., Sutton, G., Gl?ckner, F. O., Gilbert, J. A., Nelson, W. C., Hallam, S. J., Jungbluth, S. P., Ettema, T. J. G., Tighe, S., Konstantinidis, K. T., Liu, W. T., Baker, B. J., Rattei, T., Eisen, J. A., Hedlund, B., McMahon, K. D., Fierer, N., Knight, R., Finn, R., Cochrane, G., Karsch-Mizrachi, I., Tyson, G. W., Rinke, C., Lapidus, A., Meyer, F., Yilmaz, P., Parks, D. H., Eren, A. M., Schriml, L., Banfield, J. F., Hugenholtz, P., and Woyke, T. (2018). Corrigendum: Minimum information about a single amplified genome (MISAG) and a metagenome-assembled genome (MIMAG) of bacteria and archaea. *Nat. Biotechnol.*, 36(7):660.

Breitwieser, F. P., Baker, D. N., and Salzberg, S. L. (2018). KrakenUniq: confident and fast metagenomics classification using unique k-mer counts. *Genome biology*, 19(1):198.

Brito, I. L., Yilmaz, S., Huang, K., Xu, L., Jupiter, S. D., Jenkins, A. P., Naisilisili, W., Tamminen, M., Smillie, C. S., Wortman, J. R., Birren, B. W., Xavier, R. J., Blainey, P. C., Singh, A. K., Gevers, D., and Alm, E. J. (2016). Mobile genes in the human microbiome are structured from global to individual scales. *Nature*, 535(7612):435–439.

Brooks, B., Olm, M. R., Firek, B. A., Baker, R., Thomas, B. C., Morowitz, M. J., and Banfield, J. F. (2017). Strain-resolved analysis of hospital rooms and infants reveals overlap between the human and room microbiome. *Nature communications*, 8(1):1–7.

Buchfink, B., Xie, C., and Huson, D. H. (2014). Fast and sensitive protein alignment using DIAMOND.

Cáliz, J., Triadó-Margarit, X., Camarero, L., and Casamayor, E. O. (2018). A long-term survey unveils strong seasonal patterns in the airborne microbiome coupled to general and regional atmospheric circulations. *Proceedings of the National Academy of Sciences*, 115(48):12229–12234.

Chaumeil, P. A., Mussig, A. J., Hugenholtz, P., and Parks, D. H. (2019). GTDB-Tk: a toolkit to classify genomes with the Genome Taxonomy Database. *Bioinformatics*.

Consortium, T. H. M. P., Human, T., Project, M., Consortium, T. H. M. P., Human, T., and Project, M. (2012). Structure, function and diversity of the healthy human microbiome. *Nature*, 486(7402):207–14.

Cooley, J. D., Wong, W. C., Jumper, C. A., and Straus, D. C. (1998). Correlation between the prevalence of certain fungi and sick building syndrome. *Occupational and Environmental Medicine*, 55(9):579–584.

Delgado-Baquerizo, M., Oliverio, A. M., Brewer, T. E., Benavent-González, A., Eldridge, D. J., Bardgett, R. D., Maestre, F. T., Singh, B. K., and Fierer, N. (2018). A global atlas of the dominant bacteria found in soil. *Science*, 359(6373):320–325.

Eckburg, P. B., Mian, M. F., Surette, M. G., Bienenstock, J., Forsythe, P., and Sargent, M. (2005). Diversity of the Human Intestinal Microbial Flora. *Science*, 308(5728):1635–1638.

Eddy, S. R. (2011). Accelerated profile HMM searches. *PLoS Computational Biology*, 7(10).

Franzosa, E. A., McIver, L. J., Rahnavard, G., Thompson, L. R., Schirmer, M., Weingart, G., Lipson, K. S., Knight, R., Caporaso, J. G., Segata, N., and Huttenhower, C. (2018). Species-level functional profiling of metagenomes and metatranscriptomes. *Nature methods*, 15(11):962–968.

Fresia, P., Antelo, V., Salazar, C., Giménez, M., D'Alessandro, B., Afshinnekoo, E., Mason, C., Gonnet, G. H., and Iraola, G. (2019). Urban metagenomics uncover antibiotic resistance reservoirs in coastal beach and sewage waters. *Microbiome*, 7(1).

Galili, T. (2015). dendextend: an R package for visualizing, adjusting and comparing trees of hierarchical clustering. *Bioinformatics*, 31(22):3718–3720.

Gardy, J. L. and Loman, N. J. (2018). Towards a genomics-informed, real-time, global pathogen surveillance system.

Gibson, M. K., Forsberg, K. J., and Dantas, G. (2015). Improved annotation of antibiotic resistance determinants reveals microbial resistomes cluster by ecology. *ISME Journal*, 9(1):207–216.

Gilbert, J. A. and Stephens, B. (2018). Microbiology of the built environment.

Hendriksen, R. S., Munk, P., Njage, P., van Bunnik, B., McNally, L., Lukjancenko, O., Röder, T., Nieuwenhuijse, D., Pedersen, S. K., Kjeldgaard, J., Kaas, R. S., Clausen, P. T. L. C., Vogt, J. K., Leekitcharoenphon, P., van de Schans, M. G. M., Zuidema, T., de Roda Husman, A. M., Rasmussen, S., Petersen, B., Bego, A., Rees, C., Cassar, S., Coventry, K., Collignon, P., Allerberger, F., Rahube, T. O., Oliveira, G., Ivanov, I., Vuthy, Y., Sopheak, T., Yost, C. K., Ke, C., Zheng, H., Baisheng, L., Jiao, X., Donado-Godoy, P., Coulibaly, K. J., Jergović, M., Hrenovic, J., Karpíšková, R., Villacis, J. E., Legesse, M., Eguale, T., Heikinheimo, A., Malania, L., Nitsche, A., Brinkmann, A., Saba, C. K. S., Kocsis, B., Solymosi, N., Thorsteinsdottir, T. R., Hatha, A. M., Alebouyeh, M., Morris, D., Cormican, M., O'Connor, L., Moran-Gilad, J., Alba, P., Battisti, A., Shakenova, Z., Kiiyukia, C., Ng'eno, E., Raka, L., Avsejenko, J., Bērziņš, A., Bartkevics, V., Penny, C., Rajandas, H., Parimannan, S., Haber, M. V., Pal, P., Jeunen, G.-J., Gemmell, N., Fashae, K., Holmstad, R., Hasan, R., Shakoor, S., Rojas, M. L. Z., Wasyl, D., Bosevska, G., Kochubovski, M., Radu, C., Gassama, A., Radosavljevic, V., Wuertz, S., Zuniga-Montanez, R., Tay, M. Y. F., Gavačová, D., Pastuchova, K., Truska, P., Trkov, M., Esterhuyse, K., Keddy, K., Cerdà-Cuéllar, M., Pathirage, S., Norrgren, L., Örn, S., Larsson, D. G. J., Heijden, T. V. d., Kumburu, H. H., Sanneh, B., Bidjada, P., Njanpop-Lafourcade, B.-M., Nikiema-Pessinaba, S. C., Levent, B., Meschke, J. S., Beck, N. K., Van, C. D., Phuc, N. D., Tran, D. M. N., Kwenda, G., Tabo, D.-a., Wester, A. L., Cuadros-Orellana, S., Amid, C., Cochrane, G., Sicheritz-Ponten, T., Schmitt, H., Alvarez, J. R. M., Aidara-Kane, A., Pamp, S. J., Lund, O., Hald, T., Woolhouse, M., Koopmans, M. P., Vigre, H., Petersen, T. N., Aarestrup, F. M., and project consortium, T. G. S. S. (2019). Global monitoring of antimicrobial resistance based on metagenomics analyses of urban sewage. *Nature Communications*, 10(1):1124.

Hoch, J. M., Rhodes, M. E., Shek, K. L., Dinwiddie, D., Hiebert, T. C., Gill, A. S., Salazar Estrada, A., Griffin, K. L., Palmer, M. I., and McGuire, K. L. (2019). Soil microbial assemblages are linked to plant community composition and contribute to ecosystem services on urban green roofs. *Front. Ecol. Evol. 7: 198. doi: 10.3389/fevo*.

Hsu, T., Joice, R., Vallarino, J., Abu-Ali, G., Hartmann, E. M., Shafquat, A., DuLong, C., Baranowski, C., Gevers, D., Green, J. L., Morgan, X. C., Spengler, J. D., and Huttenhower, C. (2016). Urban Transit System Microbial Communities Differ by Surface Type and Interaction with Humans and the Environment. *mSystems*, 1(3):e00018–16.

31

Hyatt, D., Chen, G. L., LoCascio, P. F., Land, M. L., Larimer, F. W., and Hauser, L. J. (2010). Prodigal: Prokaryotic gene recognition and translation initiation site identification. *BMC Bioinformatics*, 11.

Joseph, S. M., Battaglia, T., Maritz, J. M., Carlton, J. M., and Blaser, M. J. (2019). Longitudinal comparison of bacterial diversity and antibiotic resistance genes in new york city sewage. *MSystems*, 4(4):e00327–19.

Joyner, J. L., Kerwin, J., Deeb, M., Lozefski, G., Paltseva, A., Prithiviraj, B., McLaughlin, J., Cheng, Z., Groffman, P., and Muth, T. R. (2019). Green infrastructure design influences urban soil bacteria communities. *Frontiers in microbiology*, 10:982.

Kang, D. D., Li, F., Kirton, E., Thomas, A., Egan, R., An, H., and Wang, Z. (2019). MetaBAT 2: an adaptive binning algorithm for robust and efficient genome reconstruction from metagenome assemblies. *PeerJ*, 7:e7359.

Kang, K., Ni, Y., Li, J., Imamovic, L., Sarkar, C., Kobler, M. D., Heshiki, Y., Zheng, T., Kumari, S., Wong, J. C. Y., Archna, A., Wong, C. W. M., Dingle, C., Denizen, S., Baker, D. M., Sommer, M. O. A., Webster, C. J., and Panagiotou, G. (2018). The Environmental Exposures and Inner- and Intercity Traffic Flows of the Metro System May Contribute to the Skin Microbiome and Resistome. *Cell Reports*, 24(5):1190–1202.e5.

Kim, D., Hofstaedter, C. E., Zhao, C., Mattei, L., Tanes, C., Clarke, E., Lauder, A., Sherrill-Mix, S., Chehoud, C., Kelsen, J., et al. (2017). Optimizing methods and dodging pitfalls in microbiome research. *Microbiome*, 5(1):52.

Klein, E. Y., Van Boeckel, T. P., Martinez, E. M., Pant, S., Gandra, S., Levin, S. A., Goossens, H., and Laxminarayan, R. (2018). Global increase and geographic convergence in antibiotic consumption between 2000 and 2015. *Proceedings of the National Academy of Sciences*, 115(15):E3463–E3470.

Korownyk, C., Liu, F., and Garrison, S. (2018). Population level evidence for seasonality of the human microbiome. *Chronobiology International*, 35(4):573–577.

Koslicki, D. (2011). Topological entropy of DNA sequences. *Bioinformatics*, 27(8):1061–1067.

Krawczyk, P. S., Lipinski, L., and Dziembowski, A. (2018). PlasFlow: predicting plasmid sequences in metagenomic data using genome signatures. *Nucleic Acids Research*, 46(6):e35–e35.

Kurtz, S., Phillippy, A., Delcher, A. L., Smoot, M., Shumway, M., Antonescu, C., and Salzberg, S. L. (2004). Versatile and open software for comparing large genomes. *Genome Biol.*, 5(2):R12.

Ladner, J. T., Grubaugh, N. D., Pybus, O. G., and Andersen, K. G. (2019). Precision epidemiology for infectious disease control.

Lakin, S. M., Dean, C., Noyes, N. R., Dettenwanger, A., Ross, A. S., Doster, E., Rovira, P., Abdo, Z., Jones, K. L., Ruiz, J., Belk, K. E., Morley, P. S., and Boucher, C. (2017). MEGARes: An antimicrobial resistance database for high throughput sequencing. *Nucleic Acids Research*, 45(D1):D574–D580.

Langmead and Steven L Salzberg (2013). Bowtie2. *Nature methods*, 9(4):357–359.

Lax, S., Sangwan, N., Smith, D., Larsen, P., Handley, K. M., Richardson, M., Guyton, K., Krezalek, M., Shogan, B. D., Defazio, J., et al. (2017). Bacterial colonization and succession in a newly opened hospital. *Science translational medicine*, 9(391):eaah6500.

Letunic, I. and Bork, P. (2019). Interactive Tree Of Life (iTOL) v4: recent updates and new developments. *Nucleic Acids Res.*, 47(W1):W256–W259.

Leung, M. H., Wilkins, D., Li, E. K., Kong, F. K., and Lee, P. K. (2014). Indoor-air microbiome in an urban subway network: diversity and dynamics. *Appl. Environ. Microbiol.*, 80(21):6760–6770.

Lloyd-Price, J., Mahurkar, A., Rahnavard, G., Crabtree, J., Orvis, J., Hall, A. B., Brady, A., Creasy, H. H., McCracken, C., Giglio, M. G., McDonald, D., Franzosa, E. A., Knight, R., White, O., and Huttenhower, C. (2017). Strains, functions and dynamics in the expanded Human Microbiome Project. *Nature*, 550(7674):61–66.

Maritz, J. M., Ten Eyck, T. A., Alter, S. E., and Carlton, J. M. (2019). Patterns of protist diversity associated with raw sewage in new york city. *The ISME journal*, 13(11):2750–2763.

Martínez, J. L. (2008). Antibiotics and antibiotic resistance genes in natural environments. *Science*, 321(5887):365–367.

Mason-Buck, G., Graf, A., Elhaik, E., Robinson, J., Pospiech, E., Oliveira, M., Moser, J., Lee, P. K. H., Githae, D., Ballard, D., Bromberg, Y., Casimiro-Soriguer, C. S., Dhungel, E., Ahn, T.-H., Kawulok, J., Loucera, C., Ryan, F., Walker, A. R., Zhu, C., Mason, C. E., Amorim, A., Syndercombe Court, D., Branicki, W., and Łabaj, P. (2020). DNA based methods in intelligence - moving towards metagenomics. *Preprints*, page 2020020158.

McArthur, A. G., Waglechner, N., Nizam, F., Yan, A., Azad, M. A., Baylay, A. J., Bhullar, K., Canova, M. J., De Pascale, G., Ejim, L., Kalan, L., King, A. M., Koteva, K., Morar, M., Mulvey, M. R., O'Brien, J. S., Pawlowski, A. C., Piddock, L. J., Spanogiannopoulos, P., Sutherland, A. D., Tang, I., Taylor, P. L., Thaker, M., Wang, W., Yan, M., Yu, T., and Wright, G. D. (2013). The comprehensive antibiotic resistance database. *Antimicrobial Agents and Chemotherapy*, 57(7):3348–3357.

McInnes, L., Healy, J., Saul, N., and Großberger, L. (2018). UMAP: Uniform Manifold Approximation and Projection. *Journal of Open Source Software*, 3(29):861.

McIntyre, A. B., Ounit, R., Afshinnekoo, E., Prill, R. J., Hénaff, E., Alexander, N., Minot, S. S., Danko, D., Foox, J., Ahsanuddin, S., Tighe, S., Hasan, N. A., Subramanian, P., Moffat, K., Levy, S., Lonardi, S., Greenfield, N., Colwell, R. R., Rosen, G. L., and Mason, C. E. (2017). Comprehensive benchmarking and ensemble approaches for metagenomic classifiers. *Genome Biology*, 18(1).

McLaren, M. R., Willis, A. D., and Callahan, B. J. (2019). Consistent and correctable bias in metagenomic sequencing measurements. *BioRxiv*, page 559831.

MetaSUB International Consortium. Mason, C., Afshinnekoo, E., Ahsannudin, S., Ghedin, E., Read, T., Fraser, C., Dudley, J., Hernandez, M., Bowler, C., Stolovitzky, G., Chernonetz, A., Gray, A., Darling, A., Burke, C., ?abaj, P. P., Graf, A., Noushmehr, H., Moraes, S., Dias-Neto, E., Ugalde, J., Guo, Y., Zhou, Y., Xie, Z., Zheng, D., Zhou, H., Shi, L., Zhu, S., Tang, A., Ivankovi?, T., Siam, R., Rascovan, N., Richard, H., Lafontaine, I., Baron, C., Nedunuri, N., Prithiviraj, B., Hyat, S., Mehr, S., Banihashemi, K., Segata, N., Suzuki, H., Alpuche Aranda, C. M., Martinez, J., Christopher Dada, A., Osuolale, O., Oguntoyinbo, F., Dybwad, M., Oliveira, M., Fernandes, A., Oliveira, M., Fernandes, A., Chatziefthimiou, A. D., Chaker, S., Alexeev, D., Chuvelev, D., Kurilshikov, A., Schuster, S., Siwo, G. H., Jang, S., Seo, S. C., Hwang, S. H., Ossowski, S., Bezdan, D., Udekwu, K., Udekwu, K., Lungjdahl, P. O., Nikolayeva, O., Sezerman, U., Kelly, F., Metrustry, S., Elhaik, E., Gonnet, G., Schriml, L., Mongodin, E., Huttenhower, C., Gilbert, J., Hernandez, M., Vayndorf, E., Blaser, M., Schadt, E., Eisen, J., Beitel, C., Hirschberg, D., Schriml, L., and Mongodin, E. (2016). The Metagenomics and Metadesign of the Subways and Urban Biomes (MetaSUB) International Consortium inaugural meeting report. *Microbiome*, 4(1):24.

Meyer, K. M., Memiaghe, H., Korte, L., Kenfack, D., Alonso, A., and Bohannan, B. J. (2018). Why do microbes exhibit weak biogeographic patterns? *ISME Journal*, 12(6):1404–1413.

Moskowitz, D. M. and Greenleaf, W. J. (2018). Nonparametric analysis of contributions to variance in genomics and epigenomics data. *bioRxiv*.

Nayfach, S., Shi, Z. J., Seshadri, R., Pollard, K. S., and Kyrpides, N. C. (2019). New insights from uncultivated genomes of the global human gut microbiome. *Nature*, 568(7753):505–510.

Neiderud, C. J. (2015). How urbanization affects the epidemiology of emerging infectious diseases. *African Journal of Disability*, 5(1).

Nicolaou, N., Siddique, N., and Custovic, A. (2005). Allergic disease in urban and rural populations: Increasing prevalence with increasing urbanization. *Allergy: European Journal of Allergy and Clinical Immunology*, 60(11):1357–1360.

Nurk, S., Meleshko, D., Korobeynikov, A., and Pevzner, P. A. (2017). MetaSPAdes: A new versatile metagenomic assembler. *Genome Research*, 27(5):824–834.

O'Hara, N. B., Reed, H. J., Afshinnekoo, E., Harvin, D., Caplan, N., Rosen, G., Frye, B., Woloszynek, S., Ounit, R., Levy, S., Butler, E., and Mason, C. E. (2017). Metagenomic characterization of ambulances across the USA. *Microbiome*, 5(1):125.

Olm, M. R., Brown, C. T., Brooks, B., and Banfield, J. F. (2017). dRep: a tool for fast and accurate genomic comparisons that enables improved genome recovery from metagenomes through de-replication. *ISME J*, 11(12):2864–2868.

Ondov, B. D., Treangen, T. J., Melsted, P., Mallonee, A. B., Bergman, N. H., Koren, S., and Phillippy, A. M. (2016). Mash: fast genome and metagenome distance estimation using MinHash. *Genome biology*, 17(1):132.

Paez-Espino, D., Eloe-Fadrosh, E. A., Pavlopoulos, G. A., Thomas, A. D., Huntemann, M., Mikhailova, N., Rubin, E., Ivanova, N. N., and Kyrpides, N. C. (2016a). Uncovering Earth's virome. *Nature*, 536(7617):425–430.

Paez-Espino, D., Eloe-Fadrosh, E. A., Pavlopoulos, G. A., Thomas, A. D., Huntemann, M., Mikhailova, N., Rubin, E., Ivanova, N. N., and Kyrpides, N. C. (2016b). Uncovering earth's virome. *Nature*, 536(7617):425–430.

Paez-Espino, D., Pavlopoulos, G. A., Ivanova, N. N., and Kyrpides, N. C. (2017). Nontargeted virus sequence discovery pipeline and virus clustering for metagenomic data. *Nature Protocols*, 12(8):1673–1682.

Paez-Espino, D., Roux, S., Chen, I. M. A., Palaniappan, K., Ratner, A., Chu, K., Huntemann, M., Reddy, T. B., Pons, J. C., Llabrés, M., Eloe-Fadrosh, E. A., Ivanova, N. N., and Kyrpides, N. C. (2019). IMG/VR v.2.0: An integrated data management and analysis system for cultivated and environmental viral genomes. *Nucleic Acids Research*, 47(D1):D678–D686.

Parks, D. H., Imelfort, M., Skennerton, C. T., Hugenholtz, P., and Tyson, G. W. (2015). CheckM: assessing the quality of microbial genomes recovered from isolates, single cells, and metagenomes. *Genome Res.*, 25(7):1043–1055.

Parks, D. H., Rinke, C., Chuvochina, M., Chaumeil, P. A., Woodcroft, B. J., Evans, P. N., Hugenholtz, P., and Tyson, G. W. (2018). Author Correction: Recovery of nearly 8,000 metagenome-assembled genomes substantially expands the tree of life. *Nat Microbiol*, 3(2):253.

Pasolli, E., Asnicar, F., Manara, S., Zolfo, M., Karcher, N., Armanini, F., Beghini, F., Manghi, P., Tett, A., Ghensi, P., et al. (2019). Extensive unexplored human microbiome diversity revealed by over 150,000 genomes from metagenomes spanning age, geography, and lifestyle. *Cell*, 176(3):649–662.

Price, M. N., Dehal, P. S., and Arkin, A. P. (2010). FastTree 2–approximately maximum-likelihood trees for large alignments. *PLoS ONE*, 5(3):e9490.

Qin, J., Li, R., Raes, J., and Arumugam, M. (2010). A human gut microbial gene catalogue established by metagenomic sequencing: Commentary.

Rahman, S. F., Olm, M. R., Morowitz, M. J., and Banfield, J. F. (2018). Machine Learning Leveraging Genomes from Metagenomes Identifies Influential Antibiotic Resistance Genes in the Infant Gut Microbiome. *mSystems*, 3(1).

Rice, L. B. (2012). Mechanisms of resistance and clinical relevance of resistance to β-lactams, glycopeptides, and fluoroquinolones. In *Mayo Clinic Proceedings*, volume 87, pages 198–208. Elsevier.

Ritchie, H. and Roser, M. (2020). Urbanization. *Our World in Data*. https://ourworldindata.org/urbanization.

Schubert, M., Lindgreen, S., and Orlando, L. (2016). AdapterRemoval v2: Rapid adapter trimming, identification, and read merging. *BMC Research Notes*, 9(1).

Segata, N., Waldron, L., Ballarini, A., Narasimhan, V., Jousson, O., and Huttenhower, C. (2012). Metagenomic microbial community profiling using unique clade-specific marker genes. *Nature Methods*, 9(8):811.

Shaaban, H., Westfall, D. A., Mohammad, R., Danko, D., Bezdan, D., Afshinnekoo, E., Segata, N., and Mason, C. E. (2018). The Microbe Directory: An annotated, searchable inventory of microbes' characteristics. *Gates Open Research*, 2:3.

Singer, A. C., Shaw, H., Rhodes, V., and Hart, A. (2016). Review of antimicrobial resistance in the environment and its relevance to environmental regulators. *Frontiers in microbiology*, 7:1728.

Thanner, S., Drissner, D., and Walsh, F. (2016). Antimicrobial resistance in agriculture. *MBio*, 7(2):e02227–15.

Thompson, L. R., Sanders, J. G., McDonald, D., Amir, A., Ladau, J., Locey, K. J., Prill, R. J., Tripathi, A., Gibbons, S. M., Ackermann, G., Navas-Molina, J. A., Janssen, S., Kopylova, E., Vazquez-Baeza, Y., Gonzalez, A., Morton, J. T., Mirarab, S., Xu, Z. Z., Jiang, L., Haroon, M. F., Kanbar, J., Zhu, Q., Song, S. J., Kosciolek, T., Bokulich, N. A., Lefler, J., Brislawn, C. J., Humphrey, G., Owens, S. M., Hampton-Marcell, J., Berg-Lyons, D., McKenzie, V., Fierer, N., Fuhrman, J. A., Clauset, A., Stevens, R. L., Shade, A., Pollard, K. S., Goodwin, K. D., Jansson, J. K., Gilbert, J. A., and Knight, R. (2017). A communal catalogue reveals Earth's multiscale microbial diversity. *Nature*, 551(7681):457–463.

United Nations (2016). Political declaration of the high-level meeting of the General Assembly on antimicrobial resistance. Technical report.

United Nations (2018). World Urbanization Prospects: The 2018 Revision. Key facts. Technical report.

Van Boeckel, T. P., Brower, C., Gilbert, M., Grenfell, B. T., Levin, S. A., Robinson, T. P., Teillant, A., and Laxminarayan, R. (2015). Global trends in antimicrobial use in food animals. *Proceedings of the National Academy of Sciences of the United States of America*, 112(18):5649–54.

Venter, H., Henningsen, M. L., and Begg, S. L. (2017). Antimicrobial resistance in healthcare, agriculture and the environment: the biochemistry behind the headlines. *Essays in biochemistry*, 61(1):1–10.

Weiss, S., Xu, Z. Z., Peddada, S., Amir, A., Bittinger, K., Gonzalez, A., Lozupone, C., Zaneveld, J. R., Vázquez-Baeza, Y., Birmingham, A., Hyde, E. R., and Knight, R. (2017). Normalization and microbial differential abundance strategies depend upon data characteristics. *Microbiome*, 5(1):27.

Wilson, M. R., Sample, H. A., Zorn, K. C., Arevalo, S., Yu, G., Neuhaus, J., Federman, S., Stryke, D., Briggs, B., Langelier, C., Berger, A., Douglas, V., Josephson, S. A., Chow, F. C., Fulton, B. D., DeRisi, J. L., Gelfand, J. M., Naccache, S. N., Bender, J., Dien Bard, J., Murkey, J., Carlson, M., Vespa, P. M., Vijayan, T., Allyn, P. R., Campeau, S., Humphries, R. M., Klausner, J. D., Ganzon, C. D., Memar, F., Ocampo, N. A., Zimmermann, L. L., Cohen, S. H., Polage, C. R., DeBiasi, R. L., Haller, B., Dallas, R., Maron, G., Hayden, R., Messacar, K., Dominguez, S. R., Miller, S., and Chiu, C. Y. (2019). Clinical Metagenomic Sequencing for Diagnosis of Meningitis and Encephalitis. *New England Journal of Medicine*, 380(24):2327–2340.

Yooseph, S., Andrews-Pfannkoch, C., Tenney, A., McQuaid, J., Williamson, S., Thiagarajan, M., Brami, D., Zeigler-Allen, L., Hoffman, J., Goll, J. B., et al. (2013). A metagenomic framework for the study of airborne microbial communities. *PLoS One*, 8(12):e81862.

Zhu, Y.-G., Gillings, M., Simonet, P., Stekel, D., Banwart, S., and Penuelas, J. (2017). Microbial mass movements. *Science*, 357(6356):1099–1100.

7   Contributing Members of the MetaSUB Consortium

Marcos Abraao, Muhammad Afaq, Ireen Alam, Gabriela E Albuquerque, Kalyn Ali, Lucia E Alvarado-Arnez, Sarh Aly, Jennifer Amachee, Maria G. Amorim, Majelia Ampadu, Nala An, Núria Andreu Somavilla, Michael Angelov, Verónica Antelo, Catharine Aquino, Mayra Arauco Livia, Luiza F Araujo, Jenny Arevalo, Lucia Elena Alvarado Arnez, Fernanda Arredondo, Matthew Arthur, Sadaf Ayaz, Silva Baburyan, Abd-Manaaf Bakere, Katrin Bakhl, Thais F. Bartelli, Kevin Becher, Joseph Benson, Denis Bertrand, Silvia Beurmann, Christina Black, Brittany Blyther, Bazartseren Boldgiv, Gabriela P Branco, Christian Brion, Paulina Buczansla, Catherine M Burke, Irvind Buttar, Jalia Bynoe, Sven Bönigk, Kari O Bøifot, Hiram Caballero, Alessandra Carbone, Anais Cardenas, Ana V Castro, Ana Valeria B Castro, Astred Castro, Simone Cawthorne, Jonathan Cedillo, Salama Chaker, Allison Chan, Anastasia I Chasapi, Gregory Chem, Jenn-Wei Chen, Michelle Chen, Xiaoqing Chen, Ariel Chernomoretz, Daisy Cheung, Diana Chicas, Hira Choudhry, Carl Chrispin, Kianna Ciaramella, Jake Cohen, David A Coil, Colleen Conger, Ana F. Costa, Delisia Cuebas, Aaron E Darling, Pujita Das, Lucinda B Davenport, Laurent David, Gargi Dayama, Paola F De Sessions, Chris K Deng, Monika Devi, Felipe S Dezem, Sonia Dorado, LaShonda Dorsey, Steven Du, Alexandra Dutan, Naya Eady, Stephen Eduard Boja Ruiz, Jonathan A Eisen, Miar Elaskandrany, Lennard Epping, Juan P Escalera-Antezana, Iqra Faiz, Luice Fan, Nadine Farhat, Kelly French, Skye Felice, Laís Pereira Ferreira, Gabriel Figueroa, Denisse Flores, Marcos AS Fonseca, Jonathan Foox, Aaishah Francis, Pablo Fresia, Jacob Friedman, Jaime J Fuentes, Josephine Galipon, Laura Garcia, Annie Geiger, Samuel M Gerner, Dao Phuong Giang, Matías Giménez, Donato Giovannelli, Dedan Githae, Samantha Goldman, Gaston H Gonnet, Juana Gonzalez, Irene González Navarrete, Tranette Gregory, Felix Hartkopf, Arya Hawkins-Zafarnia, Nur Hazlin Hazrin-Chong, Tamera Henry, Samuel Hernandez, David Hess-Homeier, Yui Him Lo, Lauren E Hittle, Nghiem Xuan Hoan, Irene Hoxie, Elizabeth Humphries, Shaikh B Iqbal, Riham Islam, Sharah Islam, Takayuki Ito, Tomislav Ivankovic, Sarah Jackson, JoAnn Jacobs, Esmeralda Jiminez, Ayantu Jinfessa, Takema Kajita, Amrit Kaur, Fernanda de Souza Gomes Kehdy, Vedbar S Khadka, Shaira Khan, Michelle Ki, Gina Kim, Hyung Jun Kim, Sangwan Kim, Ryan J King, Kaymisha Knights, Ellen Koag, Nadezhda Kobko-Litskevitch, Giuseppe KoLoMonaco, Michael Kozhar, Nanami Kubota, Sheelta S Kumar, Lawrence Kwong, Rachel Kwong, Ingrid Lafontaine, Manolo Laiola, Isha Lamba, Hyunjung Lee, Lucy Lee, Yunmi Lee, Emily Leong, Marcus H Y Leung, Chenhao Li, Weijun Liang, Moses Lin, Yan Ling Wong, Priscilla Lisboa, Anna Litskevitch, Tracy Liu, Sonia Losim, Jennifer Lu, Simona Lysakova, Gustavo Adolfo Malca Salas, Denisse Maldonado, Krizzy Mallari, Tathiane M Malta, Maliha Mamun, Yuk Man Tang, Sonia Marinovic, Brunna Marques, Nicole Mathews, Yuri Matsuzaki, Madelyn May, Elias McComb, Adiell Melamed, Wayne Menary, Ambar Mendez, Katterinne N Mendez, Irene Meng, Ajay Menon, Mark Menor, Nancy Merino, Cem Meydan, Karishma Miah, Tanja Miketic, Eric Minwei Liu, Wilson Miranda, Athena Mitsios, Natasha Mohan, Mohammed Mohsin, Karobi Moitra, Laura Molina, Eftar Moniruzzaman, Sookwon Moon, Isabelle de Oliveira Moraes, Maritza S Mosella, Maritza S Mosella, Josef W Moser, Christopher Mozsary, Amanda L Muehlbauer, Oasima Muner, Muntaha Munia, Naimah Munim, Tatjana Mustac, Kaung Myat San, Areeg Naeem, Mayuko Nakagawa, Masaki Nasu, Bryan Nazario, Narasimha Rao Nedunuri, Aida Nesimi, Aida Nesimi, Gloria Nguyen, Hosna Noorzi, Avigdor Nosrati, Houtan Noushmehr, Diana N. Nunes, Kathryn O'Brien, Niamh B O'Hara, Gabriella Oken, Rantimi A Olawoyin, Kiara Olmeda, Itunu A Oluwadare, Tolulope Oluwadare, Jenessa Orpilla, Jacqueline Orrego, Melissa Ortega, Princess Osma, Israel O Osuolale, Oluwatosin M Osuolale, Rachid Ounit, Christos A Ouzounis, Subhamitra Pakrashi, Rachel Paras, Andrea Patrignani, Ante Peros, Sabrina Persaud, Anisia Peters, Robert A Petit III, Adam Phillips, Lisbeth Pineda, Alketa Plaku, Alma Plaku, Brianna Pompa-Hogan, Max Priestman, Bharath Prithiviraj, Sambhawa Priya, Phanthira Pugdeethosal, Benjamin Pulatov, Angelika Pupiec, Tao Qing, Saher Rahiel, Savlatjon Rahmatulloev, Kannan Rajendran, Aneisa Ramcharan, Adan Ramirez-Rojas, Shahryar Rana, Prashanthi Ratnanandan, Timothy D Read, Hugues Richard, Alexis Rivera, Michelle Rivera, Alessandro Robertiello, Courtney Robinson, Anyelic Rosario, Kaitlan Russell, Timothy Ryan Donahoe, Krista Ryon, Thais S Sabedot, Thais S Sabedot, Mahfuza Sabina, Cecilia Salazar, Jorge Sanchez, Ryan Sankar, Paulo Thiago de Souza Santos, Zulena Saravi, Thomas Saw Aung, Thomas Saw Aung, Nowshin Sayara, Steffen Schaaf, Anna-Lena M Schinke, Ralph Schlapbach, Jason R Schriml, Felipe Segato, Marianna S. Serpa, Heba Shaaban, Maheen Shakil, Hyenah Shim, Yuh Shiwa, Shaleni K Singh, Eunice So, Camila Souza, Jason Sperry, Kiyoshi Suganuma, Hamood Suliman, Jill Sullivan, Jill Sullivan, Fumie Takahara, Isabella K Takenaka, Anyi Tang, Emilio Tarcitano, Mahdi Taye, Alexis Terrero, Andrew M Thomas, Sade Thomas, Masaru Tomita, Xinzhao Tong, Jennifer M Tran, Catalina Truong, Stefan I Tsonev, Kazutoshi Tsuda, Michelle Tuz, Carmen Urgiles, Brandon Valentine, Hitler Francois Vasquez Arevalo, Valeria Ventorino, Patricia Vera-Wolf, Sierra Vincent, Renee Vivancos-

1423 Koopman, Andrew Wan, Cindy Wang, Samuel Weekes, Xiao Wen Cai, Johannes Werner, David Westfall,
1424 Lothar H Wieler, Michelle Williams, Silver A Wolf, Brian Wong, Tyler Wong, Hyun Woo Joo, Rasheena
1425 Wright, Ryota Yamanaka, Jingcheng Yang, Hirokazu Yano, George C Yeh, Tsoi Ying Lai, Laraib Zafar,
1426 Amy Zhang, Shu Zhang, Yang Zhang, Yuanting Zheng,

8 Supplemental Materials

Table S1: Sample Counts

Region	project city	Pilot	CSD16	CSD17	Other	Total
Control	Background Control	0.0	40	0	0.0	40
	Lab Control	0.0	20	6	0.0	26
	Positive Control	0.0	33	6	0.0	39
East Asia	Region Total	26.0	1297	0	34.0	1357
	Hanoi	0.0	16	0	0.0	16
	Hong Kong	0.0	712	0	12.0	724
	Kuala Lumpur	0.0	30	0	0.0	30
	Sendai	0.0	32	0	0.0	32
	Seoul	0.0	80	0	12.0	92
	Shanghai	0.0	0	0	10.0	10
	Singapore	0.0	192	0	0.0	192
	Taipei	0.0	94	0	0.0	94
	Tokyo	26.0	132	0	0.0	158
	Yamaguchi	0.0	9	0	0.0	9
Europe	Region Total	310.0	939	1	177.0	1427
	Barcelona	99.0	0	0	25.0	124
	Belfast	0.0	5	0	0.0	5
	Berlin	55.0	1	0	0.0	56
	Birmingham	0.0	5	1	0.0	6
	Bradford	0.0	4	0	0.0	4
	Bury	0.0	6	0	0.0	6
	Eastbourne	0.0	6	0	0.0	6
	Eden	0.0	5	0	0.0	5
	Edinburgh	0.0	6	0	0.0	6
	Islington	0.0	5	0	0.0	5
	Jaywick	0.0	6	0	0.0	6
	Kensington	0.0	6	0	0.0	6
	Kyiv	0.0	97	0	0.0	97
	Lands End	0.0	5	0	0.0	5
	Lisbon	60.0	0	0	28.0	88
	London	0.0	534	0	0.0	534
	Marseille	96.0	16	0	0.0	112
	Naples	0.0	16	0	0.0	16
	Newcastle	0.0	5	0	0.0	5
	Oslo	0.0	16	0	12.0	28
	Paris	0.0	16	0	0.0	16
	Porto	0.0	0	0	112.0	112
	Sofia	0.0	16	0	0.0	16
	Stockholm	0.0	62	0	0.0	62
	Swansea	0.0	6	0	0.0	6
	Vienna	0.0	16	0	0.0	16
	Zurich	0.0	79	0	0.0	79
Middle East	Region Total	100.0	15	0	0.0	115
	Doha	100.0	15	0	0.0	115

Table S1: Sample Counts Cont.

continent	project city	Pilot	CSD16	CSD17	Other	Total
North America	Region Total	284.0	371	276	28.0	959
	Baltimore	0.0	23	0	0.0	23
	Denver	24.0	23	0	0.0	47
	Fairbanks	141.0	0	0	0.0	141
	Mexico City	0.0	0	0	10.0	10
	Minneapolis	0.0	16	0	0.0	16
	New York City	103.0	279	276	0.0	658
	Sacramento	16.0	0	0	18.0	34
	San Francisco	0.0	30	0	0.0	30
Oceania	Region Total	94.0	32	0	0.0	126
	Auckland	16.0	0	0	0.0	16
	Brisbane	0.0	16	0	0.0	16
	Hamilton	16.0	0	0	0.0	16
	Honolulu	0.0	16	0	0.0	16
	Sydney	62.0	0	0	0.0	62
South America	Region Total	44.0	199	68	20.0	331
	Bogota	17.0	0	0	0.0	17
	Montevideo	0.0	0	0	20.0	20
	Ribeirao Preto	0.0	93	0	0.0	93
	Rio De Janeiro	0.0	77	68	0.0	145
	Santiago	27.0	0	0	0.0	27
	Sao Paulo	0.0	29	0	0.0	29
Sub Saharan Africa	Region Total	116.0	192	0	0.0	308
	Ilorin	90.0	134	0	0.0	224
	Offa	26.0	58	0	0.0	84

Table S2: Covariate Variance. The sample variance that can be explained by each factor, in isolation.

Factor	Variance Explained
City	19%
City Population Density	0%
City Ave June Temp	4%
City Elevation	2%
Coastal City	1%
Surface Material	4%
Koppen Climate Classification	8%
Setting	2%
Above/Below Ground	7%
Continent	11%
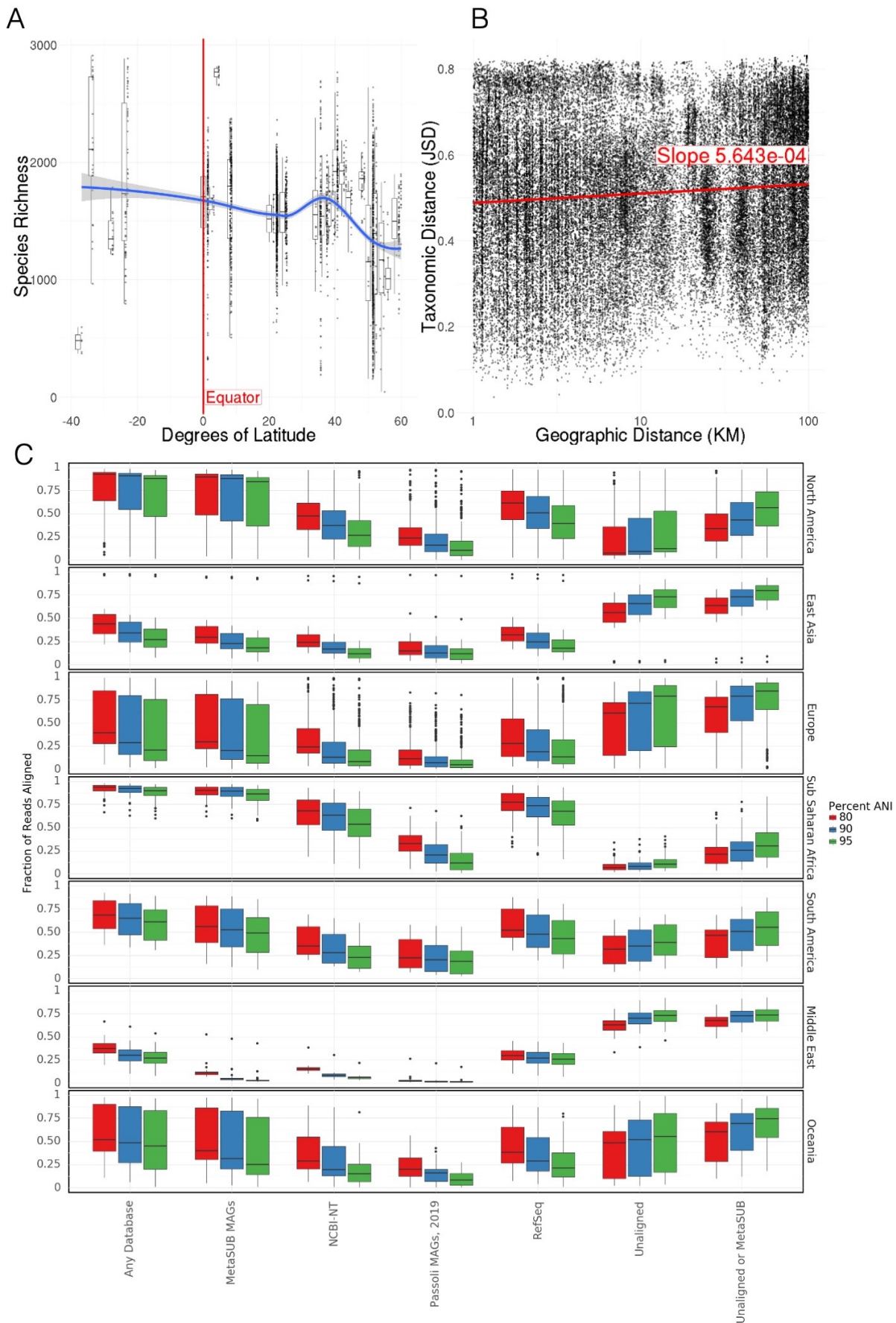
Figure S1: Ecological relationships with taxa. A) Correlation between species richness and latitude. Richness decreases significantly with latitude B) Neighbourhood effect. Taxonomic distance weakly correlates with geographic distance within cities. C) Fraction of reads assigned to different databases by BLAST for each region, at different levels of average nucleotide identity
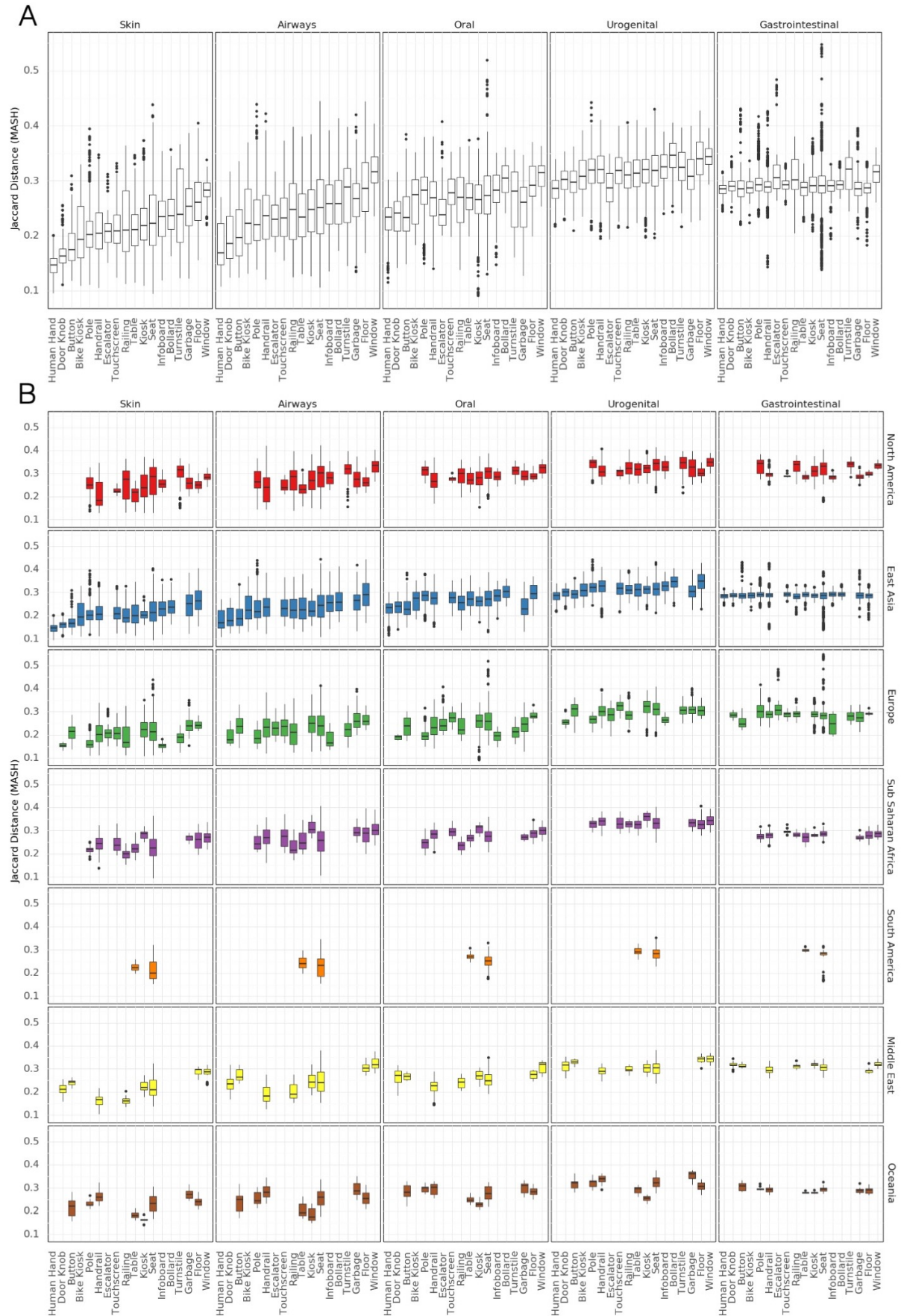
Figure S2: Comparison to Human Microbiome Project. A) Jaccard similarity of MASH indices to HMP samples for different surface types. B) Jaccard similarity of MASH indices to HMP samples for different surface types by region.

Figure S3: Microbial Signatures, supplemental. A) Classification accuracy that would be achieved by a random model predicting features (rows) for held out cities (columns) B) Endemicity Score (Term Frequency Inverse Document Frequency for taxa in cities
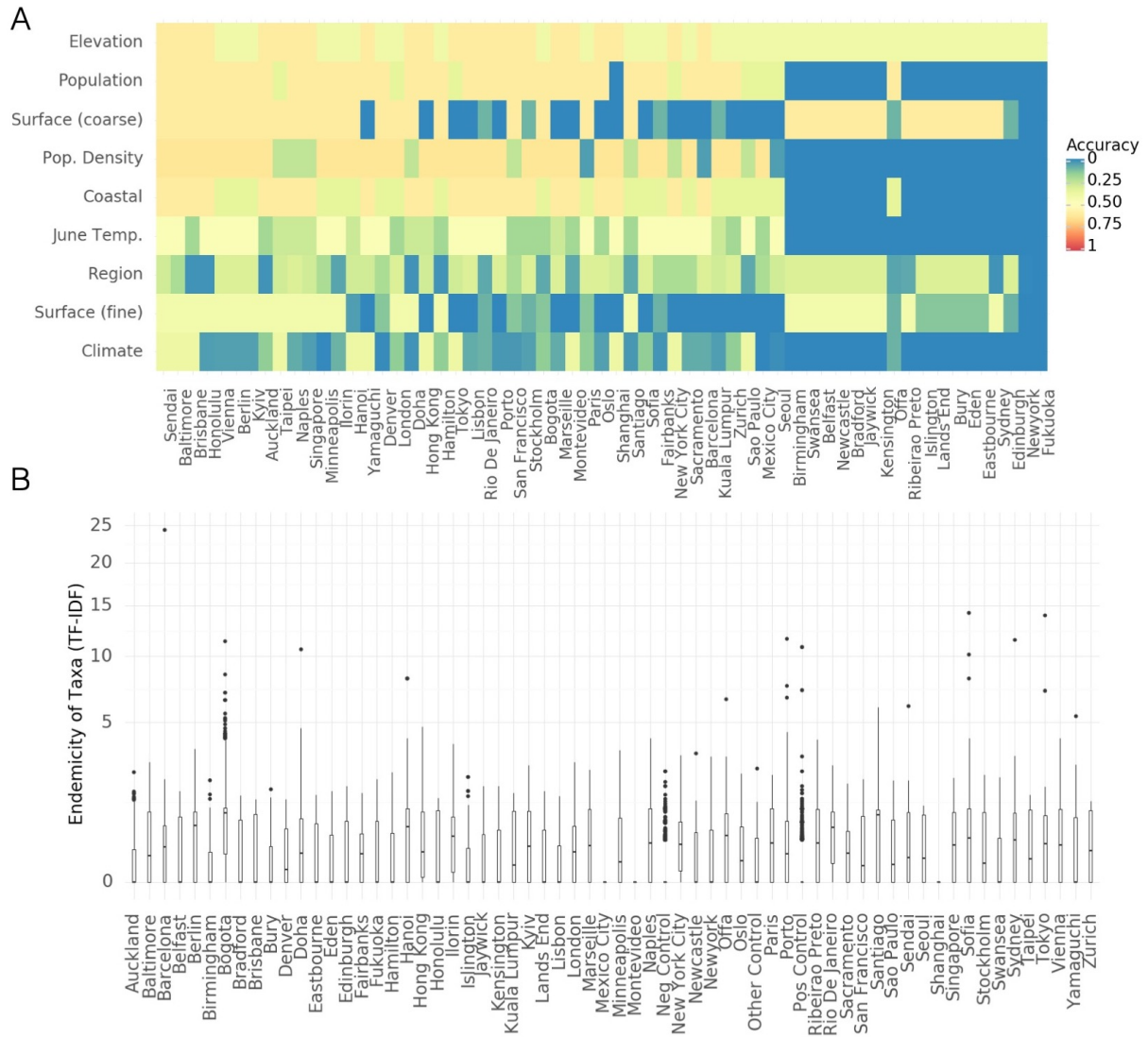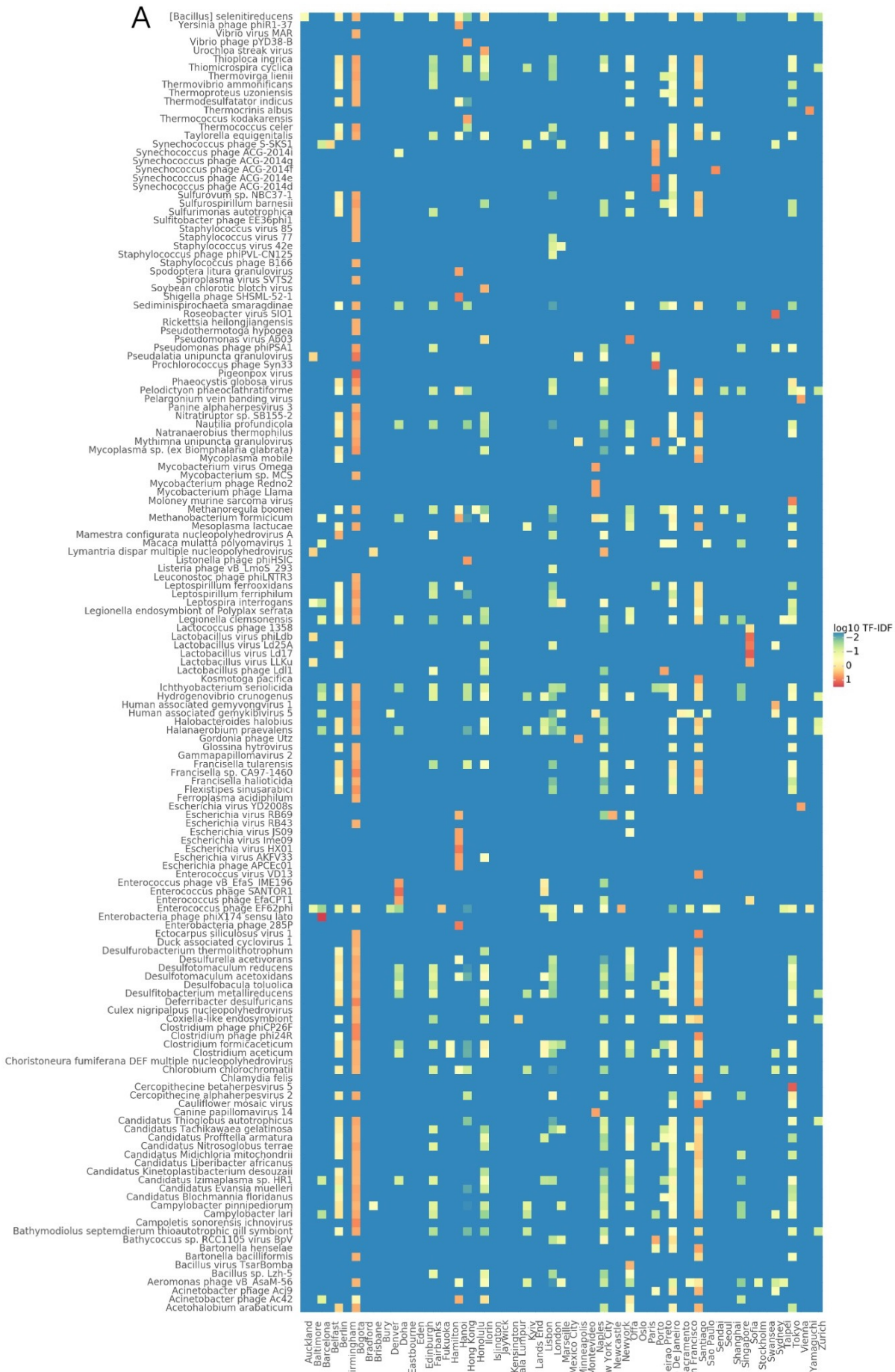
Figure S4: Endemicity scores of particular taxa. A) Heatmap showing the endemicity scores (term-frequency inverse document frequency) for taxa in different cities. This table is filtered to show only taxa with high endemicity scores in at least one city.
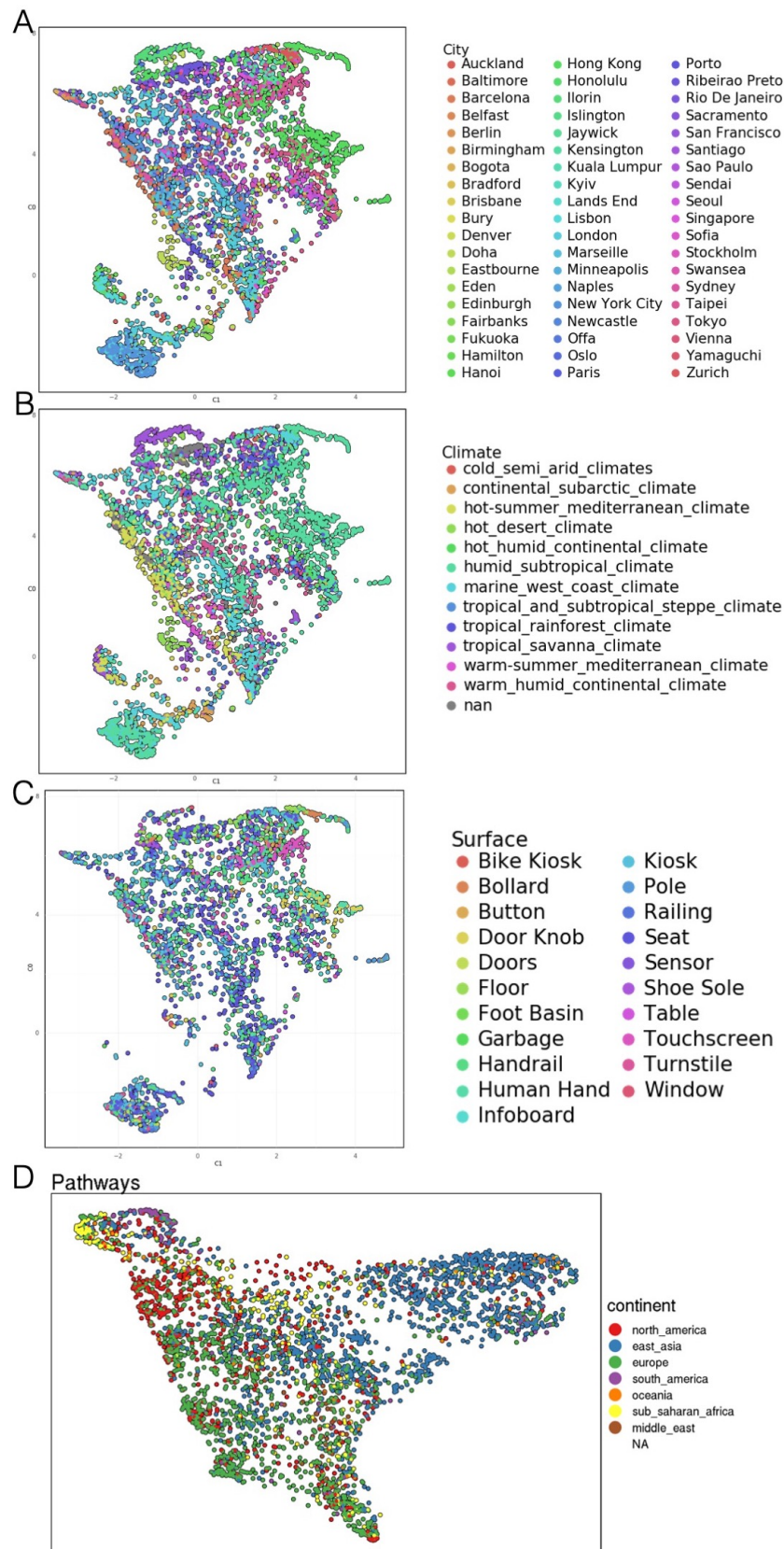
Figure S5: A) UMAP of taxonomic profiles colored by city B) UMAP of taxonomic profiles colored by climate classification C) UMAP of taxonomic profiles colored by surface type D) UMAP of functional profiles colored by region
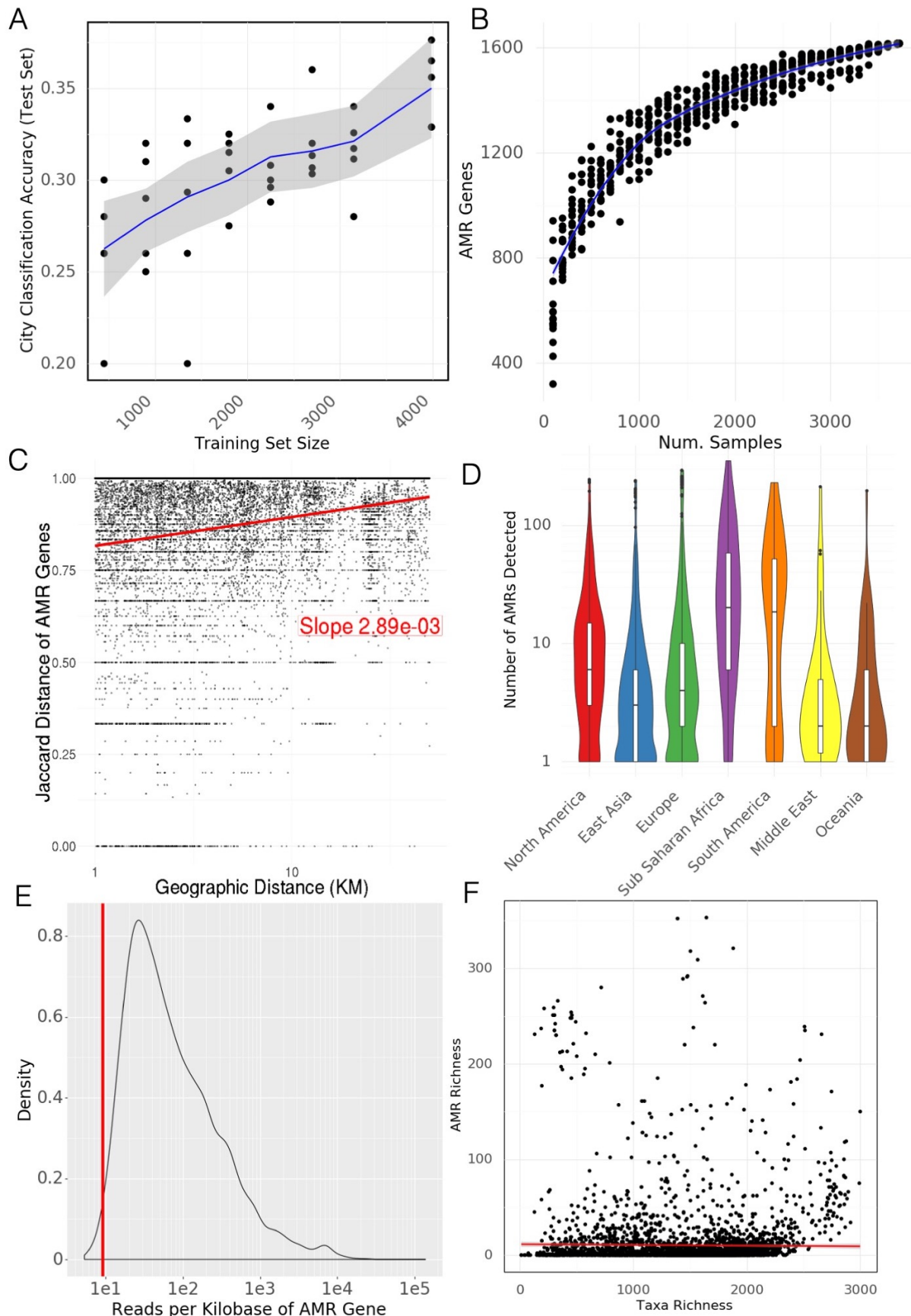
Figure S6: Antimicrobial Resistance Genes, supplemental. A) Classification accuracy of a random forest model predicting city labels for held out samples from antimicrobial resistance genes. B) Rarefaction analysis of antimicrobial resistance genes. Curve does not flatten suggesting we would identify more AMR genes with more samples. C) Neighbourhood effect. Jaccard distance of AMR genes weakly correlates with geographic distance within cities. D) Number of AMR genes detected for samples in each region. E) Distribution of reads per gene (normalized by kilobases of gene length) for AMR gene calls. The vertical red line indicates that 99% of AMR genes have more than 9.06 reads per kilobase and would still be called at a lower read depth.

47
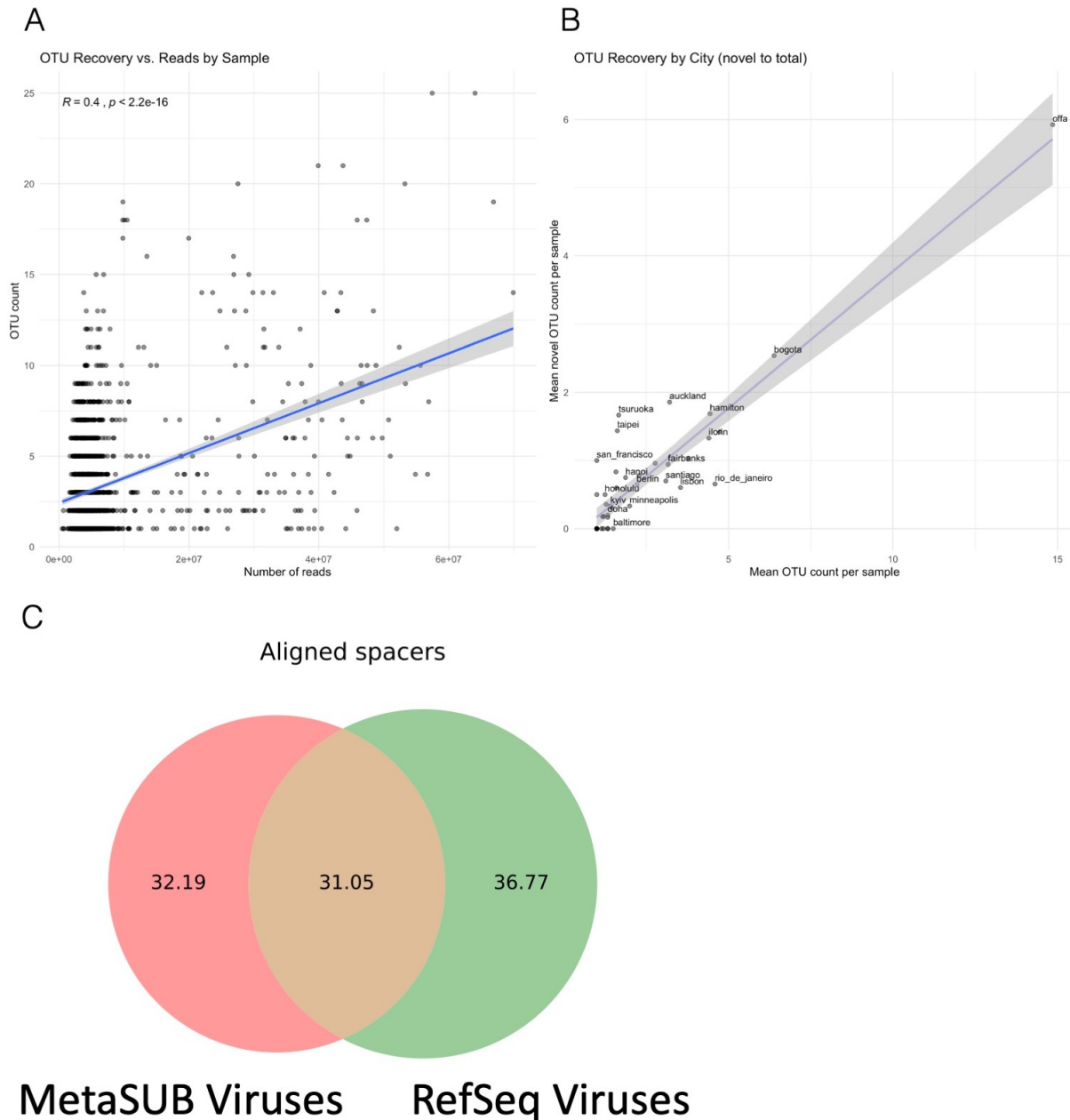
Figure S7: Novel biology, supplemental. A) Relation of read depth to the number of identified bacterial Metagenome Assembled Genomes (MAGs) in a sample. B) Discovery rate for baterial MAGs in each city. C) Total fraction of CRISPR spacers aligned to MetaSUB viral MAGs and viral genomes in RefSeq.
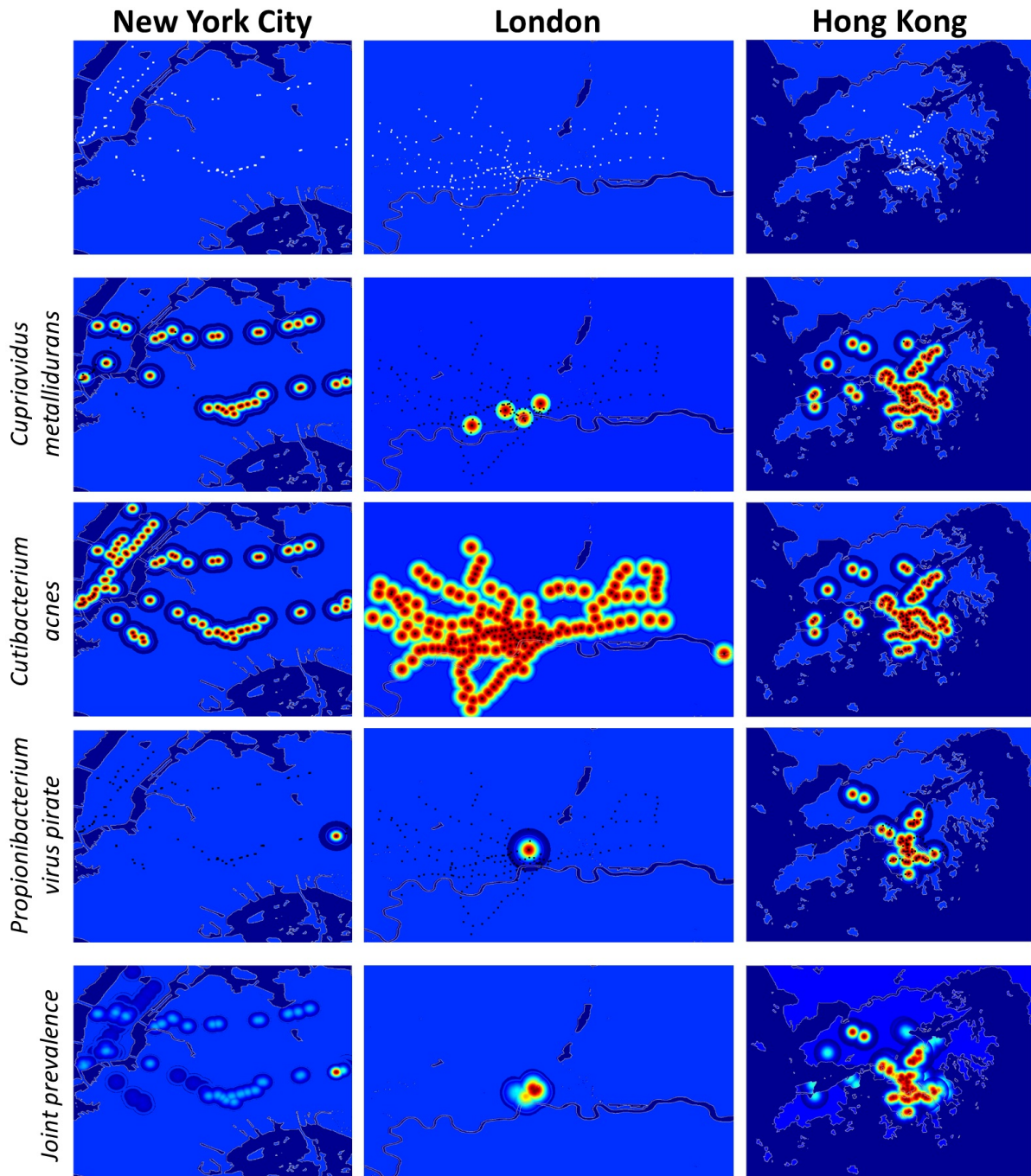
Figure S8: Example Geographic taxonomic Distributions. Distributions of taxa were estimated by fitting Gaussian distributions to sampling locations where the taxa was found with standard deviations based on the geographic distance between observations. Top Row) Sampling sites in three major cities Rows 2-4) Estimated distribution of different example species in major cities Row 5) Estimated distribution of three species together in major cities
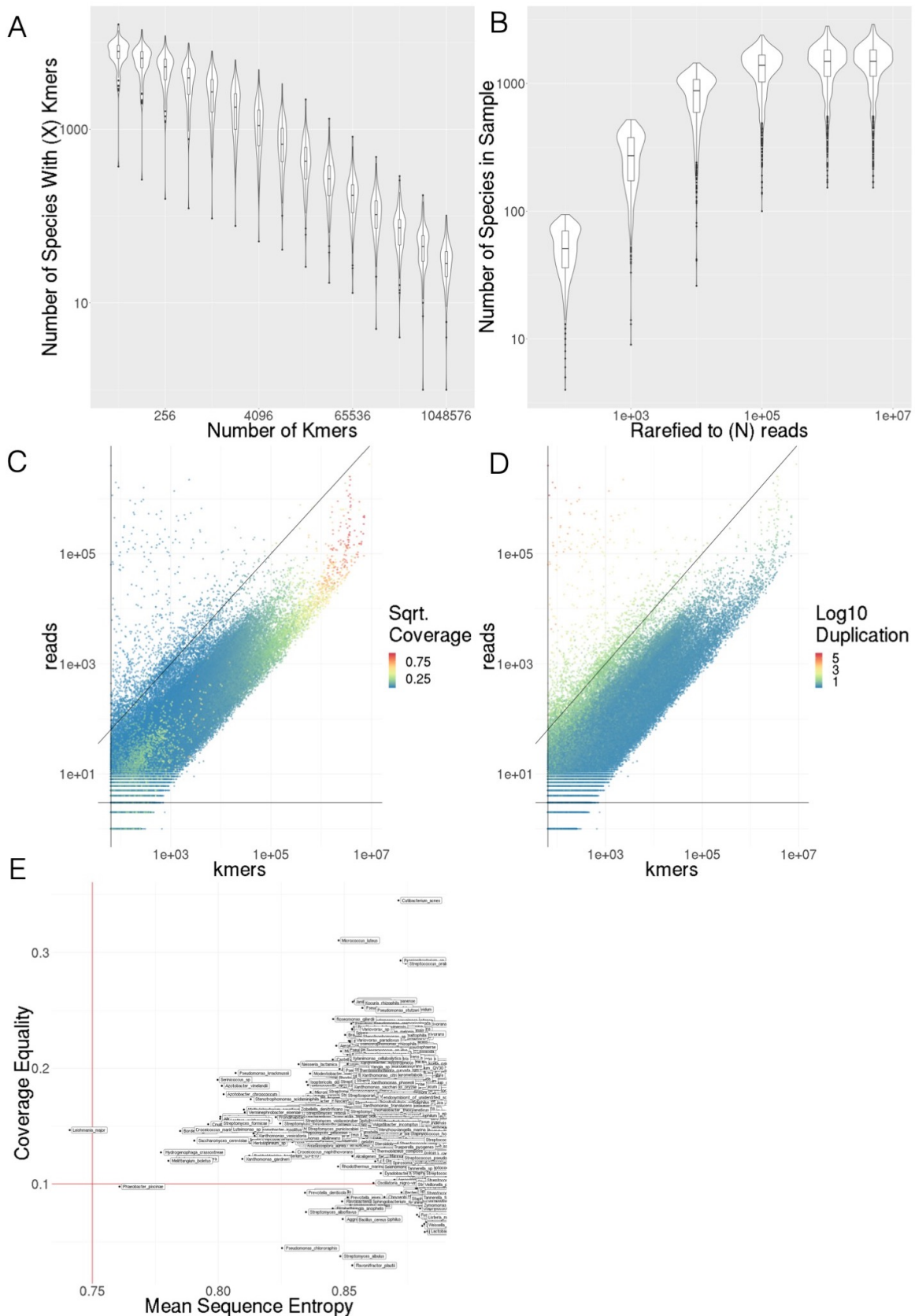
Figure S9: A) Number of species detected as k-mer threshold increases for 100 randomly selected samples B) Number of species detected as number of sub-sampled reads increase C) k-mer counts compared to number of reads for species level annotations in 100 randomly selected samples, colored by coverage of marker k-mer set D) k-mer counts compared to number of reads for species level annotations in 100 randomly selected samples, colored by average duplication of k-mers E) Comparison of Mean Sequence Entropy and Coverage Equality for core and sub-core taxa. Thresholds are shown by red lines.
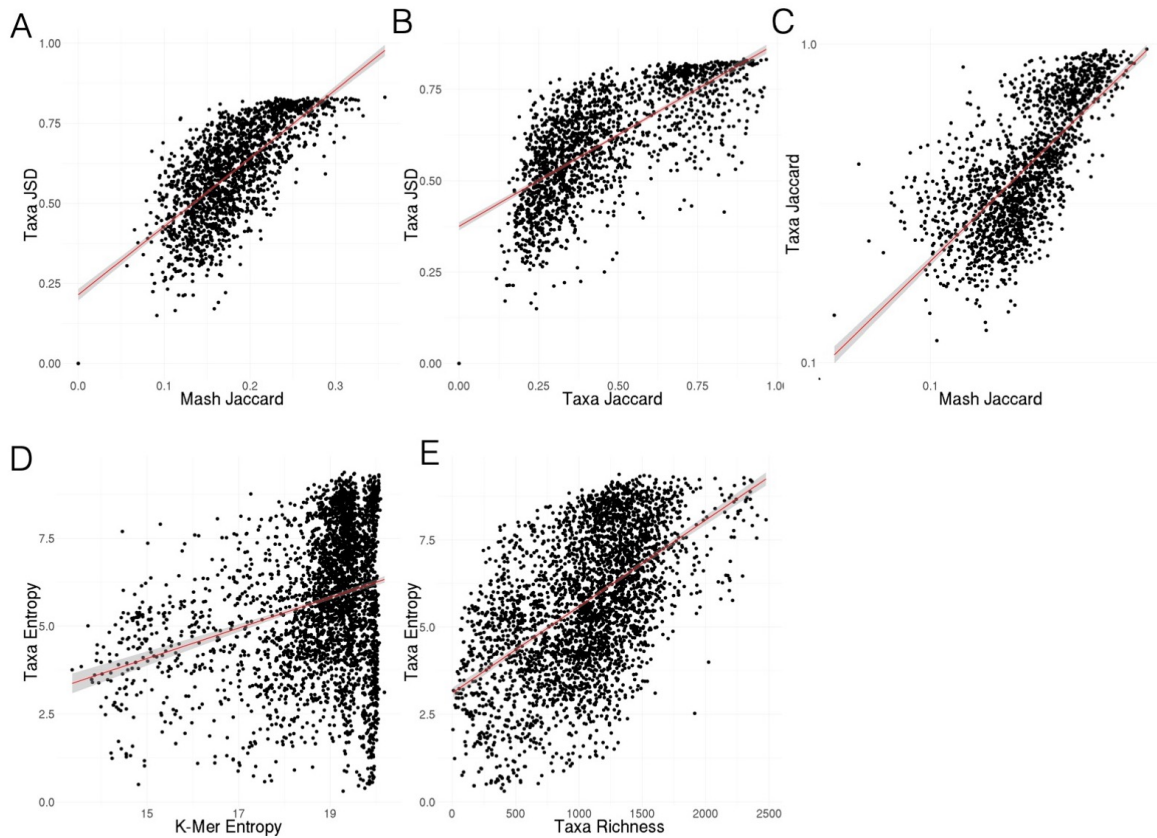
Figure S10: A) Jensen-Shannon Divergence of taxonomic profiles vs MASH Jaccard distance of k-mers B) Jensen-Shannon Divergence of taxonomic profiles vs Jaccard distance of taxonomic profiles. C) Jaccard distance of taxonomic profilesvs MASH Jaccard distance of k-mers D) Shannon's Entropy of taxonomic profiles vs Shannon's Entropy of k-mers E) Taxonomic richness (number of species) vs Shannon's Entropy of taxonomic profiles
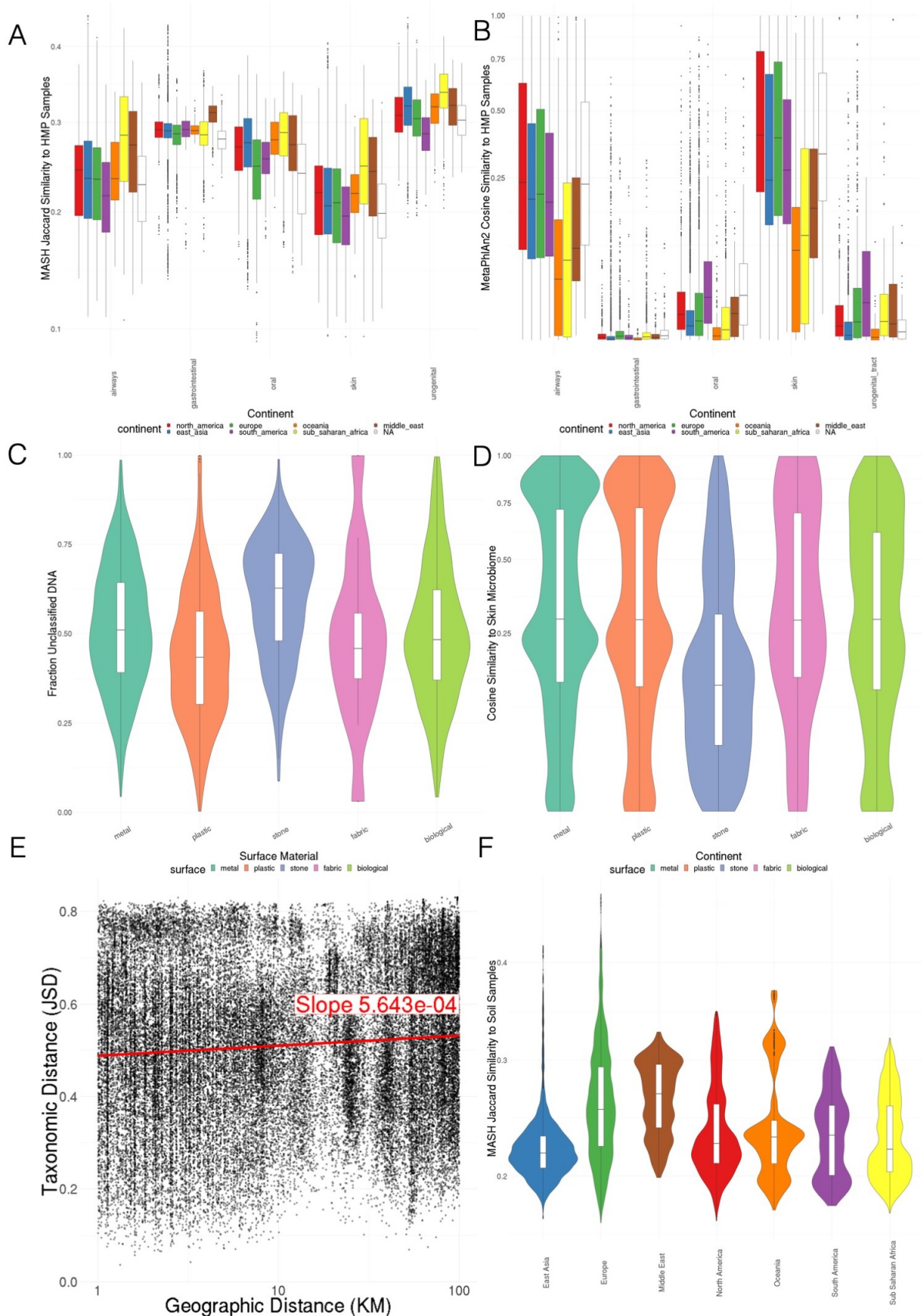
Figure S11: A) MASH k-mer Jaccard similarity to representative HMP samples, colored by continent B) MetaPhlAn v2.0 cosine similarity to representative HMP samples, colored by continent C) Fraction unclassified DNA by surface material D) Cosine similarity to MetaPhlAn v2.0 skin microbiome profile by surface E) Jensen-Shannon distance between pairs of taxonomic profiles vs Geographic Distance F) MASH k-mer Jaccard similarity to representative soil samples, colored by continent
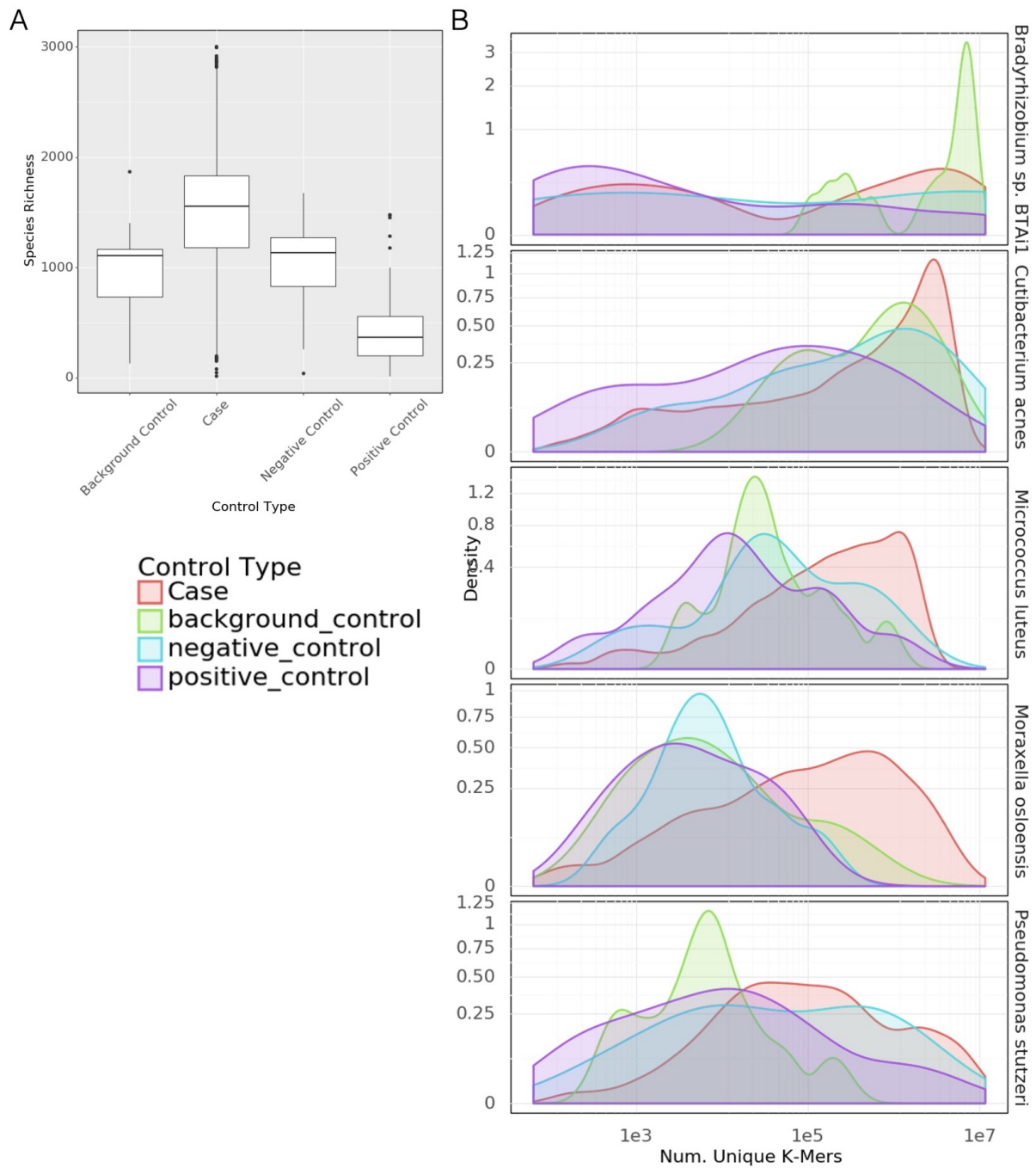
Figure S12: A) Taxonomic Richness in Cases vs. Types of Controls B) Distributions of k-mer counts in control types vs cases for 5 most abundant taxa. k-mer count is a marker of assignment confidence.
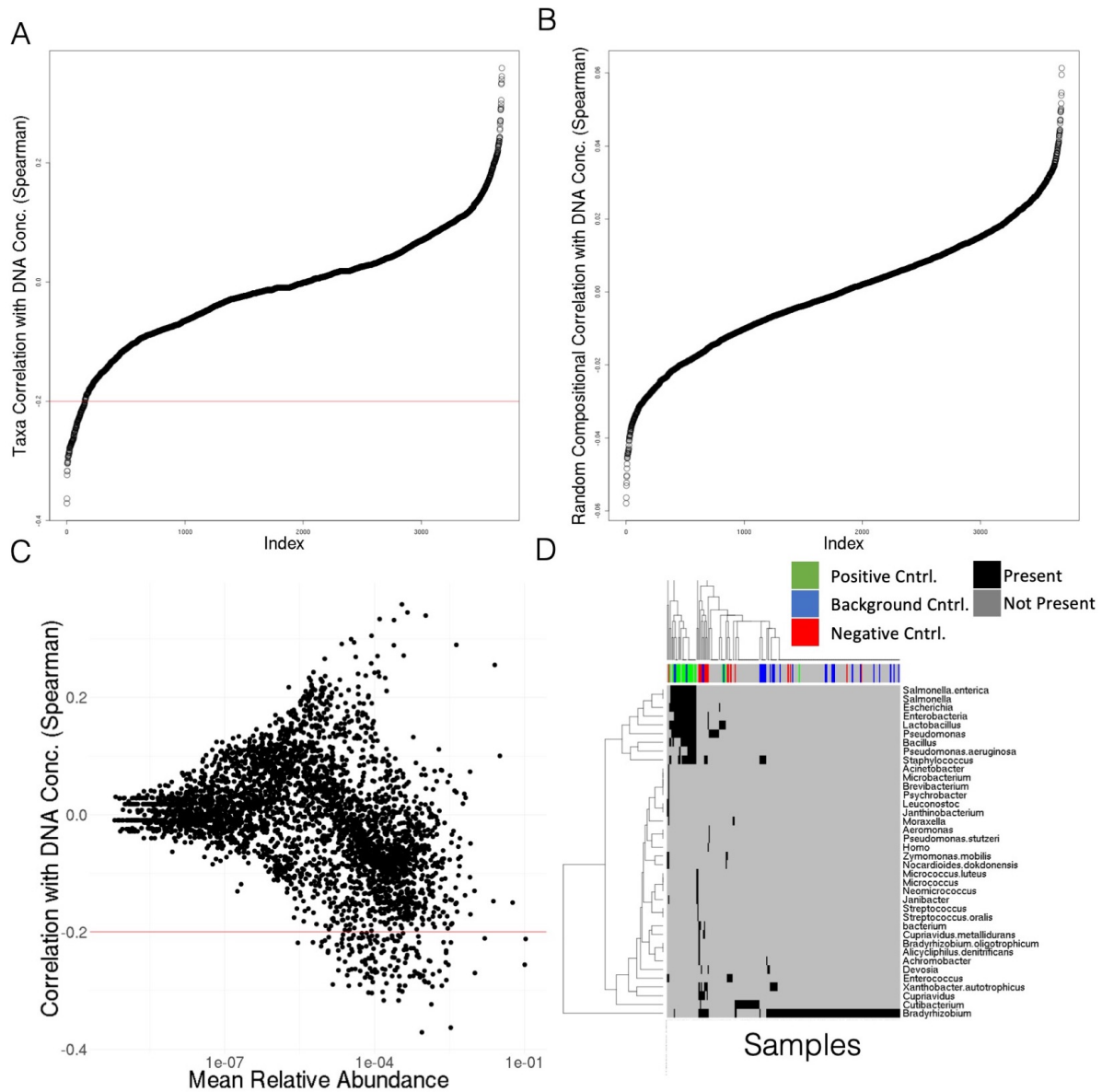
Figure S13: A) Correlation of taxonomic (species) relative abundances with DNA concentration B) Correlation of randomly generated compositional vectors with DNA concentration. Note the same shape but lower magnitude C) Correlation of taxa with DNA Concentration vs the mean relative abundance of that taxa D) Presence (black) absence (grey) heatmap of taxa found in controls and other samples. Colored bar at top, red are negative controls, blue are background, green are positive. Case samples with homology are grey. Case samples without homology to control sequences are not shown.
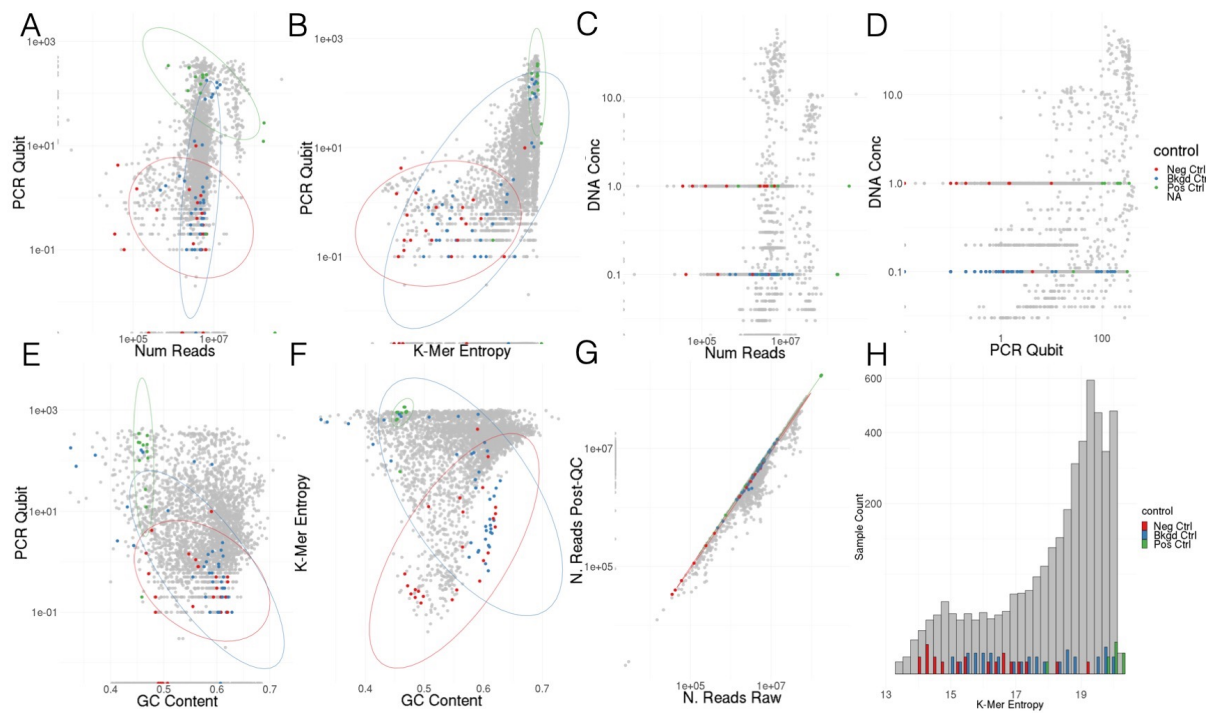
Figure S14: Comparisons of different seuqeuncing quality control metrics with controls marked. A-F) Comparisons of the raw reads, PCR Qubit scores, manually recorded DNA concentrations, k-mer Shannon entropy, and GC fraction of quality controlled reads G) Comparison of read counts before and after quality control but before human reads were removed H) Histogram showing the number of samples with different k-mer entropies.
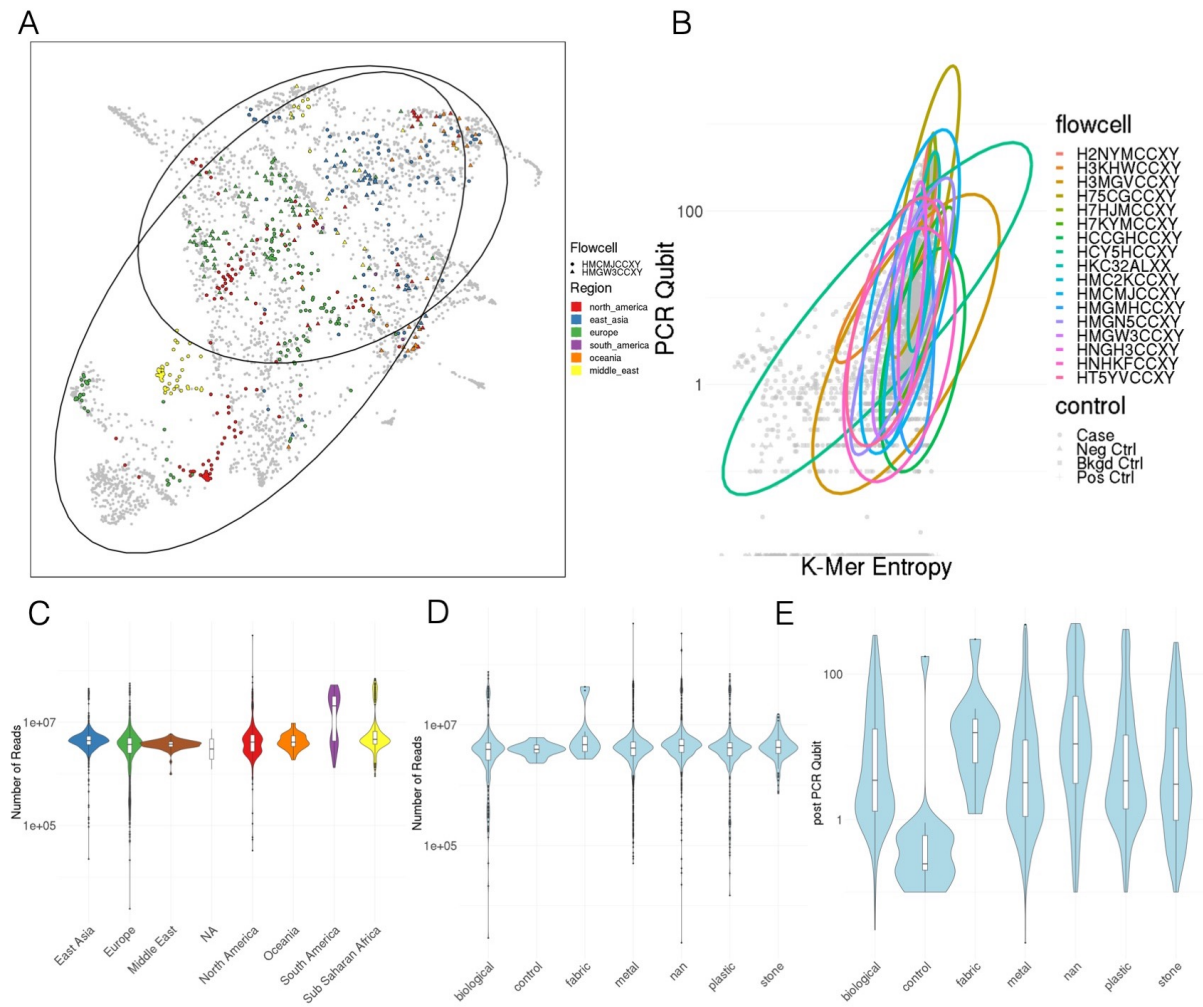
Figure S15: A) UMAP of taxonomic profiles from geographically diverse flowcells B) Flowcells vs quality control metrics C) Number of reads by region D) number of reads by surface material E) PCR Qubit by surface material